Optical characterization of InGaAsN / GaAs quantum wells:

Effects of annealing and determination of the band offsets

DISSERTATION

zur
Erlangung des Doktorgrades
der Naturwissenschaften
(Dr. rer. nat.)

dem Fachbereich Physik
der Philipps-Universität Marburg
vorgelegt von

Massimo Galluppi

aus Rom (Italien)

Marburg / Lahn 2005

Vom Fachbereich Physik der Philipps-Universität Marburg

als Dissertation angenommen am 09.12.2005

Erstgutachter: Dr. habil. Wolfgang Stolz

Zweitgutachter: Prof. Dr. Sergei Baranovski

Tag der mündlichen Prüfung am 15.12.2005

Table of contents

Table of contents

Table of contents

Figures

Chapter 1

Figures

Figures

Chapter 2

Chapter 3

Figures

Figures

Chapter 4

Figures

Figures

Introduction

Arsenide and phosphide based III-V semiconductors have been extensively researched for many years, resulting in mature technologies that are used for many of today's electronics and optoelectronics. These materials are however limited to medium and narrow band gap applications, preventing the fabrication of wide gap devices such as high power electronics and short wavelength optoelectronics. The development of wide gap material has been slow and problematic, nevertheless, advances in nitrides such as the development of blue LEDs and lasers, have given great importance to these alloys.[1] This has led to an explosion of research interest, and the natural progression was to bridge the gap between the wide gap nitrides and the medium gap arsenides. However, the addition of a small amount of nitrogen to GaAs was found to result in a rapid reduction of the band gap instead of the expected increase.[2] This unusual behaviour has attracted considerable interest both from a fundamental physics point of view as well as for potential narrow gap applications. These new alloys, which have become known as "dilute nitrides", are the main topic of this thesis work.

Practical interest in dilute nitrides began in the mid nineties after Kondow et al. published results on the quaternary system InGaAsN.[3] This new alloy allowed independent control over the In:Ga and N:As ratios. Increasing the In:Ga ratio causes a reduction in the band gap and an increase in lattice parameter, while increasing the N:As ratio also causes a band gap reduction, but a decrease in the lattice parameter. This potential for band-gap tailoring opened up a wide range of possible applications, but the 1.3 µm lasers based on GaAs for optical communication were identified as a key-application. At this wavelength, silica fibre has zero dispersion and relatively low attenuation, providing an attractive

means of high-speed data communication. In the past few years significant progress has been made towards 1.3 μm (and longer wavelengths) lasers.[4,5,6] In particular, great attention has been given to GaAs-based vertical-cavity surface–emitting lasers (VCSELs) due to their promising use as transmitter devices for short and mid-range optical networks.[7,8,9,10] In addition to lasers, dilute nitrides have been used in a number of other devices such as solar cells,[11] resonant cavity enhanced photodetectors,[12] electro-absorption modulators,[13] and heterojunctions bipolar transistors.[14]

Despite promising applications and encouraging experimental results, many open questions remain about the physical properties of these alloys. The band structure and its dependence on composition, for example, are still not completely understood. Also, the correct values of the electron effective mass and of the band offsets for varying composition are still topic of debate. In addition, the difficulty of incorporating nitrogen into (In)GaAs while maintaining good optical quality has provoked much work to establish an understanding of the underlying factors determining the optical quality of InGaAsN such as composition, growth and annealing conditions.

The principal aim of this thesis is to give more clarity to some intriguing aspects which characterise dilute nitride quantum well structures. For this reason, two important problems have been considered: the influence of annealing on the morphological and optical properties of InGaAsN / GaAs single quantum well (SQW) samples and the determination of the band offsets for the same type of structures.

As a main conclusion, it has been found that morphology and photoluminescence (PL) efficiency are not always correlated while the PL efficiency directly depends on the density of non-radiative recombination centres. These results have been obtained by combining continuous wave and time resolved photoluminescence measurements with transmission electron microscopy analysis. As a novelty, samples were annealed in different atmospheres, namely Ar and H_2.

In addition to that, the band offsets of InGaAsN / GaAs SQW samples have been determined by employing a method based on surface photovoltage measurements and conceived at Infineon Technologies. At first, the understanding of this technique has been broadened and refined by comparing measurements of dedicated series of samples with results obtained by electro reflectance

and by simulations. Then, a quantitative description of the influence of nitrogen and indium content on the valence and conduction band states has been presented. It has been shown the first direct experimental evidence that nitrogen influences mostly the conduction band states and leaves the valence band states almost unaltered.

Various part f this thesis have already been published.

The thesis is organised as follows:

- Chapter 1. An overview of the main properties characterising dilute nitrides is presented. In the first part of this chapter, the peculiar variation of the band gap and of the effective mass with varying nitrogen content is described taking examples from literature. Two of the most important theoretical models used to describe these peculiarities are illustrated. In the second part, the influence of nitrogen on the morphological and optical properties of InGaAsN / GaAs systems is described introducing also the concept of carrier localization.

- Chapter 2. Gives a description of the experimental techniques employed to grow and characterise the samples used in this thesis. The molecular beam epitaxy machine, the annealing apparatus and procedures, and the photoluminescence and the surface photovoltage set-ups are illustrated in detail.

- Chapter 3. A study of the influence of growth temperature and indium content on the PL intensity and PL peak position of $In_xGa_{1-x}As_{1-y}N_y$/GaAs SQWs are presented. Also an analysis of the degree of localization is performed. As a main part of this chapter, the modifications of the optical and morphological properties of these samples after annealing in different atmospheres are extensively discussed. At the end of the chapter, a speculative model describing the possible defects present in InGaAsN structures and their role in the PL efficiency of the quantum well is proposed.

- Chapter 4. The first part of this chapter illustrates a revised interpretation of the information which can be obtained employing a method, based on surface photovoltage measurements,

and created at Infineon Technologies to determine the band offsets of quantum well structures. The advantages of using this technique compared to other optical techniques are also emphasized. In the second part, this method is employed to determine the value of the band offsets of $In_xGa_{1-x}As_{1-y}N_y$/GaAs SQWs with varying quantum well composition and other parameters such as the quantum well width. At the end, an example is presented how to obtain information about the band offsets of laser structures without performing any type of theoretical calculation.

Chapter 1

Characteristics of Dilute Nitrides

Nitrogen containing III-V alloys, such as (In)GaAsN and (In)GaPN have in recent years emerged as a subject of considerable experimental and theoretical interest, due to their very unique physical properties and a wide range of possible device applications. In spite of the high interest in III-N-V ternary and quaternary alloys, the knowledge of their physical properties is still very poor. A complete understanding of the variation of the band gap with nitrogen content is far from complete despite many experimental and theoretical studies. [2,3,15,16] Other physical properties of these materials such as the dependence of the effective mass on nitrogen concentration or the band alignment are also basically unknown.

In this chapter, an overview about the fundamental properties of dilute nitrides will be presented. In the first part (§ 1.1), the peculiarities of the band structure of N-containing III-V compounds will be described. Employing different approaches, very far from those used to describe the properties of conventional III-V semiconductors, several theoretical models have been developed. Among these, the two most significant will be presented and compared in §1.1.2. In the last part of the section, the concept of potential fluctuations will be introduced. The morphological origin of these fluctuations will be discussed in §1.2, and the optical consequences in terms of carrier localization will be examined in §1.3. In addition, other optical properties typical for dilute nitrides will be described. In particular, all the results presented in this last section were obtained in the course of this PhD thesis.

1.1 Fundamental band structure properties and theories on dilute nitrides

The understanding of conventional III-V alloys has been built up through a range of approaches. Much progress was based on the use and application of relatively simple models, such as effective mass theory[17] and the envelope function method[18] to describe electronic states in quantum wells (QWs) and heterostructures. These simple and well established models are supported by more detailed and fundamental theoretical calculations, as well as by comparison with a wide range of experimental data. However, the presence of a small amount of nitrogen in III-V alloys induces a markedly different behaviour of the energy gap and the effective mass compared to conventional semiconductors. For this reason, appropriate theoretical models had to be developed to describe the main properties of dilute nitrides.[19,20] In the following section the fundamental band structure properties of dilute nitrides will be explained. The problem of the giant band gap bowing, the new features found in the conduction band, the increased value of the effective mass, and the band alignment will be discussed considering a variety of experimental results taken from the literature. In addition, two of the most important theoretical models will be presented.

1.1.1 Giant bowing of the band gap energy

In conventional $A_xB_{1-x}C$ isovalent III-V alloys the band gap E_g (x) deviates from the composition-weighted linear average of the constituents by

$$\Delta E_g(x) \equiv E_g(x) - [(1-x)E_{AC} + xE_{BC}] = -bx(1-x) , \qquad (1.1)$$

where b is the bowing coefficient and E_{AC} and E_{BC} are the band gap values of the AC and BC binary alloys, respectively. The bowing coefficient is composition independent and usually a fraction of an eV.[21] Two binary compounds such as InAs and GaAs can form the ternary compound InGaAs. InAs has a smaller band gap in comparison to the GaAs one (0.356 eV compared to 1.425 eV) and a greater lattice

_____

constant (6.54 Å compared to 5.65 Å). Inserting gallium into InAs, the band gap of the resulting

compound progressively increases and the lattice constant decreases. This is shown in figure 1.1 in

which the relationships between the band gap energy and the lattice constant of III-V semiconductors

are depicted.
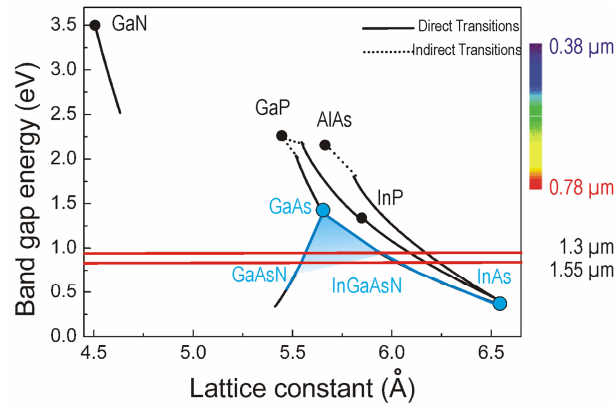
Figure 1.1.: Relationship between the lattice constant and the band gap energy in III-V compound semiconductors.

For the $GaAs_{1-y}N_y$ compound, however, the behaviour is completely different. Although the energy gap

of GaN is greater than the GaAs one (about 3.50 eV compared to 1.43 eV, at room temperature), the

$GaAs_{1-y}N_y$ alloy does not show the expected blue shift from the GaAs band gap. This ternary compound

shows instead a considerable red shift in absorption and photoluminescence (PL) measurements near

the band edge, suggesting a decrease in the band gap energy with increasing nitrogen content.[2,22,23]

Theoretical predictions of the $GaAs_{1-y}N_y$ electronic structure depend strongly on the model used and

show contradictory results.[24,25] Sakai et al.,[24] using Van Vechten's model,[26] predicted a negative band

gap for nitrogen concentrations in the range of 0.09 – 0.87, giving this material a semimetal nature in

this N content range. In contrast, calculations of Bellaiche et al.,[16] based on a supercell representation

of the alloy, confirmed the previous suggestion of Wei and Zunger[27] that $GaAs_{1-y}N_y$ is a semiconductor

rather than a semimetal for the whole range of nitrogen concentrations, and that the bowing parameter

is strongly composition dependent, unlike the case of conventional III-V alloys. In GaAsN structures

grown on GaAs for example, b ≈ 26 eV at [N] < 1% and ≈ 16 eV at [N] > 1%.[28] The behaviour of the

bowing coefficient has been explained in Ref. 16 by first principle local density approximation (LDA)

calculations of the band structure. Based on the analysis of the highly localized nature of the perturbation introduced by N atoms due to a large chemical and size difference between N and the other group V-anions it replaces, two regions in the band gap variation of the III-N-V alloys have been predicted for N concentrations less than 50%. An impurity-like region with a large and composition-dependent bowing coefficient is expected for low N concentrations up to 10%, whereas a band-like region with a much smaller and nearly constant bowing coefficient is predicted for intermediate concentrations ([N] = 10% - 40%).

In addition to that, it has been shown that the compositional dependence of the GaAsN band gap is rather different when measured on GaP instead of GaAs substrates. This implies that the bowing coefficient depends also on the internal strain in the GaAsN epilayers.[15,29]

InGaAsN alloys show similar band gap properties as GaAsN structures. However, being constituted of four elements, a clear description of the band gap properties is more complicated. On the other hand, for InGaAsN structures there are more possibilities to grow materials with different energy gaps. In particular, combining nitrogen and indium in the right way, it is possible to obtain structures lattice-matched to GaAs suitable for long-wavelength-range emitting devices.

1.1.2 Theoretical models

Owing to the peculiar behaviour of their band gap, dilute nitrides have been the subject of many theoretical works aimed to partly or wholly account for the puzzling phenomenology mentioned above. In particular, two different theoretical models have been presented:

I. The band anti-crossing (BAC) model. In this phenomenological model the band gap reduction and the electron effective mass increase (see § 1.1.4) in (In)GaAs upon nitrogen incorporation are ascribed to the perturbation induced into the conduction band by *isolated* nitrogen atoms;[19,30]

II.   The pseudopotential theory of dilute nitrides. This theory takes into account the presence of both *isolated* nitrogen atoms and nitrogen *clusters*, based on a "polymorphous model" which acknowledges the existence of a plurality of local atomic environments, all characterized by different atomic arrangements and distances. In this case, even a random distribution of impurities creates by chance a cluster.[31]

Both models imply that the states of the valence band exhibit negligible nitrogen dependence.

1.1.2.1 The band anti-crossing model

In this model, firstly proposed by W. Shan et al.,[19] it is assumed that the incorporation of isolated nitrogen atoms into a host matrix compound (GaAs or InGaAs) leads to a strong interaction between the conduction band and the narrow resonant band formed by the nitrogen states. The interaction between the extended conduction states of the matrix semiconductor and the localized nitrogen states is treated as a perturbation which leads to the following eigenvalue problem:

$$\begin{vmatrix} E - E_M & V_{NM} \\ V_{NM} & E - E_N \end{vmatrix} \qquad\qquad (1.2)$$

where E_M is the energy of the unperturbated conduction band of the matrix semiconductor and E_N is the energy of the nitrogen level (both relative to the top of the valence band). V_{NM} measures the strength of the interaction potential. The alignment of the localized N level E_N in GaAs has been modelled using tight-binding calculations.[32] At very low nitrogen fractions the wavefunctions of individual nitrogen atoms do not significantly overlap, hence they act as isoelectric impurities with energy around 1.65-1.70 eV. However, as the nitrogen fraction increases (above $\approx$ 0.2%) the wavefunctions start overlapping, forming a resonant energy band E_N. Solving the eigenvalue problem, the following subbands energies are given:

$$E_\pm = \frac{E_M + E_N \pm \sqrt{[E_M - E_N]^2 + 4V^2{}_{NM}}}{2} \; . \qquad\qquad (1.3)$$

E_-, mixture of highly localized (E_N) and extended states (E_M), is the new conduction band minimum and

it is depicted along with the other subband E_+ in figure 1.2.[33]
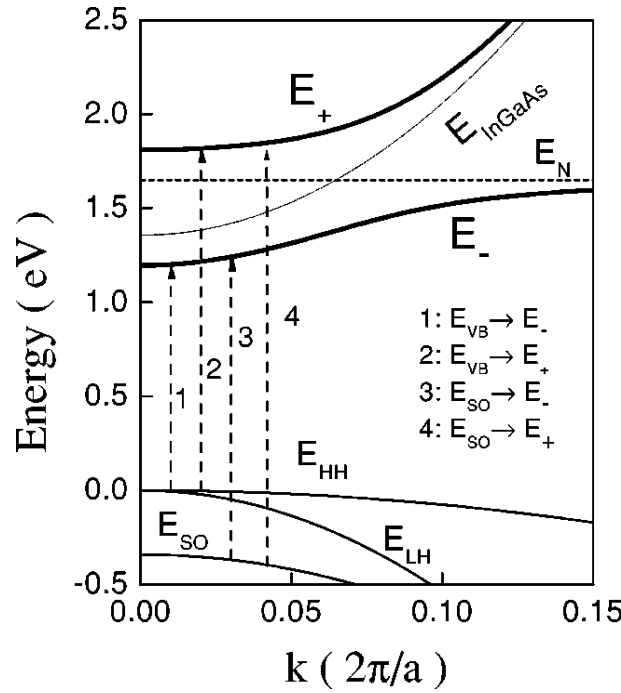
Figure 1.2.: E-k diagram of an $In_{0.04}Ga_{0.96}As_{0.99}N_{0.01}$ structure calculated using the BAC approach
and the corresponding optical transitions (arrows). (From Ref. 33)

Since the dispersion of the new conduction band is *strongly non parabolic* due to the anti-crossing

interaction with the N-related resonant level, the electron effective mass m^*_e depends on the

wavevector k. For small wavevectors one obtains

$$\frac{1}{m^*_e(k=0)} \approx \left(\hbar^2 \left| \frac{k}{\partial E_-/\partial k} \right|_{k=0} \right)^{-1} = \frac{1}{2m_M} \left[1 - \frac{E_M(k=0) - E_N}{\sqrt{[E_M(k=0) - E_N]^2 + 4V^2_{NM}}} \right], \qquad (1.4)$$

where m_M is the electron effective mass of the host semiconductor matrix, i.e. GaAs for GaAsN

structures.

This model yields a remarkably good description of the physical properties of the fundamental band

gap and of E_+. For example, the flattened dispersion explains the increase in electron effective mass

(§ 1.1.4), and the low-pressure coefficient of the nitrogen level explains the reduced pressure

dependence of the conduction band minimum[33] (§ 1.1.3). Because this model provides a simple and

satisfactory fit to many characteristics of the alloy, it is very popular. It has been expanded to a 10-band

k·p model,[34] it has been supported by a more sophisticated analysis,[35] and tight-binding versions have also been proposed.[34,36] On the other hand, the BAC model assumes that the nitrogen resonant states form a well-behaved band, in contradiction with simple phenomenological arguments and more elaborate theoretical models.

1.1.2.2 Pseudopotential theory of dilute nitrides

Kent et al.[20,31] have used a pseudopotential supercell technique to model the band structure of GaAsN. This work studied the conduction band states of GaAsN starting from very dilute concentrations up to 1% N. The main interesting aspect of this calculation is that more than one nitrogen atom was included in the supercell, therefore nitrogen atom interactions could be studied.

Adding a few nitrogen atoms to a GaAs matrix produces resonant and bound states, above and below the conduction band, respectively. At ultra low concentration, these states are relatively isolated from each other. At higher concentration, their spatial density increases and their mutual interactions induce broadening and splitting. The resulting effects were analysed with an "effective" conduction band density of states as reported by Kent and Zunger. It was found that nitrogen produces a complex distribution of localized and quasi-localized states both above and below the conduction band edge. According to these results, the quasi-localized states or perturbed host states are resonant with the conduction band and are the most likely origin for E_+ as measured in experiments. The localized states result from nitrogen aggregates in the band gap and are associated with E_-.

This calculation explicitly takes into account the complex interactions between nitrogen states and it was found that the single nitrogen states and the multiple pair configurations states interact and merge together. This result raises an important issue concerning the appropriateness of the BAC model since this phenomenological model neglects the multiple and diverse configurations nitrogen atoms can take.

1.1.3 Conduction band states

The discovery of an additional feature, denoted E_+ in the electro-[37] and photoreflectance[19] spectra of (In)GaAs$_{1-y}$N$_y$ alloys with $y > 1\%$ and the observation of the unusual pressure dependence of the alloy band gap has given further insight into the nature of the band states in III-N-V structures.

A typical electroreflectance (ER) spectrum measured from thick GaAs$_{0.978}$N$_{0.022}$ epilayers grown on GaAs substrates is shown in figure 1.3.[37] Three fundamental transitions are clearly visible: the band gap transition (denoted as either E_0 or E_-); the transitions from the spin-orbit split-off valence band ($E_0+\Delta_0$), which are intrinsic to all zinc blende III-V semiconductors; and an additional feature E_+, which appears in the spectra of GaAs$_{1-y}$N$_y$ samples with $y > 0.8\%$ and in In$_x$Ga$_{1-x}$As$_{1-y}$N$_y$ samples with $y \geq 1.2\%$.[37]
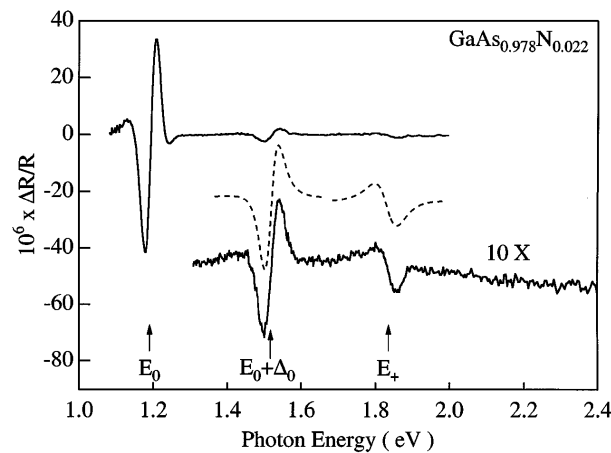
Figure 1.3.: Electroreflectance spectra taken at room temperature for a 2 µm thick GaAsN film. The transitions E_0 and $E_0+\Delta_0$ are easily visible. The additional feature E_+ is more clearly visible in the second spectrum, magnified and offset for clarity. The dashed line is the fitted line shape for the $E_0+\Delta_0$ and E_+ transitions. (From Ref. 37)

The evolution of the ER spectra as a function of nitrogen content is described in figure 1.4. With increasing nitrogen content in the alloy the spectral position of the transition E_- shifts towards lower energies showing the giant band gap bowing effect discussed in section 1.1.1. Also the transition from the top of the spin-orbit split-off valence band to the bottom of the conduction band ($E_-+\Delta_0$) moves to lower energies with increasing N concentration. On the contrary, the transition E_+ shifts toward higher energies with increasing N and its intensity increases relative to the E_- intensity. It is important to note that while the energy difference E_+-E_- increases with increasing nitrogen content, the spin-orbit splitting

energy Δ_0 is about 0.3 eV for all measured samples and does not depend on the nitrogen concentration.

These results demonstrate that the incorporation of N into (In)GaAs affects mostly the conduction band

and has a negligible effect on the electronic structure of the valence band. Moreover, they show that the

E_+ transition does not correspond to an electronic transition from within the valence band to the

conduction band minimum but to an electronic transition between the valence band maximum and a

level above the conduction band minimum.[37]
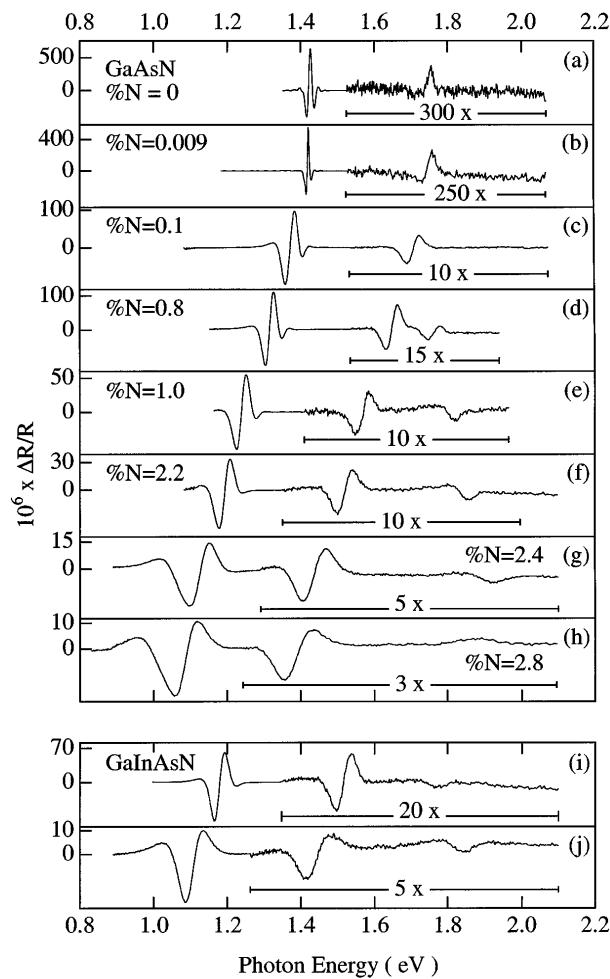
Figure 1.4.: Electroreflectance spectra taken at room temperature for thick GaAsN (a)-(h) and InGaAsN (i)-(j) films. For the GaAsN samples, [N] ranges from y = 0% (a) to y = 2.8% (h): For InGaAsN samples, the compositions are $In_{0.05}Ga_{0.95}As_{0.987}N_{0.013}$ (i) and $In_{0.08}Ga_{0.92}As_{0.978}N_{0.022}$ (j). (From Ref. 37)

Another peculiarity of dilute nitrides is the pressure dependence of the band gap. In strong contrast

to the (In)GaAs material, where the fundamental bandgap energy increases linearly under applied

hydrostatic pressure, the bandgap energy in N-containing alloys (corresponding to the E_- transitions)

exhibits a much weaker sublinear pressure dependence with a tendency to saturate at high pressures.

This unusual pressure behaviour of the bandgap energy has been detected both via

photoreflectance[19,38] and photoluminescence[39] measurements.
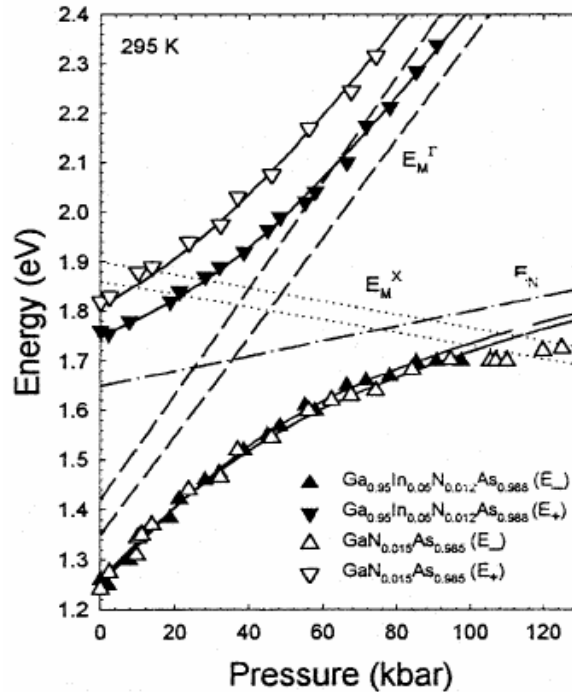
Figure 1.5.: Fundamental bandgap variation of different $In_xGa_{1-x}As_{1-y}N_y$ samples as a function of hydrostatic pressure. The solid line is a best linear fit to the experimental data obtained from the $In_{0.08}Ga_{0.92}As$ sample. (From Ref. 38)

On the other hand, the pressure dependence of the E_+ transition undergoes a change opposite to E_-,

i.e. the E_+ energy position depends weakly on the applied pressure at low pressures and demonstrates

a much stronger linear increase at high pressures. Some representative experimental data are shown in

figure 1.5, for $GaAs_{1-y}N_y$ and $In_xGa_{1-x}As_{1-y}N_y$ alloys. These data, taken from Ref. 38, are in good

agreement with the fits (solid lines in the figure) obtained employing the band anti-crossing model.

1.1.4 Conduction band dispersion: electron effective mass

The knowledge of the carrier effective masses provides valuable information on the fundamental

nature of the band states in the alloy and is also very important for a full exploration and optimisation of

III-N-V alloys in device applications.

In contrast to conventional semiconductors, in which the value of the effective mass decreases with decreasing band gap energy, in dilute nitrides it increases with increasing nitrogen composition and thus with decreasing band gap energy.[32,39,40] In addition, as described in § 1.1.2 the conduction band in the alloys is predicted to be very non-parabolic, leading to a strong energy dependence of the effective mass.[32]

For GaAsN / GaAs quantum well structures the compositional dependence of the electron effective mass m^*_e has directly been determined by using optically detected cyclotron resonance measurements.[41] The results show that m^*_e increases up to 0.190 m_0 (from 0.067 m_0 for GaAs) with increasing nitrogen content up to 2%, where m_0 is the free electron rest mass.

For InGaAsN structures, most experimental values of m^*_e have been obtained using indirect methods[42,43,44] such as the analysis of the carrier confinement energies. It has been found that for an $In_xGa_{1-x}As_{1-y}N_y$ / GaAs structure with [In]≈30%, the incorporation of 1% of nitrogen induces an increase of the electron effective mass up to about 0.080 m_0 (from 0.054 m_0 for $In_{0.30}Ga_{0.70}As$). Concerning direct measurements, infrared reflection has been employed by Skierbiszewski et al. [45] to investigate the conduction band dispersion of InGaAsN alloys. They found a strong increase of the electron effective mass with the addition of nitrogen and, even more severe, with electron concentration.

1.1.5 Band alignment

A comprehensive knowledge of physical parameters such as band alignment in quantum structures and band offsets values is extremely important in order to apply (In)GaAsN alloy systems for the realization of optoelectronic devices. Furthermore, information about band alignment is also valuable in examining the validity of the approximations made by theoretical models, and thus the understanding of the fundamental band structure of nitrogen containing III-V alloys.

Optical transition measurements, capacitance-voltage techniques, and photoemission spectroscopy are some of the common methods employed to experimentally determine the band offsets of quantum

well structures.[46,47,48] However, in order to apply these methods successfully, other parameters of the structures have to be known accurately. For example, when the optical absorption is used to determine the band offsets, the energies of the optical transitions between the discrete levels in the QW are first experimentally determined. The band offsets are then calculated using fitting procedures under the assumption that the other parameters of the structure are known: the effective masses of electrons and holes, the geometry of the structure, and the QW potential. If one of these parameters is not known accurately, the results of the fitting procedures are not precise.

Due to the fact that in dilute nitrides some physical phenomena are not fully understood and that the value of some parameters is not univocally determined, experimental information about band offsets of dilute nitrides are rare in literature.[43] A profound understanding of the evolution of the band states with nitrogen content has in fact so far been lacking. For example, although it is commonly accepted that the addition of nitrogen into (In)GaAs mainly affects the conduction band states leading to a large conduction band offset and only a small valence band discontinuity, direct experimentally proofs of that are basically absent. In particular, nobody has so far presented a quantitative description of the influence of nitrogen on the conduction and valence band states in dilute nitrides. Experimental results for this question are a main finding of this thesis and will be presented and discussed in chapter 4.

Regarding the band alignment, different groups,[49,50,51] employing different experimental techniques such as X-ray photoemission spectroscopy, photoluminescence polarization measurements and optically detected cyclotron resonance studies have investigated GaAsN / GaAs heterostructures. However, the exact band configuration for these systems is still under debate. Both experimental studies and theoretical calculations have in fact not univocally established if GaAsN / GaAs structures have a type I or type II band alignment. Concerning the InGaAsN / GaAs systems, their band configuration has been studied mainly by analysing the effect of quantum confinement on the energies of the optical transitions detected from strained InGaAsN / GaAs quantum wells. Photoluminescence,[52] optical absorption,[53] and polarized photoluminescence excitation spectroscopy[43] have been employed to demonstrate that these heterostructures show a type I band alignment and a strong increase of the

conduction band offset with increasing nitrogen composition. The estimated rate is about 100 meV per 1% of N.

1.2 Structural properties

Dilute nitrides are very different from conventional III-V semiconductors, not only for their electronic properties but also because of the very large range of miscibility gap in the alloys. Most ternary or quaternary semiconductors, such as AlGaAs and InGaAsP, have complete miscibility across the entire alloy range. Due to the low solubility of nitrogen in (In)GaAs, this is not possible for (In)GaAsN structures, which are therefore metastable materials and are very sensitive to growth conditions.

Employing microscopic analysis, such as transmission electron microscopy (TEM),[54,55,56] high resolution X-ray diffraction (HRXRD),[57] or reflection high energy electron diffraction (RHEED)[58] it is possible to investigate the effect of nitrogen on the structures dilute nitrides.
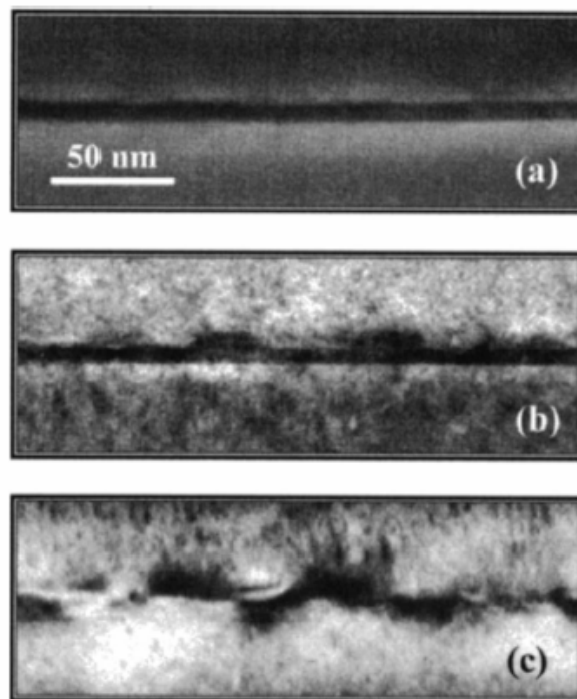
Figure 1.6.: Bright field cross-sectional TEM images of the (a) $In_{0.28}Ga_{0.72}As$/GaAs and (b) $In_{0.28}Ga_{0.72}As_{0.972}N_{0.028}$/GaAs SQWs. (c) (400) dark field image of the $In_{0.28}Ga_{0.72}As_{0.972}N_{0.028}$/GaAs SQW. (From Ref.55)

In figure 1.6 (a-b) are shown bright field cross-sectional TEM micrographs of InGaAs/GaAs and InGaAsN/GaAs SQW samples, respectively.[55] The N-free single quantum well shows flat interfaces and good homogeneity. The incorporation of 2.8% nitrogen induces well width fluctuations from 6 nm to 12 nm. Moreover, the (400) dark field image, shown in figure 1.6 (c), reveals local strain fluctuations that can be attributed to variations in composition. This means that the presence of nitrogen strongly influences the homogeneity of the structure. Structural investigations of InGaAsN /GaAs multi quantum wells have been performed also on MOVPE samples. Transmission electron microscopy analysis in combination with energy filtering have shown that changing the growth parameters of the group V precursors, can result in a structural deterioration in the quantum wells. A roughening transition from planar to an island growth is observed, resulting in an inhomogeneous indium distribution in the [001] direction as well as in a pronounced thickness modulation across the wells.[59] Combining cross-sectional TEM results with photoluminescence measurements, Xin et al.[56] have interpreted the strong lateral variation in strain in $In_{0.30}Ga_{0.70}As_{0.98}N_{0.02}$/GaAs multi quantum wells as composition fluctuations (In- and N-rich regions). In particular, they have shown a quantum dot-like behaviour for these structures due to the non-uniformity of indium and nitrogen concentration in the QWs.

This variation of the morphology has been considered the origin of localized states in dilute nitrides.[60,61] Well width and / or compositional fluctuations affect the carriers collected by the well. The carriers in fact, locate in regions where the well width and / or the [In] and [N] are maximum.

As mentioned before, the low equilibrium solubility of N in (In)GaAs gives to the growth conditions of dilute nitrides a fundamental role. The growth temperature, for example, has been found to be a crucial parameter during the growth of dilute nitrides. In fact, in order to incorporate nitrogen atoms in percentage range, it is necessary to lower the temperature by about 100 °C compared to the usual growth temperature for the N-free parent-compounds. Moreover optical properties, such as the PL intensity and the peak emission energy, are strongly affected by the growth temperature. Nevertheless, the origin of this strong influence remains still obscure and works addressed to give more details about the relations between growth conditions and sample properties are very few.

Pinault and Tournié[58] have studied the influence of the growth rate (R_{gr}) and growth temperature (T_{gr}) on the growth mode and structural properties of GaAs$_{0.972}$N$_{0.028}$ SQWs grown by molecular beam epitaxy (MBE). Based on RHEED observations during the growth of these GaAsN SQWs, the authors of Ref. 58 have created a surface phase diagram. This is shown in figure 1.7.
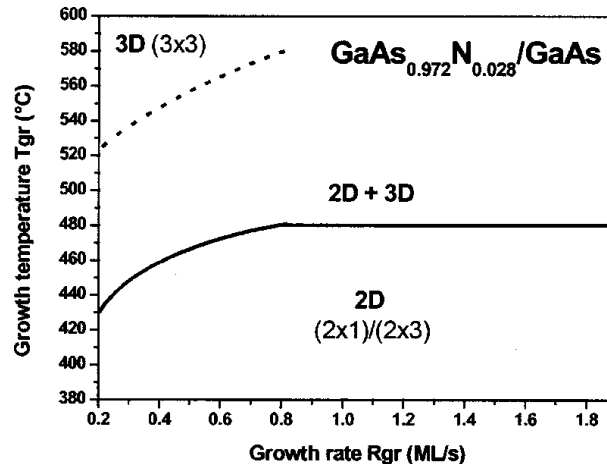
Figure 1.7.: Surface phase diagram deduced from RHEED observation during MBE growth of GaAs$_{0.972}$N$_{0.028}$/GaAs SQWs. (From Ref. 58)

The sets of R_{gr} and T_{gr} conditions located below the solid line result in smooth two-dimensional (2D) growth. For the conditions above the solid line, the growth is initiated in 2D mode but turns progressively to three-dimensional (3D) mode. For a given R_{gr}, the RHEED pattern degrades faster and more severely at higher temperatures. At low growth rates and high temperatures the surface results in 3D growth mode.

As mentioned above, although surface phenomena come into play during epitaxial growth and help to stabilize the N content in percentage range,[62] GaAsN alloys remain fundamentally metastable. Single phase alloys can then be obtained only by imposing kinetic restrictions on the system, i.e. lowering the growth temperature[63] and / or increasing the growth rate[64]. Figure 1.7 show that if one wants to increase growth temperature it becomes necessary to increase R_{gr} to preserve a 2D growth mode. Correspondingly, if one wants to decrease the growth rate it becomes necessary to decrease T_{gr} to preserve the 2D growth mode. The 2D+3D growth mode transition is related to the potential fluctuations of the metastable GaAsN alloy.

Several groups have studied the problem of the spinodal decomposition. [65, 66] In particular, Asomoza et al.[66] have presented a description of spinodal decomposition range of the $In_xGa_{1-x}As_{1-y}N_y$ alloys with the interaction parameters estimated by valence-force field model. This range is defined as the region where the phase separation fluctuations decrease the internal energy of the alloy. They found that the temperature at which the spinodal decomposition starts to appear depends on nitrogen and indium content. In particular, the spinodal decomposition temperature strongly increases with increasing N content. Furthermore, for a fixed nitrogen concentration value, this temperature decreases with increasing the lattice mismatch to GaAs.

1.2.1 Annealing effects on the structure of dilute nitrides

It has been found that a thermal treatment not only strongly modifies the optical properties of (In)GaAsN systems (this will be discussed in more detail in the next section) but modifies also the morphology of the structures. Different groups tried to find a correlation between the optical and morphological modifications after annealing.[60,67,68,69] However a clear and unambiguous picture is still lacking.

The main structural effects of annealing can be found in a general homogenisation of the system[*] and / or a reorganisation of the atoms configuration.

In an interesting work, Klar et al.[67] have shown that the band gap structure of $In_xGa_{1-x}As_{1-y}N_y$ for $y \approx 1$ to 3% is strongly dependent on the dominating nearest-neighbours environment of N. They have shown that annealing modifies the atomic configuration around the nitrogen atoms. In particular, after annealing the system passes from a Ga-rich configuration (four gallium atoms are the nearest-neighbours of the nitrogen atom) to an In-rich configuration (four indium atoms are the nearest-neighbours of the nitrogen atom). This is explained considering that, during annealing, the local strain is reduced by the formation of In-N bonds. Performing Fourier transform infrared absorption spectroscopy

---

[*] The general homogenisation has been shown mostly for samples grown by MBE.

(FTIR), contradictory results have been obtained regarding the nearest-neighbours environment of nitrogen in samples grown by different techniques. While Kurtz et al.[70] have shown that annealing change the structure of MOCVD InGaAsN samples confirming the results of Ref. 67, Alt et al.[71] have shown that in InGaAsN MQW structures gown by MBE, nitrogen is surrounded only by nearest-neighbours gallium atoms and that after annealing this configuration is not modified.

In order to investigate morphological modifications in terms of well width and / or composition fluctuations, TEM analysis have been employed.
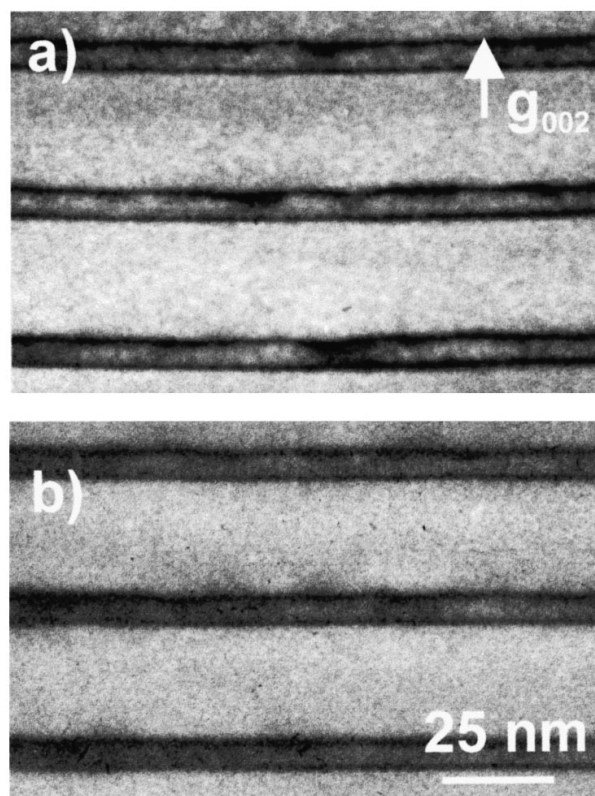
Figure 1.8.: Dark-field image using the (002) reflection of $In_{0.36}Ga_{0.64}As_{0.981}N_{0.019}$ MQW sample before (a) and after annealing (b). (From Ref. 68)

Figure 1.8 shows a comparison between (002) dark-field images of an $In_{0.36}Ga_{0.64}As_{0.981}N_{0.019}$ MQW sample before and after annealing. The quantum wells can be seen as dark stripes between even darker horizontal lines. The as-grown samples exhibit pronounced lateral fluctuations of the dark-field intensity along the quantum well, whereas the annealed sample does not. Based on a quantitative structural analysis, the authors of Ref. 68 have found that the observed dark-field fluctuations are due to

compositional fluctuations. In particular, the compositional analysis has shown that after annealing there is a diffusion of nitrogen out of the well and dissolution of In-rich inclusions present in the as-grown QW structures. On the other hand, other authors[69] believe that after annealing there is a diffusion of nitrogen inside the well rather than out of the well. However all agree that thermal annealing tends to homogenise the structure of the QW layers decreasing the depth of the potential fluctuations.

1.3 On the radiative and non-radiative recombination processes in dilute nitrides

Among the main motivations for the rapidly expanding fundamental and applied research in dilute nitride alloys is a wide range of optoelectronic applications both for efficient light emitting devices operating within the near infrared region[6,7,10] and for many other electronic devices.[11,12,13,14] For this reason many groups have investigated the optical properties of dilute nitride systems, and a number of phenomena that are characteristic for these materials has been observed many times. These findings are exemplified in this subsection by measurements that are made during this PhD work.

From numerous optical experiments it is concluded that the radiative efficiency of the (In)GaAsN alloy rapidly degrades with incorporation of nitrogen.[2,52,72] A drastic decrease in the PL intensity is typically observed with increasing nitrogen concentration. Considering for example an $In_{0.34}Ga_{0.66}As_{1-y}N_y$ SQW sample, with increasing the nitrogen concentration from [N] = 0.34% to [N] = 2.43%, the photoluminescence intensity decreases by about 30 times, as shown in figure 1.9.
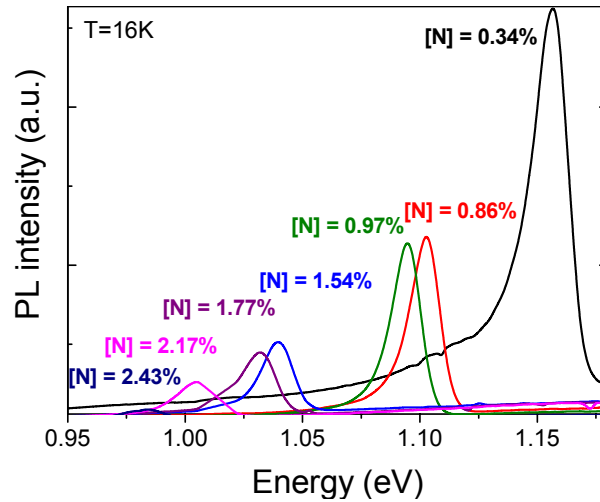
Figure 1.9.: Evolution of the PL peak emission energy taken at 16 K with varying nitrogen content for an $In_{0.34}Ga_{0.66}As_{1-y}N_y$ / GaAs SQW sample.

The observed degradation of the alloy optical quality is commonly attributed to non-radiative centres which are associated to the presence of nitrogen in the system, such as nitrogen interstitials.[73] Moreover, as described in §1.2, the insertion of N into (In)GaAs QW structures induces morphological modifications to the system. It has been shown that a variation of the well width and / or an inhomogeneous distribution of In and N in the system yields potential fluctuations. These fluctuations trap carriers in localized states and strongly influence the optical properties of dilute nitrides.[55,60] In the following, comparing N-free and N-containing structures, the main effects of the presence of nitrogen in terms of carrier localization and optical emission efficiency will be discussed.

1.3.1 Low energy tail of the photoluminescence spectrum
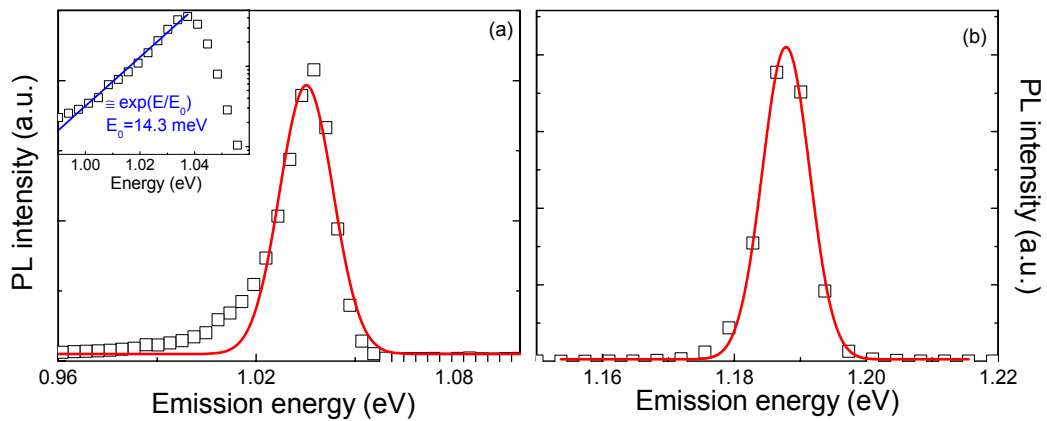
Figure 1.10.: (a) PL emission spectrum taken at 20 K of an $In_{0.30}Ga_{0.70}As_{0.984}N_{0.016}$ / GaAs SQW sample (open squares) and gaussian fit (solid line). In the inset, part of the PL spectrum (open squares) and a fit of the low-energy tail (solid line) are plotted in semi-logarithmic scale. (b) PL emission spectrum taken at 20 K of an $In_{0.37}Ga_{0.63}As$ / GaAs SQW sample (open squares) and theoretical fit (solid line).

In figure 1.10, the PL spectra taken at 20 K of $In_{0.30}Ga_{0.70}As_{0.984}N_{0.016}$ (a) and $In_{0.37}Ga_{0.63}As$ (b) SQW samples are compared. The experimental data (open squares in the figures) clearly show that the presence of nitrogen leads to an asymmetric lineshape of the spectrum. In fact, while the data of the InGaAs sample are well fitted by a gaussian function (solid line), this is not the case for the InGaAsN data for which an "additional tail" for energies up to 1.02 eV is present. The reason for the asymmetric lineshape can be simply understood by looking at the picture in figure 1.11. In the figure, the potential landscape of the conduction band (on the left) and the PL spectrum in semi-logarithmic scale (on the right) is schematically shown.
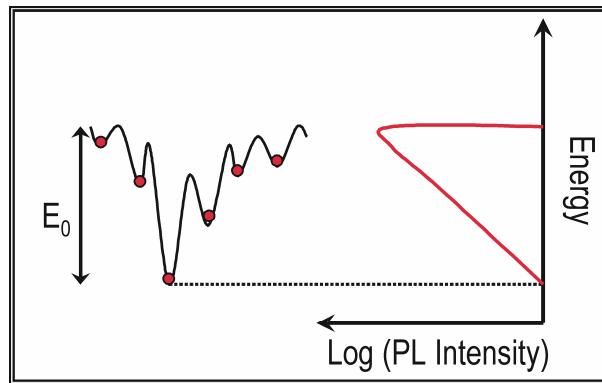
Figure 1.11.: Schematic explanation of the origin of the asymmetric lineshape of the PL spectrum. Potential fluctuations on the conduction band states (on the left) and their effect on the PL lineshape (on the right).

The presence of random fluctuations in alloy composition in these materials causes a smearing of the band edges and formation of tails in the density of states extending into the band gap. At low temperatures, photo-generated carriers can be trapped by these localized states at the band tails and recombine from them. The typical spectral shape of such emissions is very asymmetric, where the low energy tail reflects the energy distribution of the density of states within the band tail, while the sharp high energy cut-off corresponds to the distribution at the band edge. In this way it is possible to introduce a localization energy value E_0 which represents the degree of the potential fluctuations. The deeper the potential fluctuations, the stronger the asymmetric lineshape, the bigger will be the value of E_0.

The probability to find carriers in potential minima close to the band edge is higher than to find them in minima far from the band edge. It has been reported by many groups[22,74,75] that the density of states caused by potential fluctuations is described by an exponential function. For this reason, the slope of the PL low-energy tail in a semi-logarithmic scale can be used for a rough estimate of the localization energy.[74] In the inset of figure 1.10 (a), the low-energy region has been fitted employing the exponential function $f(E) \approx \exp(E/E_0)$, where E_0 is the characteristic localization energy. The fit confirms the exponential behaviour and gives a localization energy value for this sample of about $E_0 = 14.3$ meV.

1.3.2 Temperature dependence of the PL peak energy and PL linewidth

The temperature behaviour of the PL peak emission energy and of the PL linewidth also provides evidence of carrier localization.[55,60,76,77] In figure 1.12 the evolution of the PL peak energy with temperature is shown for an $In_{0.30}Ga_{0.70}As_{0.984}N_{0.016}$ SQW sample. The spectra show that, with increasing temperature, the PL peak energy at first shifts to lower energies, then moves to higher energies and finally for T > 70 K shifts to lower energies again. This red-blue-red shift behaviour describes an "S" shape and is marked in the figure by a dashed line.
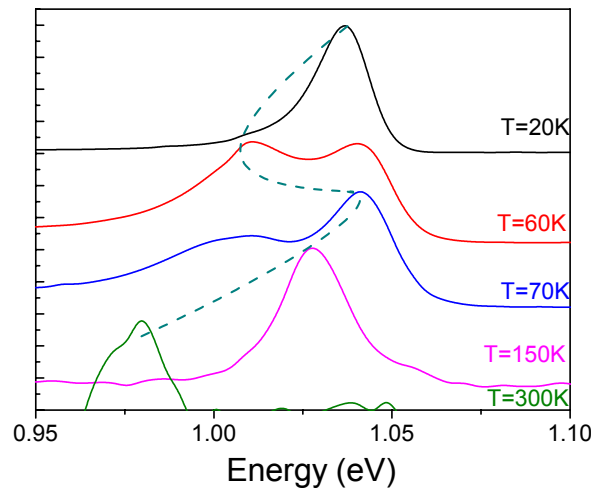
Figure 1.12.: Temperature dependence of the PL emission spectrum of an $In_{0.30}Ga_{0.70}As_{0.984}N_{0.016}$ / GaAs SQW sample. The dashed line follows the evolution of the PL maximum with increasing temperature: red-blue-red shift (S-shape).

This particular temperature-induced emission shift is attributed to the band-tail states in the density of states (DOS). In order to describe this phenomenon, the energy values of the PL peak emission of the $In_{0.30}Ga_{0.70}As_{0.984}N_{0.016}$ SQW sample are plotted as a function of the measured temperature and are compared with the same energy quantities of an $In_{0.37}Ga_{0.63}As$ SQW in figure 1.13 (a). The red-blue-red shift, that is completely absent for the N-free sample (open triangles), characterises the InGaAsN structure (open squares). In this figure is also shown a schematic picture of the variation of the position of the carriers in the potential landscape of the conduction band at three characteristic temperatures. As described in 1.3.1, dilute nitrides are characterized by potential fluctuations which trap carriers at the

band tails. At very low temperatures, the carriers are localized in potential minima close to the conduction band edge. With increasing temperatures, the probability to find carriers in lower potential minima increases. The carriers in fact gain sufficient thermal energy to overcome the small potential barriers and become trapped in adjacent lower levels of the DOS from where the recombination takes place. This corresponds to the first red shift (up to 60 K). At 60 K, the carriers have enough thermal energy to overcome all the potential fluctuation barriers and to reach the lowest energy possible level (the deepest potential fluctuation). The following blue shift (about 30 meV for this sample) is a result of the thermal population of higher energy states of the DOS. Here, a transition from the localized states in the quantum well takes place. At even higher temperatures (T > 100 K) the temperature-shift of the PL emission is mainly determined by the behaviour of the band gap and can be described by the Varshni equation[78] (solid line in the figure). As said above, the InGaAs sample (open triangles) does not show the S-shape and the PL emission energy position decreases monotonously with increasing temperature. The Varshni equation (solid line) fits the data for all the measured temperatures very well.
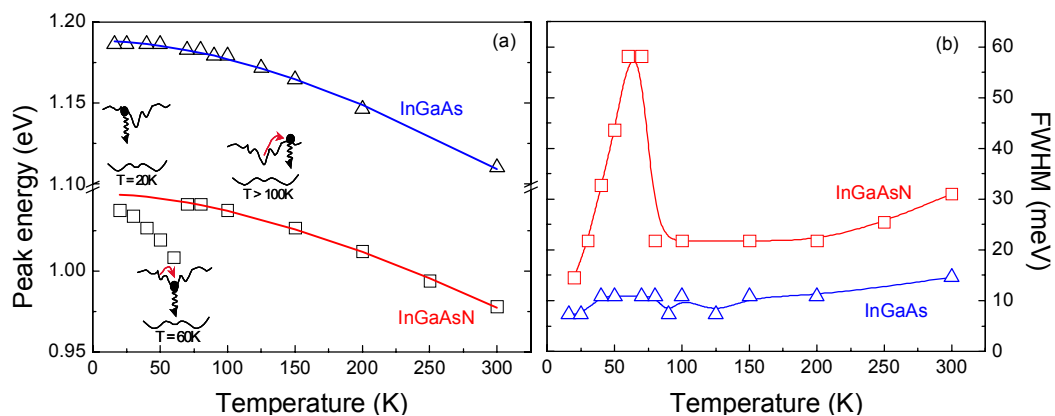
Figure 1.13.: (a) Temperature dependence of the PL emission energy of an $In_{0.30}Ga_{0.70}As_{0.984}N_{0.016}$ / GaAs SQW sample (open squares) and of an $In_{0.37}Ga_{0.63}As$ / GaAs SQW sample (open triangles). The solid lines represent the behaviour employing the Varshni model. (b) Temperature dependence of the FWHM of an $In_{0.30}Ga_{0.70}As_{0.984}N_{0.016}$ / GaAs SQW sample (open squares) and of an $In_{0.37}Ga_{0.63}As$ / GaAs SQW sample (open triangles). The solid lines in plot b are guidelines to the eye.

Considering the InGaAsN sample, the energy difference between the empirical Varshni behaviour and the experimental data at low temperatures can give an estimation of the localization degree in the

sample. The maximum value of localization energy is about 35 meV at 60 K. At 20 K the energy difference is about 10 meV and is consistent with the value found in section 1.3.1.

Most notably, at temperatures 60 – 70 K, the PL spectra clearly show the presence of two peaks (figure 1.12). In this range of temperatures, the carriers start to reach the delocalized region but they are not yet fully delocalized. For this reason the simultaneous emission from localized and non-localized states is present in the PL spectra.

The presence of localized states is also reflected in the peculiar behaviour of the full width at half maximum (FWHM) of the PL emission peak with varying temperature.[60] The comparison between the T-dependence of the FWHM of the InGaAs and the InGaAsN structure [figure 1.13 (b)] shows that while in the case of the N-free sample the PL linewidth increases monotonously with temperature, the presence of localized states induces a maximum in the value of the FWHM corresponding to the temperature at which the localization is strongest. This odd evolution can be explained as follows. When increasing the temperature above 20 K, the less localized carriers become mobile and sample an average of the potential fluctuations while the more localized carriers remain trapped. This leads to an increase of the linewidth. When approaching the full-delocalization temperature (60 K < T < 100 K), even the most localized carriers become progressively mobile. The carrier distribution narrows or stabilises, as does the linewidth. With a further increase in the temperature, thermal broadening of the carrier distribution occurs and the linewidth increases accordingly.

1.3.3 Power dependence of the PL peak emission

It is well known that with increasing excitation power, the PL spectra of structures containing localized states under the energy of the band gap show a blue shift.[79] This is also the case for dilute nitride samples.[77, 80] In figure 1.14 are compared the PL spectra taken at 50 K of an $In_{0.30}Ga_{0.70}As_{0.984}N_{0.016}$ SQW sample employing an excitation power density of P (solid line) and 45 P (dashed line), where P is about 100 W / cm^2.
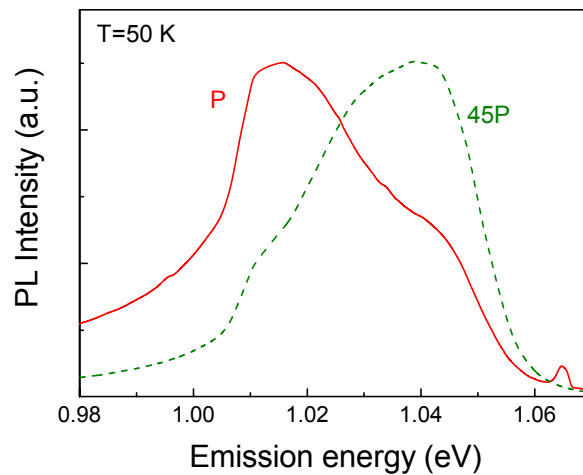
Figure 1.14.: PL spectra taken at 50 K of an $In_{0.30}Ga_{0.70}As_{0.984}N_{0.016}$ / GaAs SQW sample excited with a power density P (solid line) and 45 P (dashed line), where P ≈ 100 W / cm². The two spectra are normalized to the PL maximum.

When the excitation power density P is increased by about 45 times, the PL peak moves from a value of 1.013 eV to a value of 1.039 eV, yielding a blue shift of 26 meV. This phenomenon is explained considering that by raising P the number of photo-generated carriers increases. Consequently, the lower-energy localized states are progressively saturated. In order to make this point clearer, in figure 1.15 are plotted the evolution with temperature of the PL peak emission energy (plot a) and of the FWHM (plot b), restricted to the localized region considering the two different power densities.
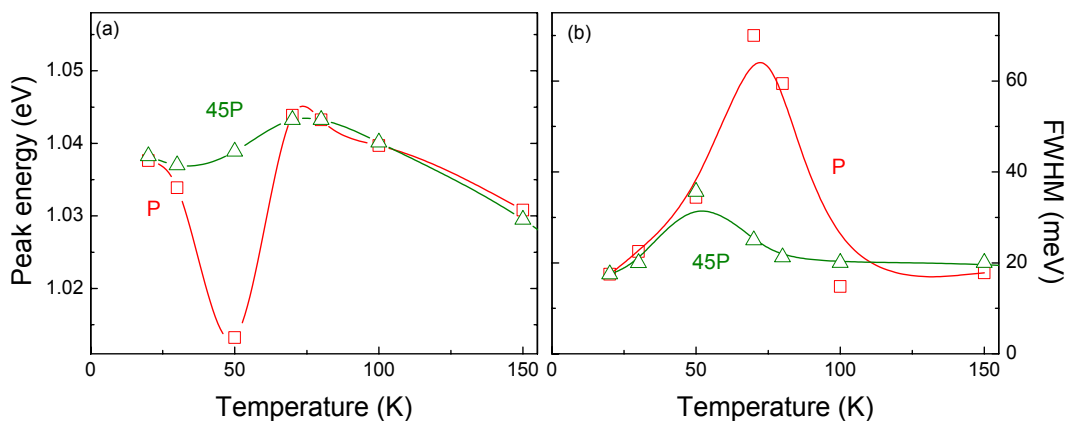
Figure 1.15.: (a) PL peak position with varying temperature of an $In_{0.30}Ga_{0.70}As_{0.984}N_{0.016}$ / GaAs SQW sample excited with a power density P (open squares) and 45 P (open triangles). (b) FWHM with varying temperature of the same sample excited with a power density P (open squares) and 45 P (open triangles). P is about 100 W / cm². The solid lines are guidelines to the eye.

As also noticed in figure 1.14, the increase of the value of P moves the PL peak emission to higher energies. Looking at figure 1.15 (a), it is clear that the blue shift involves only the localized states, which

are filled by the excess of photo-generated carriers. For T > 70 K the different power density does not produce any effect. The PL linewidth values are affected by the change in the power density as well. This is shown in plot (b). Employing a power density P, the FWHM shows a maximum value at about 60 K. The reason of that is the presence of localized states as explained in § 1.3.2. With increasing the excitation power density (45 P), the maximum value of the FWHM decreases confirming the saturation of the low-energy localized states.

1.3.4 PL decay time

Localization effects in dilute nitrides can also be analysed with the help of photoluminescence transient data.[22,81] In figure 1.16 (a) the PL spectrum (solid line) and the spectral dependence of the PL decay time (open spheres) taken at 2 K of an $In_{0.37}Ga_{0.63}As_{0.983}N_{0.017}$ SQW sample are shown. With increasing energy the decay time strongly decreases. This is clear looking at plot (b) in which the decay curves taken at two different photon energies are compared. Passing from 0.990 eV, below the energy of the PL peak, to 1.025 eV, above the energy of the PL peak, the decay time decreases by one order of magnitude (from about 2 ns to about 200 ps). This is because the decay is predominantly radiative for the strongly localized excitons (i.e., the lowest PL energies) and is shortened at the high energy side of the localized exciton spectra due to transfer of the excitons from the localized into the delocalized states. Thus the exciton activation into the delocalized states can be monitored by the shortening of the PL decay at a given PL energy.[81,82]
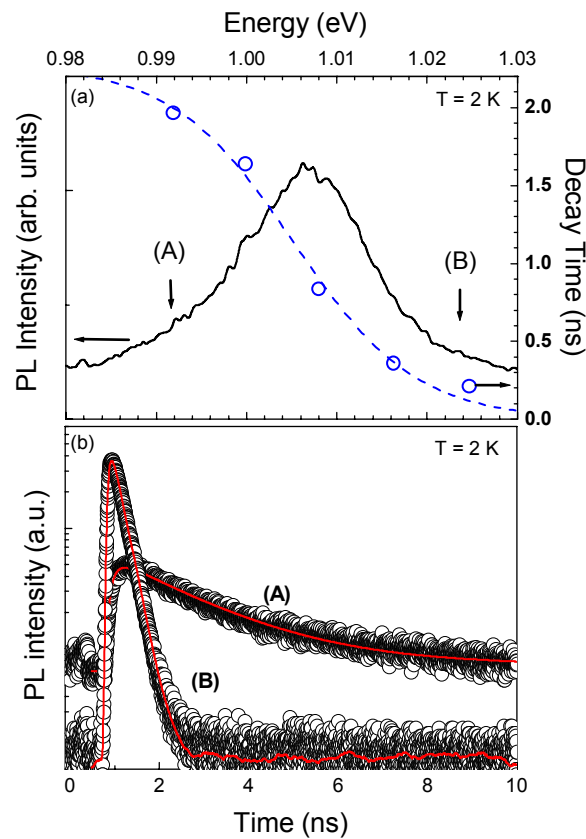
Figure 1.16.: (a) PL spectrum and PL decay time taken at 2 K of an $In_{0.37}Ga_{0.63}As_{0.983}N_{0.017}$ / GaAs SQW sample (solid line and open spheres, respectively). The dashed line is a guideline to the eye. (b) PL decay curves measured at 0.99 eV (A) and 1.025 eV (B).

1.3.5. Annealing effects

As described in section 1.2 thermal annealing influences the morphology of dilute nitride QW structures. On the basis of high resolution TEM images, a general homogenisation of the QW layers has been found.[68] Accordingly, the potential fluctuations, responsible for localized states, are decreased. The reduction of the localization degree has evident consequences on the symmetry of the PL spectra, on the evolution with temperature of the peak energy position and on the variation of the peak emission energy with the excitation power density.

In addition, annealing remarkably affects the PL efficiency of the QWs. A thermal treatment, such as oven annealing or rapid thermal annealing, generally improves the PL intensity.[61,69] This is the main motivation for this treatment and for research aimed at elucidating the accompanying phenomena. However, the exact mechanism of such an improvement has not been determined in the majority of the

studies. The effect has naturally been attributed to the elimination of some grown-in competing non-radiative channels.[73] So far, only limited information is available regarding the nature of these competing non-radiative defects / impurities.

An additional intriguing effect of annealing is the blue shift of the PL emission peak. Different explanations have been proposed in literature. One of these takes into account the compositional modification of the quantum well. Regarding this solution however, contradictory results have been found. While some groups[69] have shown nitrogen diffusion inside the QW after annealing, other groups[68,83] have found an out-diffusion of N from the QW.[*] A further explanation of the blue shift has been proposed by Klar et al.[67] according to which there is a rearrangement of the nearest-neighbours' environment of nitrogen. The authors of Ref. 67 have shown that for the same QW composition, different discrete band gaps can occur by ranging the nitrogen environment from 4 Ga nearest-neighbours to 4 In nearest-neighbours.
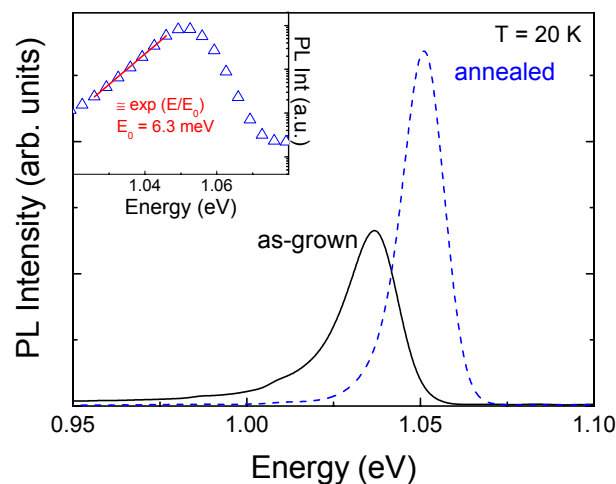
Figure 1 17.: PL spectrum taken at 20 K of an $In_{0.30}Ga_{0.70}As_{0.984}N_{0.016}$ / GaAs SQW sample as-grown (solid line) and annealed (dashed line). In the inset, detail of the PL spectrum of the annealed sample plotted in semi-logarithmic scale (open triangles) and fit of the low-energy tail (solid line).

In figure 1.17 are compared the PL spectra taken at 20 K of an $In_{0.30}Ga_{0.70}As_{0.984}N_{0.016}$ / GaAs SQW sample before (solid line) and after annealing (dashed line). Annealing induces an evident improvement

---

[*] A possible explanation of the out-diffusion of nitrogen can be the decrease, after annealing, of nitrogen interstitial defects, which can be created during the MBE growth.

___

of the PL intensity, a blue shift of the peak position, and a reduction of the PL linewidth. Most notably, the photoluminescence spectrum becomes more symmetric, as the characteristic low-energy tail is reduced. In the inset is plotted the PL spectrum of the annealed sample in semi-logarithmic scale. Employing the same approach used in section 1.3.1, the localization energy has been estimated. The exponential fit (solid line in the inset) gives a value of the localization energy $E_0 = 6.3$ meV. Comparing the result obtained for the as-grown case (§ 1.3.1), the thermal treatment produced, for this particular sample, a reduction of the localization energy at very low temperature of about 55 %.
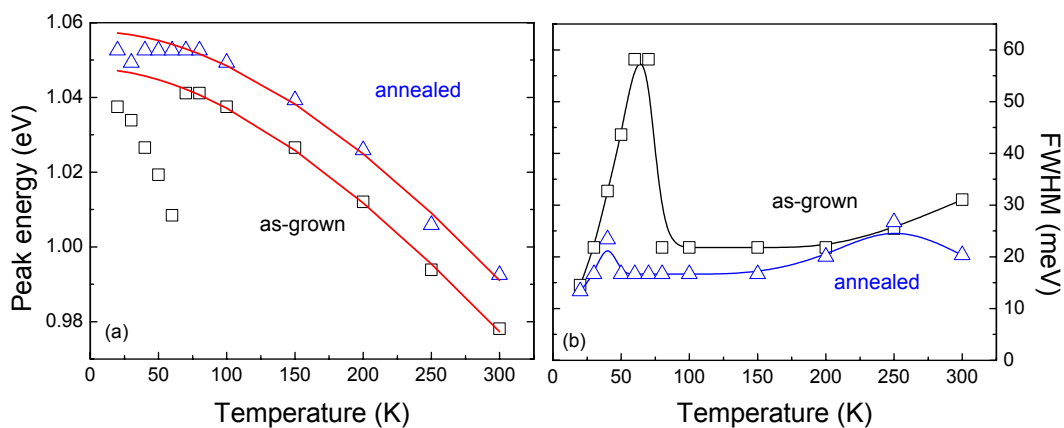
Figure 1.18.: (a) Temperature dependence of the PL emission energy of an $In_{0.30}Ga_{0.70}As_{0.984}N_{0.016}$ / GaAs SQW sample as-grown (open squares) and annealed (open triangles). The solid lines represent the behaviour employing the Varshni model. (b) Temperature dependence of the FWHM of an $In_{0.30}Ga_{0.70}As_{0.984}N_{0.016}$ / GaAs SQW sample as-grown (open squares) and annealed (open triangles). The solid lines in plot b are guidelines to the eye.

In figure 1.18 (a) is shown the value of the PL peak emission energy as a function of the measured temperature for an as-grown $In_{0.30}Ga_{0.70}As_{0.984}N_{0.016}$ / GaAs SQW sample (open squares). This behaviour is compared with the T-dependence of the PL peak energy for the same sample but after a thermal treatment (open triangles). From the experimental data it is possible to notice that after annealing the S-curve is modified and the localization degree is reduced. Considering the fit employing the Varshni equation (solid line in the figure), the effects of annealing can be determined by the deviation from the experimental data. In this situation in fact, the energy difference between the experimental points and the empirical expression leads to a maximum value of the localization energy $E_0 = 4.4$ meV at 20 K, that is consistent with the estimation found above.

After the annealing process, also the PL linewidth is modified. Comparing the as-grown and the annealed case [open squares and triangles in figure 1.18 (b), respectively], one can see that the maximum value of the FWHM is extremely reduced after the thermal treatment. In this particular case, it becomes less than the half.
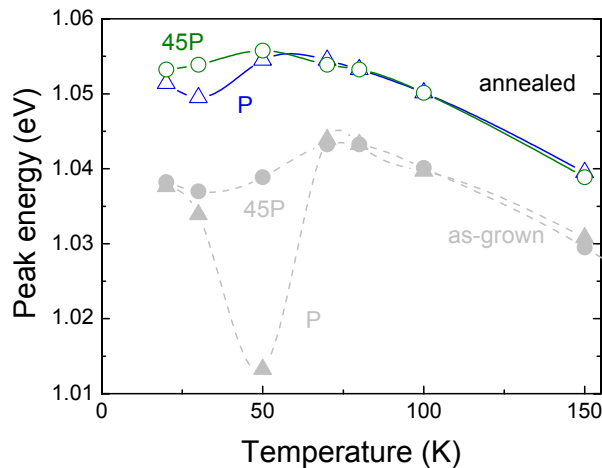
Figure 1.19.: PL peak position with varying the temperature of an annealed $In_{0.30}Ga_{0.70}As_{0.984}N_{0.016}$ / GaAs SQW sample excited with a power density P (open squares) and 45 P (open triangles). P is about 100 W / cm^2. With dashed lines, the results for the as-grown sample.

Figure 1.19 shows the evolution with temperature of the PL peak emission energy of an annealed $In_{0.30}Ga_{0.70}As_{0.984}N_{0.016}$ / GaAs SQW sample for two different excitation power densities, P and 45 P where P $\approx$ 100 W / cm^2. Comparing these results with those of the as-grown sample (dashed lines in the figure), it is possible to notice a difference in the blue shift due to raising P. While for the as-grown case the maximum energy variation is about 25.6 meV, for the annealing case it is only 4.4 meV. This is another confirmation that after annealing the potential fluctuations, and then the localized states, are strongly reduced. In addition, figure 1.19 shows that in the annealed case, the localized states are almost totally filled up employing an excitation power density of 45 P. In fact, the peak emission energy decreases nearly monotonously with the temperature (open spheres in figure). On the other hand, in the as-grown case, the number of photo-generated carriers produced by a power density of 45 P is not enough in order to completely fill up the localized states. The dashed line with closed spheres in fact shows still a strong localization degree.

1.3 Conclusions of the first chapter

In this chapter, an overview of the fundamental properties of dilute nitrides has been presented. It has been shown that (In)GaAsN materials behave in a different way as compared to the conventional III-V semiconductors. The insertion of small quantities of nitrogen in (In)GaAs induces a strong red shift in the band gap and an increase of the value of the effective mass although the standard theory of III-V compounds predicted a completely opposite behaviour. For this reason, in order to theoretically describe the properties of these materials in a satisfactory way, new methods, far from the conventional ones, have been developed. Due to its simple application and due to the good results obtained to describe the characteristics of dilute nitrides, the band anti-crossing model has become very popular. This model assumes that the incorporation of isolated nitrogen atoms into (In)GaAs leads to a strong interaction between the conduction band and the narrow resonant band formed by the nitrogen states. With the band anti-crossing model it has been possible to explain, besides the behaviour of the band gap and of the effective mass, also the presence of an additional conduction band level denoted E_+, above the conduction band minimum.

Although an explanation of the main peculiarities of dilute nitrides can be found in the theoretical models developed in the last few years, a quantitative knowledge of fundamental parameters, such as a complete description of the band gap with varying the alloy composition or the exact value of the electron effective mass is still missing. In particular, the value of the band offsets of InGaAsN heterostructures has been shown so far only as the result of indirect measurements. Direct measurements of these quantities, which are very important for the realisation of optoelectronic devices, are very few if not absent in literature. In chapter 4 of this thesis, important questions about the influence of nitrogen on the band offsets of InGaAsN / GaAs quantum wells (QWs) will be finally answered.

Due to their wide range of possible device applications, dilute nitrides have attracted the interest of the optoelectronic world. For this reason, the morphological and optical properties have been investigated by several groups. The effect of the insertion of nitrogen in (In)GaAsN QWs has been studied employing different investigation techniques. Using transmission electron microscopy images for example, it has been shown that the presence of nitrogen causes inhomogeneity of the system leading, in some cases, to three-dimensional structures. However, the exact origin of this non-uniformity is still unclear. Different groups have reported variation of the quantum well width, modification of nitrogen and / or indium composition, or a combination of both. Furthermore, it has been shown that the dominating nearest-neighbours environment of nitrogen strongly influences the band gap of InGaAsN materials.

This morphological non-uniformity produces potential fluctuations in the system which have repercussions on the optical properties of the (In)GaAsN structures. The carriers in dilute nitrides are in fact strongly localized at low temperatures. The asymmetry of the photoluminescence spectra, the peculiar behaviour of the peak emission energy and of the linewidth with varying measuring temperature, the decrease of the photoluminescence decay with increasing photon energy, and the blue shift of the peak emission energy with increasing the excitation power density, for example, are phenomena which can offer an estimate of the localization degree in dilute nitrides.

In addition to that, the presence of nitrogen strongly reduces the photoluminescence efficiency of (In)GaAsN quantum well structures, suggesting the presence of defects or impurities related to the presence of nitrogen atoms.

It has been shown that annealing reduces such defects improving the quantum wells photoluminescence efficiency remarkably. Moreover, after annealing a substantial homogenisation of the structure has been verified with a consequent reduction of the potential fluctuations and of the degree of localization.

Although several groups have dedicated their efforts to understand the influence of nitrogen on the morphological and optical properties of dilute nitrides, a clear picture about the origin of the modifications of the morphology and of the photoluminescence efficiency after annealing and a possible

correlation between them is still lacking. These problems will be intensively discussed in chapter 3 of this thesis. Approaches of investigation which are new in literature will be proposed to shade on light on the understanding of the influence of annealing on the morphological and optical properties of dilute nitrides.

Chapter 2

Experimental Techniques

In the following chapter the main experimental techniques employed to grow and characterise the samples shown in this work will be presented. Section 2.1 is dedicated to illustrate the growth method and the general structure of the samples. Section 2.2 describes the annealing system and the employed thermal profile. Finally, in section 2.3 the two optical techniques mostly used in this work (photoluminescence spectroscopy and surface photo voltage spectroscopy) are presented along with the corresponding experimental set-ups. Additional characterization techniques are illustrated at the end of the chapter. Unless otherwise explicitly mentioned, all the experimental measurements were performed at Infineon Technologies.

2.1 Growth

The growth of optoelectronic devices based on InGaAsN material has been a new challenge for the epitaxy research field due to divergent properties of arsenides and nitrides. Indeed, $GaAs_{1-y}N_y$ is an alloy composed of group V elements with large differences in ionic radii (0.75 Å for As as compared with 1.2 Å for N) as well as in the electro-negativity values ($\approx$ 2 for As as compared with $\approx$ 3 for N, in Pauling´s scale). Also, the crystal structure of the binary parent compounds of this alloy is the zinc-blende structure for GaAs and the zinc-blende or wurtzite structure for GaN. These characteristics are the origin of a miscibility gap with phase separation.[65,66] Furthermore, the equilibrium solubility of N in GaAs is known to be extremely low ([N] < 10^{14} cm^{-3} at T = 650 °C).[62] By growing high nitrogen InGaAsN

multi quantum wells, phase separation and segregation processes of the elements contained in the wells have been observed. In particular, a phase-diagram has been built. In this diagram it is shown that the nitrogen concentration, at which the phase separation starts to appear, increases with decreasing the indium concentration.[84] This new epitaxy challenge requires for a suitable growth technique to choose an appropriate N-based growth precursor and to optimise specific growth conditions of N-containing alloys. Due to the nitrogen solubility limitations, growth techniques far from the thermodinamical equilibrium such as solid or gaseous molecular beam epitaxy (SSMBE, GSMBE), chemical beam epitaxy (CBE) or metal-organic vapour phase epitaxy (MOVPE) have been employed.[85] So far, several improvements in N-containing material quality as well as in laser performances have been obtained both by MBE[6,7] and MOVPE.[10]

2.1.1 MBE at Infineon: sample structure

Molecular beam epitaxy (MBE) is a common method used to grow III-V compound semiconductors as well as several other materials and structures. Indeed, MBE can produce high-quality layers with very abrupt interfaces and good control of thickness, doping and composition. Because of the high degree of control possible with MBE, it is a valuable tool in the development of sophisticated electronic and optoelectronic devices. [85]

Essentially, MBE consists in "irradiating" the substrate with molecular or atomic beams of the alloy constituents, obtained by heating very pure chemical elements in special containers, called effusion cells. The substrate is heated (at a temperature called growth temperature) and rotated. To obtain high-purity layers it is critical that the material sources be extremely pure and that the entire process be done in an ultra-high vacuum (UHV) environment. Each effusion cell is independently heated until the desired material flux is achieved. Typically growth rates are on the order of few Å / sec and the shutters in front of the various sources can be opened and closed on the time scale of less than a monolayer growth,

allowing for nearly atomically abrupt transitions from one material to another. The sample holder continuously rotates for an improved uniformity of the epitaxial layer thickness.

In its standard state, nitrogen is an extremely stable molecule (N_2). Injecting N_2 into the MBE chamber would only lead to a very small amount of interstitially incorporated N_2. In order to incorporate nitrogen into the lattice, one must create a more reactive form. The most successful method of obtaining reactive atomic nitrogen has been the use of a radio-frequency plasma source. Dissociated atomic and molecular radicals and ions are generated in the plasma and escape from a front aperture plate towards the substrate, depositing in substantial concentrations.

It is important to note that MBE growth takes place in conditions far away from thermodynamic equilibrium and is rather dominated by kinetic effects. Molecular or atomic elements coming from the cells and hitting the growing surface undergo diffusion and find a place in the crystal lattice. Atoms which are not incorporated into the lattice (due to desorption) are finally caught by the cryo-shield around the growth chamber. The growth process depends on the growth temperature, the fluxes of each element, and on the previous growth history by means of the surface morphology.

All the samples employed in this thesis work have been grown by MBE at Infineon Technologies. The general structure of a typical InGaAsN/GaAs SQW sample employed in this thesis is illustrated in figure 2.1. The relative dimensions of the layers are only indicative. Typically, on a semi-insulating GaAs (001) substrate are grown 3000 Å of undoped GaAs. After that, the growth is basically symmetric: a 65 Å-InGaAsN SQW is grown between two 2000 Å-GaAs-layers and two 6-double-layers-AlAs/GaAs (super lattice) with a periodicity of 50 Å. Finally, on top of the structure, 100 Å GaAs are grown. In the figure the temperature profile of the substrate during growth is also shown. Before starting the growth process, the surface of the substrate, which is oxidized, must be prepared. This is done by heating the substrate at 650 °C[*], during this process the As-shutter is open in order to compensate for the Arsenic desorption.

---

[*] This temperature is 60-70 °C greater than the oxide-desorption temperature value taken from the literature (582 °C). The oxide-desorption is determined with the help of reflection high energy electron diffraction (RHEED).
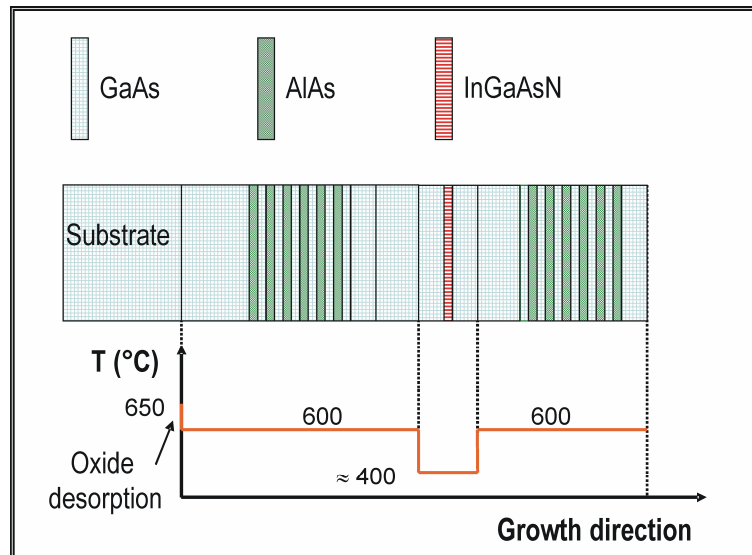
Figure 2.1.: Structure of a typical InGaAsN / GaAs SQW sample employed in this thesis work. The evolution of the temperature is also shown. For clarity reasons the dimensions of the structure are purely indicative.

The probability for an atom which reaches the growing surface to be integrated into the crystal lattice is called "sticking coefficient". For reactive nitrogen, this coefficient is about 1 at temperatures below 520 °C and decreases at temperatures over 520 °C.[86] Due to the large miscibility gap of InGaAsN, however, the optimum growth temperature for this structure is lower by 100 °C, i.e. 400-430 °C.

The AlAs/GaAs barriers prevent photo-excited carriers from non-radiative recombination in the substrate or at the surface, therefore their quality is very important. In order to avoid nitrogen incorporation in these super lattices (SL), the plasma ignition must take place after the growth of the first Al/As SL and the cell must be switched off before the second SL is grown. During the plasma operational time, in fact, a small quantity of nitrogen reaches the sample and is incorporated (around 0.3%) even if the respective shutter is closed. This leads to the formation of a parasitic GaAsN quantum well, which can be seen in photoluminescence spectra. However, the position of its PL peak is usually located close to the peak associated to the emission from the GaAs barrier and does not influence at all the emission of the InGaAsN QW.

All the experimental results shown in chapter 1 and 3 refer to samples having the structure shown in figure 2.1. Of course, QW parameters such as the width, the growth temperature, and the QW and

barrier composition are varied each time in order to investigate specific topics. The samples presented in chapter 4 have a different structure. As will be explained in section 2.3, in surface photo voltage measurements the carriers must be collected at the surface of the samples. This means that the sample must be grown without the presence of the Al/As superlattices. Also, an n^+-doped substrate is required to realise a built-in electric field used to move the carriers to the surface. In addition to that, the samples presented in § 4.2.1 have a p-doped region on top of the structure in order to increase the electric field and therefore to improve SPV intensity. In chapter 4 samples with a laser structure are also presented (§ 4.2.2 and § 4.3.2), that means that the QW is embedded in a 4000-Å-thick GaAs layer sandwiched between two 1.5-μm-thick AlGaAs layers, that are p and n doped, respectively. The SQWs of these samples are surrounded by 50-Å-thick $GaAs_{0.986}N_{0.014}$ barriers.

2.2 Annealing

As shown in § 1.2.1 and § 1.3.5, annealing strongly affects the morphological and optical properties of dilute nitride structures. Till now, different approaches have been employed: long or rapid thermal annealing in *in-situ* or *ex-situ* conditions.[60,61,67,68,69] *In-situ* means that the annealing process is performed in the growth-chamber after the growth. On the contrary, under *ex-situ* conditions the samples are annealed after removal from the growth-chamber in a different set-up.

At Infineon Technologies an oven-system is used to perform post-growth thermal treatments on the samples. The system allows the annealing of the samples in different gas environments, which are hydrogen and argon, in the specific case of this thesis. A temperature controller regulates and modifies automatically the chamber temperature on the basis of the thermal profile set in advance.
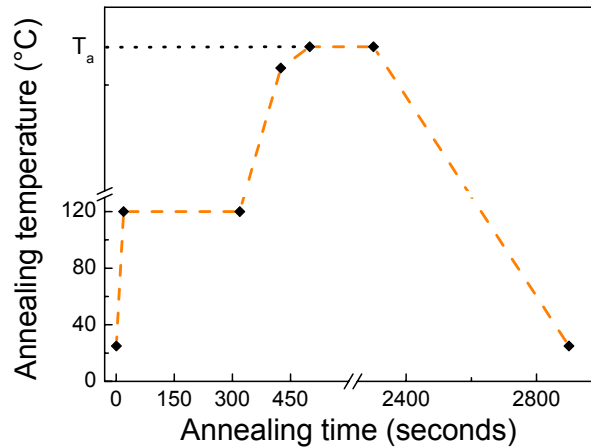
Figure 2.2.: Typical thermal profile employed to anneal the samples of this thesis work.

In figure 2.2 is plotted a typical thermal profile employed to anneal the samples studied in this thesis work. The profile can be divided into three main parts. In the first step the temperature of the sample reaches 120 °C and remains at that temperature for about 5 minutes. During this time, water is eliminated from the chamber. In the second part, the system reaches the annealing temperature T_a gradually. An abrupt thermal variation would cause a thermal instability in the system, meaning that the chamber would have a different (higher) temperature compared to T_a, at least at the beginning of the annealing process. In the last step, the system remains at the annealing temperature for a set time. The desired annealing temperature must be corrected by an offset which has been determined separately for Ar and H_2. Finally, the temperature of the chamber decreases monotonously till the ambient temperature value.

During this thesis work two different thermal profiles were employed. All the samples shown in chapter 1 and those in section 3.3.1 are annealed in hydrogen atmosphere at $T_a \approx 720$ °C and for an annealing time of 30 minutes. The samples shown in section 3.3.2 are annealed in either hydrogen or argon at $T_a \approx 680$ °C for 109 minutes. The latter thermal profile simulates that one employed during the growth of a QW laser structure. During the annealing process, the samples are covered with a face down GaAs sample in order to avoid As desorption.

2.3 Sample characterization

2.3.1 Photoluminescence spectroscopy

Photoluminescence (PL) spectroscopy is an extremely powerful technique for assessing material quality. It is quite possibly the most useful technique when developing a new (direct band gap) material system. It is non-destructive and requires no sample preparation or complex device structures. In addition, variation of different parameters, such as the temperature or the excitation power, can be used to identify several optical transitions and even explore the structural quality of the system. In its simplest form, photoluminescence spectroscopy consists of an incident pump beam with photon energy larger than the band gap of the material investigated, optics to focus and collect the light, and a spectrometer and detector to measure the emission spectrum of the sample.
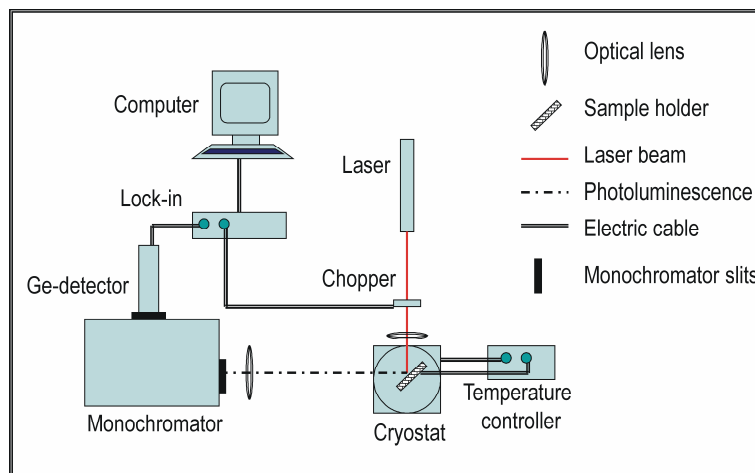
Figure 2.3.: Experimental set-up for the photoluminescence measurements.

In figure 2.3 the experimental set-up employed for the low-temperature PL measurements is illustrated. Two different laser sources have been employed: a Helium-Neon laser (633 nm) having a power density of about 100 W / cm^2 and an InGaAlP solid state laser (680 nm) having a variable power density up to about 5 kW / cm^2. Through an optical lens, the laser beam is focused on the sample in a spot with a diameter of less than 100 μm. The sample is fixed on a sample-holder located inside a He-

closed-cycle cryostat able to reach a minimum temperature of about 15 K. A temperature controller regulates the temperature of the sample in the range of 15 – 300 K. The photoluminescence produced by the sample (dotted-dashed line in the figure) is collected by an optical lens and focused on the entrance-slit of a 1m-spectrometer. At the exit-slit the signal is detected by a Ge-detector operating at 77 K. In order to improve the signal-to-noise ratio, the lock-in technique has been employed. The spectral sensitivity of the Ge-detector is between 800 nm and 1700 nm. In this range the spectral sensitivity of the system (spectrometer plus detector) varies roughly over two orders of magnitudes with a maximum around 1300 nm. For this reason, all the acquired spectra have to be normalized to this spectral sensitivity. The data acquisition program does this normalization automatically.

The room-temperature PL measurements shown in chapter 3 for the series of samples grown at different temperatures have been performed employing a different photoluminescence apparatus. In this case a Nd:YAG-laser emitting at 532 nm with power density of about 1 kW / cm[2] as excitation source and an InGaAs-detector have been used.

2.3.2 Surface photo voltage spectroscopy

The surface photo voltage (SPV) spectroscopy is a well-known electrical-optical characterization technique. In a previous PhD thesis at Infineon Technologies, G. Dumitras developed a technique that employs SPV in order to measure the band offsets of QW structures.[87] In the course of the present PhD work, the understanding of the underlying processes was extended and refined.

As mentioned in § 2.1.1, the structure of the samples employed for SPV measurements differs from that of samples used for photoluminescence investigations. The samples, grown on n-doped substrate, contain a QW embedded in the middle of a GaAs layer of about 3000 – 4000 Å thickness. The QW and the grown GaAs layer are not intentionally doped. A modified structure with an additional p-doped region on top of the sample has been also employed. In figure 2.4 the sample structure and the SPV experimental set-up are described. The sample is sandwiched between the massive copper plate of the

sample-holder (put in the cryostat in order to have the possibility to vary the measuring temperature) representing the ground contact and a transparent electrode (ITO - Indium Tin Oxide, on glass). The distance between the sample and the electrode is a few μm. This allows a capacitive contact between these two elements. Monochromatic light, generated by the halogen lamp passing through a monochromator, illuminates the sample on an area of about 5x5 mm^2 through the transparent electrode. The photovoltage signal taken from the ITO is applied to a high impedance amplifier (few GΩ) and measured by standard lock-in technique. The monochromatic light is chopped with a frequency of about 30 Hz causing periodical variation in the photovoltage generated in the sample.
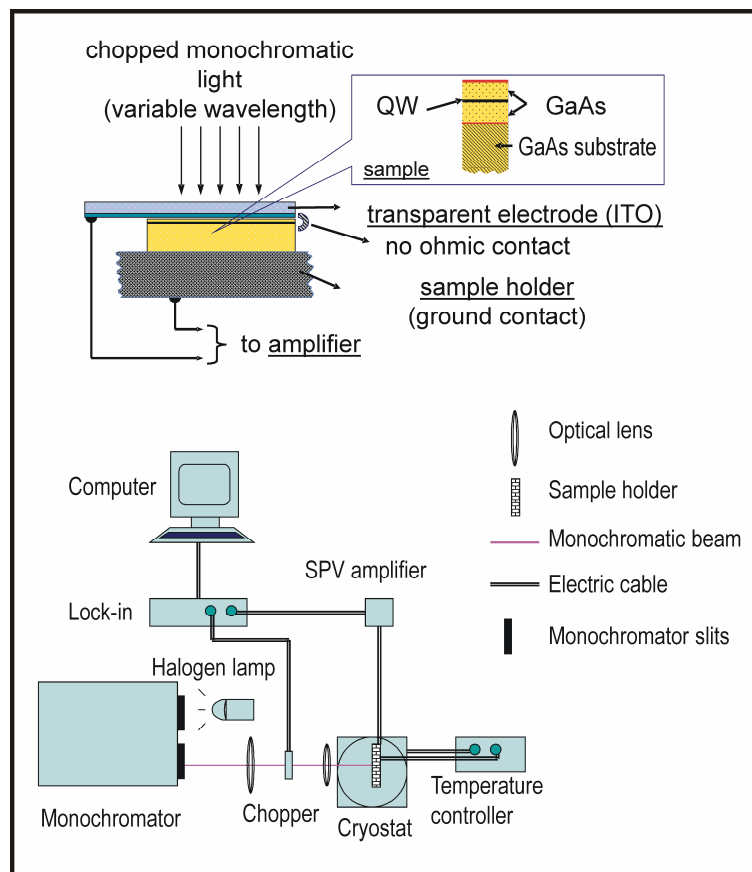
Figure 2.4.: Sample structure and experimental set-up for the surface photo voltage measurements.

Using this method, small variations in the photovoltage, generated near the surface of the sample, are measured. The mechanism of SPV generation can be explained in the following using a simple model. As assumptions, the energy of the photons is only slightly above the GaAs band gap and the surface Fermi level is pinned at 0.7 eV under the conduction band.

When light is applied, the built-in electric field* separates the photo-generated electron-hole pairs (EHPs). These carriers come out from the QW due to thermal escape and / or tunnelling and are collected at the surface of the sample. This gives rise to a current (I_{ph}) which charges the capacitor between the surface and the substrate. This current must compete against the volume (I_V) and the surface (I_s) recombination currents. It has been calculated that the main contribution to the SPV signal comes from the carriers outside the QW (see figure 2.5). In this way, the SPV signal can be written as:

$$SPVsignal \propto \alpha_{QW}(E) \cdot \left[f_e(E,T)d_2 + f_h(E,T)d_1 \right],\qquad\qquad(2.1)$$

where $\alpha_{QW}(E)$ is the QW absorption coefficient, $f_e(E,T)$ and $f_h(E,T)$ are the escape efficiency of the generated electrons and holes from the QW, respectively, and d_1 and d_2 are the distances between the surface and the QW and between the QW and the substrate, respectively.
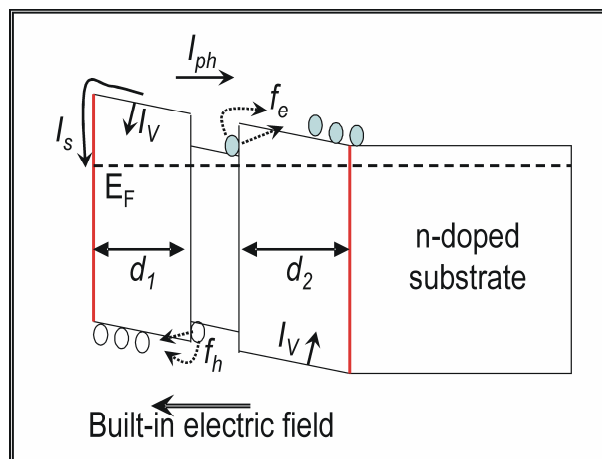
Figure 2 5.: Mechanism of the SPV signal generation.

By performing this measurement it is possible to distinguish EHPs generated by bound-to-bound transitions, such as e_1-hh_1 or e_2-hh_2 from EHPs due to transitions involving extended states (e_1-ch*, ce-ch). A more detailed description of the theoretical principles of this method can be found elsewhere.[88,89]

The main advantages of this method are its sensitivity (several optical transitions can be detected for a single quantum well structure) and its simplicity (no ohmic contacts to the sample are required).

---

* The highly doped substrate ($\approx 2 \times 10^{18}$ cm^{-3}) creates a built-in electric field ($E \approx 10^4$ V / cm) in the undoped region between the surface and the substrate.
* The letter "c" stays for "continuum". In the course of this thesis, transitions involving extended states of electrons and holes will be marked as "ce" and "ch", respectively.

Moreover, the band alignment, and than the band offset, result straightforwardly by examining the SPV spectrum without the need of fitting procedures. A more comprehensive description of the advantages and potentialities of this method as compared to other optical techniques will be presented in § 4.1.4.

2.3.3 Other characterization techniques

The studies presented in this thesis required also other experimental characterization techniques, both optical and morphological.

Contactless Electro Reflectance (ER) measurements have been employed on the samples presented in section 4.1.1 in order to determine, with a different optical technique than SPV, the optical transitions in the SQW samples. ER is in fact a useful tool to analyse the band structure of a semiconductor sample by measuring the changes in spectral reflectance. In electro reflectance, an applied electric field is modulated so as to produce a periodic variation in the dielectric function. The electric field is applied putting the sample in a light transparent capacitor. The ER measurements shown in this thesis were performed at the University of Karsruhe in Germany.

Time Resolved Photoluminescence (TRPL) measurements were performed at Technical University of Berlin in Germany on the samples presented in § 3.3.2. The measurement principle is basically the same as for standard PL. The main difference is the application of a short-pulse laser to excite the sample and a system to synchronize the laser pulse with the detected signal. Using TRPL it is possible to investigate the different recombination processes present in a quantum structure.

For a morphological analysis of the samples presented in § 3.3.2 *Transmission Electron Microscopy (TEM)* has been employed. On the basis of the interaction with the material of the transmitted electrons in the sample, it is possible to obtain information regarding the composition and the strain of the material.

TEM analysis has been carried out at the University of Erlangen-Nuremberg and at the Institute of

Crystal Growth (IKZ) in Berlin.

Chapter 3

Effects of Growth Parameters and Annealing Conditions on the Optical Properties of Dilute Nitrides

Dilute nitride systems have been demonstrated to be important materials for applications in the optoelectronic field.[6,7,8,9,10,11,12] For this reason, much work has been devoted to analysing their optical properties.[22,43,60] In particular, the improvement of the photoluminescence efficiency and the modification of the photoluminescence energy position after annealing have been intensively investigated in literature.[61,69,90] In addition, it has been shown that thermal treatments also influence the morphology of the quantum wells. Although several groups dedicated much effort to studying these problems, a clear and unique picture about the influence of annealing on the optical and morphological properties of the quantum wells and the dependence on of growth parameters is still missing.

In this chapter, comparing different types of photoluminescence (PL) measurements with microscopic analysis such as transmission electron microscopy (TEM) studies, information regarding the influence of the MBE growth temperature and indium content on the optical properties and on the structure of the quantum wells will be presented. For the first time, a comparison of the results of samples annealed in different environments will be employed. Combining results obtained from PL measurements and TEM images, a possible correlation between the optical and morphological properties of InGaAsN quantum wells will be established. As a conclusion, it will be found that during the growth of InGaAsN samples at least two different types of optical defects are created. The density of these defects, related to the presence of nitrogen and to the combined presence of nitrogen and indium,

depends on the growth temperature and is modified by annealing. The improvement of the photoluminescence efficiency of the quantum wells is mainly attributed to the removal or to the passivation of these optical defects rather than to the morphological modifications of the structure.

3.1 Influence of the growth temperature on the optical and morphological properties of InGaAsN

As justified above, in the last years the improvement of the optical quality of (In)GaAsN alloys and the identification of the dominant mechanisms of light emissions have been intensively investigated. [61,69,77] At Infineon Technologies, dilute nitrides have been employed for the realisation of QW laser structures.[6,7] Therefore, it has been paid attention to optimise the optical properties of the test-structures[*] such as the PL efficiency and PL peak emission energy taken at room temperature.

In section 1.2 it has been shown that growth parameters such as the growth temperature (T_g) strongly affect the morphology of the quantum wells. For this reason, a study of the influence of T_g on the optical properties of (In)GaAsN systems is a good way to find a correlation between the morphology and the optical recombination processes of the QW.

In figure 3.1 the values of the PL intensity (a) and of the peak emission energy (b) taken at 300 K are shown for an as-grown $In_{0.37}Ga_{0.63}As_{0.983}N_{0.017}$ SQW sample with varying growth temperature from 360 to 480 °C.

---

[*] Test-structures are samples employed for the optoelectronic characterization. Usually these samples simulate, in a simplified way, the structure of a final device. In § 2.1.1 it is possible to find the description of the structure employed in this thesis.
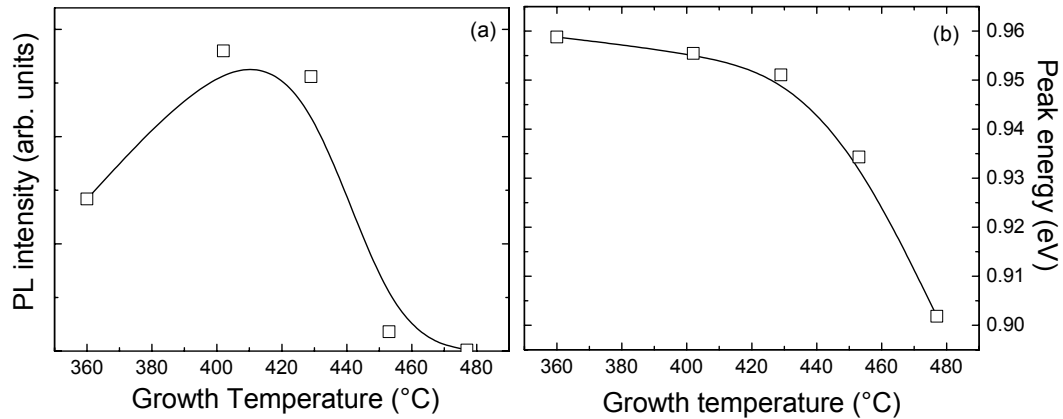
Figure 3.1.: (a) PL peak intensity and (b) PL peak position of an $In_{0.37}Ga_{0.63}As_{0.983}N_{0.017}$ SQW sample with varying growth temperature.

The results show that both the PL intensity and the peak emission energy depend on the growth temperature. In particular, the photoluminescence intensity reaches a maximum value at 400 °C < Tg < 430 °C and strongly decreases at very low ($\approx$ 360 °C) and very high ($\approx$ 480 °C) growth temperatures. On the other hand, the peak position decreases monotonously with increasing Tg. Regarding the PL red shift as Tg is increased, similar results have been found in the literature,[90,91] but no explanations have been given. With a dedicated series of samples, Pavelescu et al.[92] have tried to clarify these phenomena. They found that the reason of the dependence of the PL intensity and peak position on Tg should be found in the growth conditions after the growth of the QW layer. In particular, they have shown that if the layer above the QW (usually GaAs) is grown at higher temperature compared to that of the QW layer there is a decrease of the PL intensity and a blue shift of the peak position with decreasing the QW Tg. On the other hand, if the QW and the above layer are grown at the same temperature any difference in PL intensity and emission energy due to Tg is completely eliminated.[*] This effect is called *self-annealing*. As an explanation, the authors of Ref. 92, performing X-ray diffraction measurements, found that during (self-)annealing In-N bonds form instead of Ga-N bonds and that this process is enhanced with decreasing Tg. They also found that the creation of In-N bonds is a point-

---

[*] Concerning the samples shown in figure 3.1, after the QW a layer of GaAs is grown at 600 °C, that means $\approx$200 °C higher than the temperature at which the InGaAsN quantum well is grown. More details about the sample structure can be found in § 2.1.1.

defect assisted phenomenon. The lower Tg the more defects, the easier is the formation of In-N bonds. As a consequence, more In-N bonds are created, a larger band gap is obtained.[67] In addition, they found that the PL line-shift with Tg occurs without noticeable changes in macroscopic alloy composition or quantum well structure.

Hierro et al.[93] have found an influence of the growth temperature on the PL intensity and peak position of InGaAsN QWs as well. However, in contrast to the conclusions in Ref. 92, employing dark-field TEM images they have shown a strong correlation between the growth temperature of the QW and compositional fluctuations in the system.

The self-annealing process explains the influence of the growth temperature on the emission energy of the QW in a satisfactory way however an unambiguous correlation with the morphological properties is not present.

In order to investigate the effect of the growth temperature on the structure of the samples described in figure 3.1, a comparison between the evolution of the PL peak position with the measured temperature and TEM images will be presented in the following. The results for the samples grown at 360 °C and 480 °C are excluded from this analysis. At these two growth temperatures, in fact, the quality of the InGaAsN sample starts to strongly degrade.

Figure 3.2 shows that with increasing the growth temperature from 400 °C to 450 °C, the typical red-blue-red shift (S-curve) characteristic of dilute nitrides and illustrated in section 1.3 strongly increases. As explained in chapter 1, the S-curves give information about the localization of the carriers in the QW: the more marked the S-curve, the stronger is the localization degree. Therefore, considering these results, one can say that with increasing Tg, the localization degree increases.
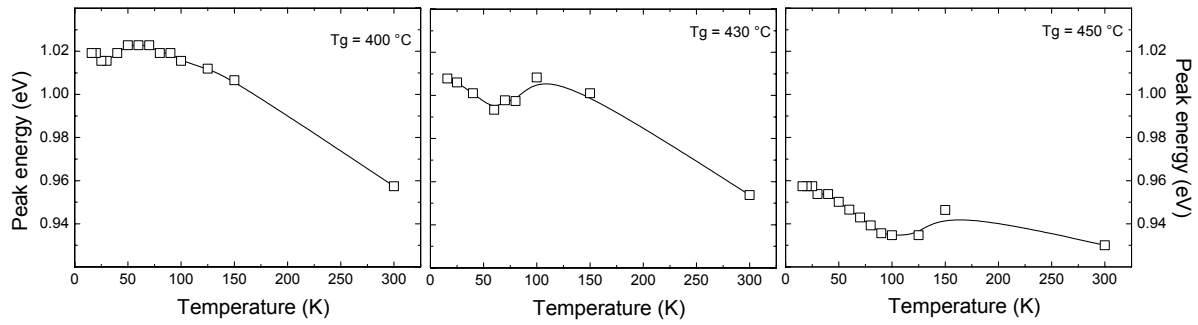
Figure 3.2.: Variation with temperature of the PL peak emission for $In_{0.37}Ga_{0.63}As_{0.983}N_{0.017}$ SQW samples grown at 400 °C, 430 °C and 450 °C.

In figure 3.3 are shown (002)- and (004)-TEM micrographs of the same series of samples. The dark-field (002) images, also called "chemically sensitive reflection" images, give information on the local composition of the investigated material. On the other hand, dark-field (004) images are only weakly affected by local composition variations and are more sensitive to strain fluctuations.

Considering the two extreme cases (Tg = 400 °C and Tg = 450 °C), there is a strong difference in the morphology of the quantum well. While for the sample grown at low temperature the QW interfaces are almost flat (two-dimensional structure), for the sample grown at high temperature it is possible to notice a strong undulation especially for the upper interface. For this sample, the presence of asymmetric islands (three-dimensional structure) has been determined. Concerning the sample grown at 430 °C, the (002)-dark field image does not reveal substantial differences from that of the sample grown at 400 °C. On the other hand, the (004)-dark field image analysis visibly shows an increase of the strain fluctuations passing from Tg = 400 °C to Tg = 430 °C. These results clearly show that an increase of the growth temperature induces inhomogeneity of the QW layer and a roughness of the interfaces (at least of the upper one).

The comparison of figure 3.2 and 3.3 gives important information. In fact, as also shown by other groups,[60,61] there is a clear correlation between the localization of the carriers and the inhomogeneity of the QW layer. Structural non-uniformity of (In)GaAsN quantum wells gives rise to potential fluctuations. As described in chapter 1, these fluctuations trap the carriers in localized states strongly affecting the

optical properties of the QWs. In particular, an increase of the inhomogeneity of the QW causes an increase of the localization degree in the system.
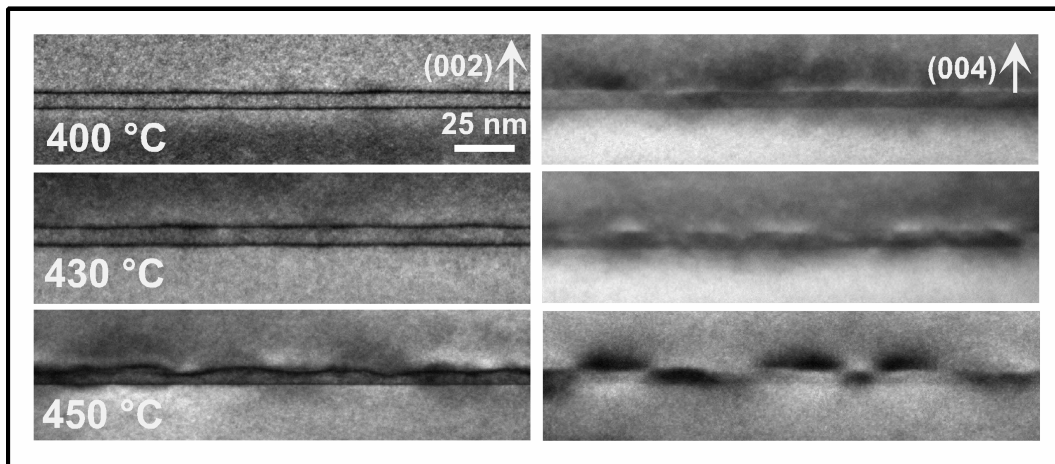
Figure 3.3.: (002)- and (004)-dark field TEM images of $In_{0.37}Ga_{0.63}As_{0.983}N_{0.017}$ SQW samples grown at 400 °C, 430 °C and 450 °C.

The influence of growth parameters, such as the growth temperature, on the morphology of dilute nitride structures has been investigated in the past by many groups,[64,66] but a correlation also with the optical properties of these materials is a quite new subject in literature. Only few studies,[93,94] and published during the course of this thesis work, have been dedicated to this topic. The results presented by these authors confirm those in this section according to which the growth temperature strongly influences the morphology and the optical properties of the quantum well structures. Moreover, the degree of localization is indicative of the extent of structural inhomogeneity. Thus, the time-consuming investigation by TEM can be limited to selected samples.

3.2 Influence of the indium content on InGaAsN quantum wells

Quantum well composition is an important parameter to take into account in order to investigate the optical properties of the system. In particular, it has been shown that indium in InGaAsN structures is a determining factor for the presence of carrier localization in dilute nitrides.[60] For this reason, in the following, the influence of indium content on the optical and structural properties of InGaAsN QWs will be analysed.

Figure 3.4 shows the PL intensity (a) and the PL peak position (b) taken at 300 K for two series of InxGa1-xAs0.84N0.016 / GaAs SQW samples grown at 400 °C and 430 °C. The indium content is varied between 26 % and 38 %. As already noticed in the previous section, the growth temperature influences the PL intensity of the QWs. Independently of the indium content, the samples grown at the lower Tg have always the stronger PL intensity. In addition, figure 3.4 shows for the samples grown at 400 °C an increase of the PL intensity with increasing indium content till [In] = 34 % and a strong decrease for an indium concentration of 38%. A similar trend is present for the samples grown at 430 °C. In this case, however, the highest PL intensity is reached at lower indium contents ([In] = 30%). For the sample with [In] = 38% the PL is not detectable at 300 K[*]. Most interestingly, in both growth temperature cases the PL intensity strongly degrades for high indium contents. This is probably due to the strong presence of non-radiative recombination centres generated for example by dislocations due to the strain relaxation induced by the high indium concentration.

As expected, with increasing indium content the peak emission energy decreases. However, the energy values of the samples grown at Tg = 430 °C are red-shifted if compared to those of the samples grown at Tg = 400 °C. As for the case presented in the previous section, this red shift can be explained considering the self-annealing process.[92]
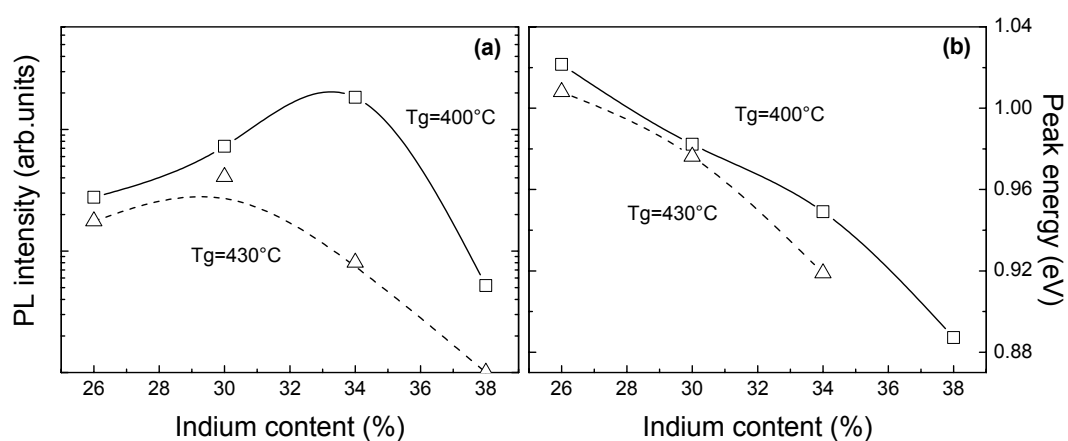
Figure 3.4.: (a) PL intensity and (b) peak energy position variation with indium content of $In_xGa_{1-x}As_{0.984}N_{0.016}$ SQW samples grown at 400 °C (solid lines) and at 430 °C (dashed lines).

---

[*] The PL intensity of the sample grown at 430 °C with [In] = 38% is plotted in figure 3.4 (a) with a data point having a value of almost zero.

Figure 3.5 shows the S-curves for the two series of samples. In both cases, with increasing indium content the localization degree increases.
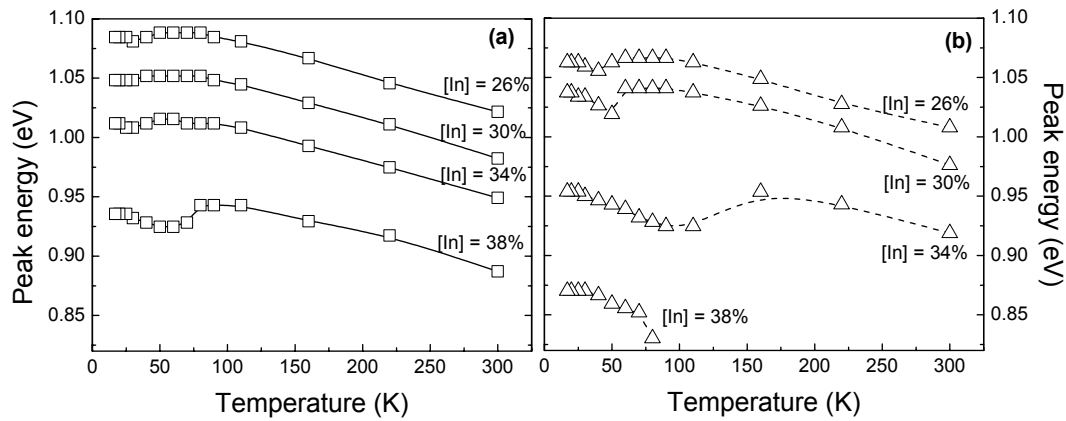
Figure 3.5.: Variation with temperature of the PL peak emission of $In_xGa_{1-x}As_{0.984}N_{0.016}$ SQW samples grown at Tg = 400 °C (a) and Tg = 430 °C (b).

For these samples there are no microscopic investigations at disposition. However, on the basis of the correlation between the S-curves and the TEM images found in the previous section, it is possible to conclude that indium affects the morphology of the system. Looking at figure 3.5 one can say that with increasing indium content the inhomogeneity of the quantum well increases. Similar results have been found for pure nitrides. From X-ray diffraction and high resolution TEM investigations, it has been shown that in InGaN / GaN quantum well structures a higher nominal indium content results in a larger indium-rich cluster sizes and more In-N phase separated clusters with a consequent increase of the localized states.[95]

In addition to that, the influence of the growth temperature can be also analysed. Taking the indium content constant, the figure 3.5 shows an increase of the carrier localization passing from Tg = 400 °C to Tg = 430 °C confirming the final conclusions of § 3.1.

The results of section 3.1 and 3.2 have shown that high growth temperatures and high indium contents cause a strong inhomogeneity of the QW layer. Also, the PL intensity is affected by these two parameters. By raising Tg and with increasing [In], the PL intensity strongly decreases. Therefore, an InGaAsN sample grown at high temperature and with high indium content will show the strongest

inhomogeneity and the weakest PL intensity (an example is the sample grown at 430 °C with [In] = 38% shown in this section).

3.3 Influence of annealing

As illustrated in § 1.3, annealing is a well established tool to improve the PL efficiency of dilute nitride QW samples. Moreover, it has been shown that thermal treatments modify also the morphology of the QW, generally reducing the inhomogeneity of the system (§ 1.2).

Usually, the gaseous atmospheres employed during annealing are As$_4$ (*in-situ* in MBE), AsH$_3$ (*in-situ* in MOCVD), or N$_2$ (*ex-situ*). Concerning the *ex-situ* procedures, the majority of the groups focused their attention on the variation of the annealing time and annealing temperature in order to find the optimal thermal treatments,[96,97] neglecting the investigation of the annealing environment.

The series of samples analysed at the beginning time of this thesis work have been *ex-situ* annealed with a standard thermal profile of 730 °C for 30 minutes only in hydrogen atmosphere. This is because H$_2$ annealing, employed at Infineon Technologies before also for other purposes, was found not to damage the sample surface. Afterwards, in order to mimic the *in-situ* annealing process of a QW laser, the annealing time and annealing temperature have been changed. In addition, to eliminate the reactive nature of the annealing atmosphere, the inert gas argon has been employed as new annealing environment. A direct comparison between the results obtained annealing the samples in these two different environments (H$_2$ and Ar) was performed, pointing out the differences from the morphological and optical point of view. This comparison has been carried out employing continuous wave and time resolved photoluminescence and transmission electron microscopy.

3.3.1 Annealing effects on the indium series

In figure 3.6 (a-b) the effects of annealing on the PL intensity and PL peak position taken at 300 K are shown for the series of samples presented in section 3.2. The samples were annealed in H_2 atmosphere at 720 °C for 30 minutes.
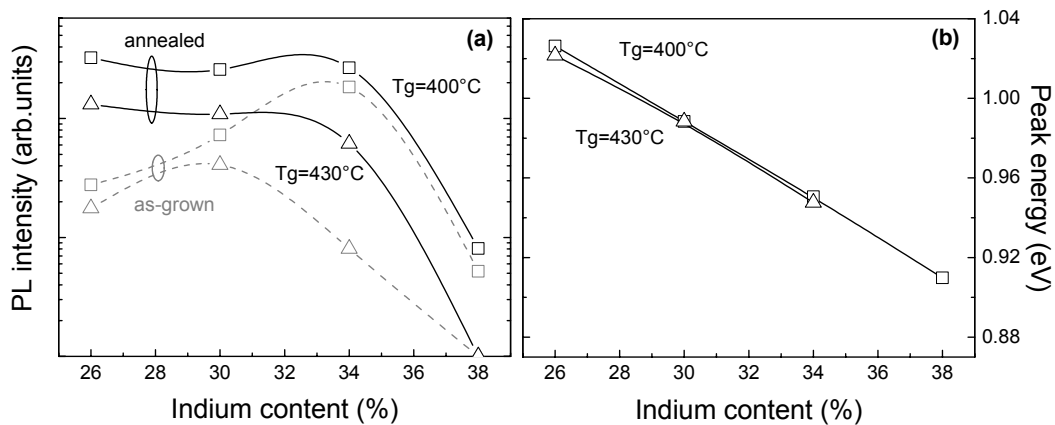
Figure 3.6.: (a) PL intensity and (b) peak energy position variation with indium content $In_xGa_{1-x}As_{0.984}N_{0.016}$ SQW samples grown at 400 °C (squares) and 430 °C (triangles).In plot (a) are shown the results for the as-grown samples (dashed lines) for comparison.

For each indium content, annealing produces an increase of the PL efficiency if compared to the as-grown case. For both the growth temperatures, there is little In-dependence of the PL efficiency with the exception of the sample with [In] = 38% for which the PL intensity is very low. As for the as-grown case, the samples grown at lower temperature show the strongest PL efficiency. Most notably, the red shift of the PL peak emission for the samples grown at 430 °C compared to the ones grown at 400 °C is completely removed after annealing [figure 3.6 (b)].

In figure 3.7 (a-b) the evolution with measurement temperature of the PL peak emission energy after annealing for the two series of samples are plotted. If compared to the curves of the as-grown samples shown in figure 3.5, the localization degree is generally reduced for each sample and is completely eliminated for the samples with low indium content.
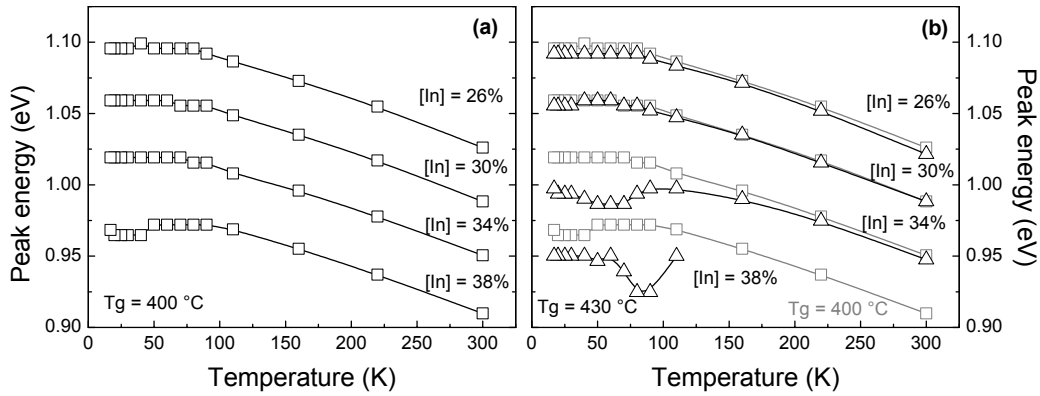
Figure 3.7.: Variation with temperature of the PL peak emission of $In_xGa_{1-x}As_{0.984}N_{0.016}$ SQW samples grown at Tg = 400 °C (squares in a) and Tg = 430 °C (triangles in b). In plot (b) the results of both growth temperatures are shown for comparison.

On the basis of the considerations made in § 3.2, it is possible to extract morphological information from these S-curves. For each growth temperature, annealing induces a general homogenisation of the QW. Moreover, as shown for the as-grown case, with increasing indium content, the inhomogeneity of the QW increases.

Comparing the results obtained for the two series of samples grown at different temperatures, it is possible to obtain interesting information. In fact, although there is still a difference in the PL efficiency and localization degree between samples grown at Tg = 400 °C and Tg = 430 °C, any difference in the peak emission energy is completely eliminated. The influence of annealing on samples grown at different temperatures will be intensively discussed in the next section.

3.3.2 Annealing effects on the optical and morphological properties of InGaAsN quantum wells grown at different temperatures

In order to simulate the *in-situ* annealing conditions during the growth of an optoelectronic device, the thermal profile of the *ex-situ* annealing has been modified. Instead of using the thermal parameters employed to anneal the samples presented in § 3.3.1 (720 °C for 30 minutes), the annealing temperature and the annealing time have been changed to 680 °C and 109 minutes, respectively.

These are the typical thermal conditions for an edge-emitting QW laser structure grown at Infineon Technologies. At first, the annealing atmosphere remained hydrogen.

In figure 3.8 (a-b) the influence of annealing on the PL intensity and PL peak position is illustrated with varying growth temperature for an $In_{0.37}Ga_{0.63}As_{0.983}N_{0.017}$ SQW sample. The described samples are those of section 3.1. Independently of the growth temperature, the PL efficiency is always improved after annealing. Moreover, the behaviour reflects that of the as-grown case: the best PL efficiency is obtained for the samples grown between 400 °C and 430 °C. As expected, after the thermal treatment there is a general blue shift of the peak emission energy, however, the strong red shift of the peak energy position with increasing Tg is remarkably reduced.
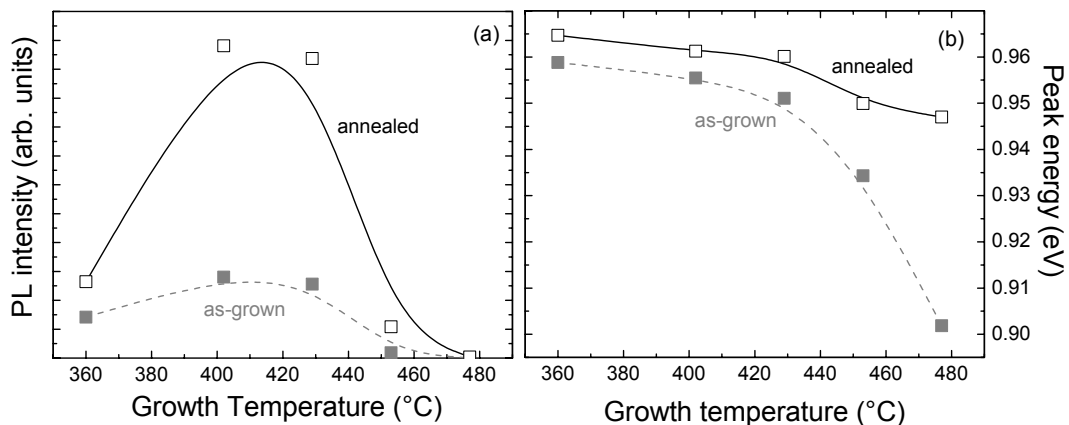
Figure 3.8.: (a) PL peak intensity and (b) PL peak position of $In_{0.37}Ga_{0.63}As_{0.983}N_{0.017}$ SQW samples after annealing (solid lines). For comparison, the results for the as-grown samples are shown with dashed lines.

The latter results are consistent with those described in Ref. 92. In their work, Pavelescu et al.[92] have shown that for annealing temperatures of exceeding T = 540 – 560 °C the energy shift between the samples grown at different T due to self-annealing starts to decrease. This is explained considering the modification after annealing of the nearest-neighbours configuration of nitrogen in InGaAsN structures. As discussed in § 1.2.1, experimental studies have shown that in as-grown InGaAsN samples nitrogen is mostly bound to gallium, while in annealed samples In-N bounds dominate[67,70,98] giving thus an explanation for the annealing induced blue shift.

According to Pavelescu`s findings (§ 3.1), the formation of In-N bonds is a point defect assisted phenomenon and the number of these bonds increases with decreasing growth temperature of the

quantum well. This means that, due to self annealing, in samples with low T_g nitrogen is preferably bound to In atoms, while in those with high T_g nitrogen is preferably bound to Ga atoms. Consequently, the as-grown samples show a blue shift in the peak energy with decreasing T_g. Post-growth annealing causes a further change in local N-bonding from Ga-rich to In-rich environment. For this reason, after annealing samples grown at high temperature show a stronger blue shift compared to that of samples grown at low temperature. With increasing annealing temperature, any difference among samples grown at different temperatures will be eliminated*. This is because the more stable configuration will be reached: the nitrogen atoms are bound only to indium atoms.

In figure 3.9 (a-c), the variation with measurement temperature of the peak emission energy for different T_g is shown comparing the as-grown and annealed case. After annealing, a clear reduction of the localization degree is evident for each T_g. This is consistent with the results in 3.3.1 and with several reports in the literature which describe a reduction of the potential fluctuations in dilute nitrides due to annealing processes. [61,69,93] Despite the general reduction of localization, the S-curves in figure 3.9 show that the localization degree depends on the growth temperature even after annealing. In particular, it increases with increasing T_g.
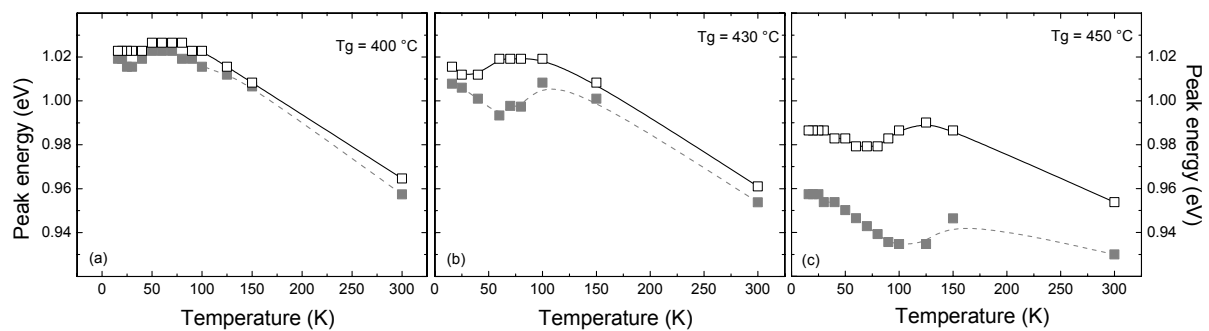
Figure 3.9.: Variation with measurement temperature of the PL peak emission for annealed $In_{0.37}Ga_{0.63}As_{0.983}N_{0.017}$ SQW samples grown at 400 °C, 430 °C and 450 °C (solid lines). For comparison, the results for the as-grown samples are shown with dashed lines.

The morphological analysis is illustrated in figure 3.10 where the (002)- and (004)-TEM micrographs are shown for the samples grown at 400 °C and 450 °C. The comparison of these images with those of

---

* However, this condition could be prevented by possible morphological damages to the QW due to too high annealing temperature.

the as-grown samples (figure 3.3) shows a general reduction of the alloy fluctuations after annealing. However, the dependence on growth temperature remains the same: with increasing Tg, the QW becomes more inhomogeneous. Also after annealing the sample grown at 450 °C shows a three-dimensional structure with the formation of islands.
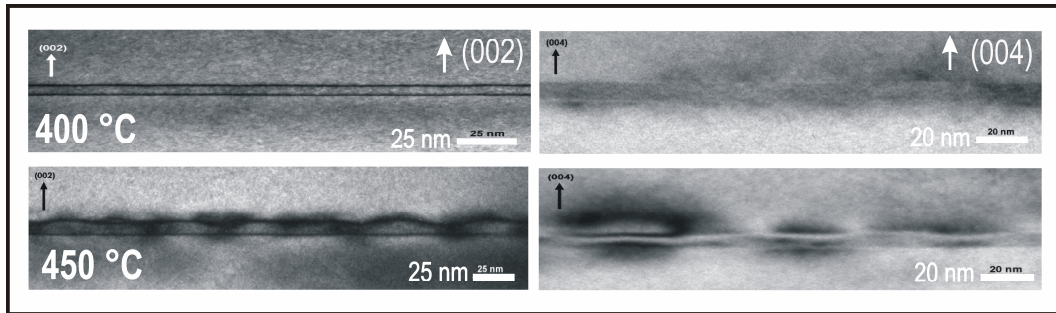

Figure 3.10.: (002)- and (004)-dark field TEM images of annealed $In_{0.37}Ga_{0.63}As_{0.983}N_{0.017}$ SQW samples grown at 400 °C and at 450 °C.

3.3.3 Influence of the annealing atmosphere on the optical and morphological properties of dilute nitrides

As already mentioned, test-structures should reproduce the results of a final device. In this way optoelectronic characterisation can be carried out on samples with a simplified structure, saving material and time. In the previous section, in order to mimic the typical thermal parameters of the *in-situ* annealing process during the growth of an edge-emitting QW laser structure at Infineon Technologies, annealing time and annealing temperature of the *ex-situ* thermal process of the test-structures have been modified.

In a recent paper [6] it has been shown that the performances of InGaAsN SQW lasers are directly correlated to their PL intensity. A typical parameter of a laser is the threshold current. The lower the threshold current, the lower is the current at which the stimulated emission of the laser sets in. It has been shown that the value of the threshold current decreases with increasing PL intensity of the QW in a linear way, independently from the composition of the active region.

In order to compare the optical properties of the QW test structures analysed so far with the performances of final devices, in figure 3.11 the PL intensity of the H_2-annealed InGaAsN SQW samples

and the threshold current values of InGaAsN SQW lasers are shown as a function of the growth temperature. The values of the threshold current shown in the figure do not perfectly match each other. This is because they are the results taken from three different series of lasers. However, the trend shows that the minimum threshold current value corresponds to high growth temperatures ($T_g \approx 450$ °C). Although the annealing time and annealing temperature are the same for the *ex-situ* annealed samples and for the *in-situ* annealed lasers, the PL intensity depends on the threshold current in the opposite way as shown in Ref. 6. In particular, when the PL intensity is maximum also the threshold current is maximum ($T_g \approx 400$ - 430 °C) and when the PL is minimum also the threshold current is minimum ($T_g \approx 450$ °C).
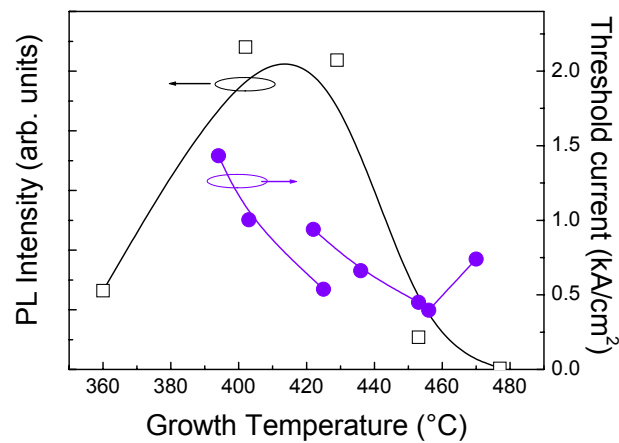
Figure 3.11.: Variation with the growth temperature of the PL intensity of H_2-annealed $In_{0.37}Ga_{0.63}As_{0.983}N_{0.017}$ SQW samples (squares) and of the threshold current of $In_{0.30}Ga_{0.70}As_{0.984}N_{0.016}$ SQW lasers (spheres).

In order to find a reason for this contradictory result, the *ex-situ* annealing parameters of the test-structures have been investigated. The main difference between the annealing procedure of the samples in § 3.3.2 and the *in-situ* annealing process during the realisation of the lasers is the annealing environment: H_2 for the test-structures and As_4 for the lasers. Annealing samples in H_2-atmosphere can lead to a small incorporation of hydrogen in the samples via diffusion process. As is well known[99,100] this could modify the optical properties of the investigated systems. For this reason, the series of $In_{0.37}Ga_{0.63}As_{0.983}N_{0.017}$ SQW samples grown at different temperatures has been annealed in inert Ar atmosphere. In this way, any chemical effect during annealing can be eliminated. As mentioned before,

the majority of the groups in literature employ N_2 as *ex-situ* annealing environment that is an inert gas as well. This gives the possibility of a direct comparison with the results taken from the literature.

The PL intensity and the PL peak position of the as-grown and annealed samples are plotted and compared in figure 3.12 (a-b). The figure shows that the peak emission energy of the Ar-annealed samples does not show any clear Tg-dependence and behaves almost like that of the H_2-annealed samples. On the other hand, the PL efficiency of Ar-annealed samples depends on the growth temperature but in a completely different way as compared to the H_2-annealed case. In contrast to the H_2-annealed samples, for the Ar-annealed samples the PL intensity is the highest at high Tg (≈ 450 °C). Moreover, at low growth temperature (Tg < 430 °C), the PL intensity of the samples annealed in Ar atmosphere gets worse if compared to the as-grown case. In this way, the results of the PL intensity of the samples annealed in Ar environment are consistent with the Tg-dependence of the threshold current of the laser structures.
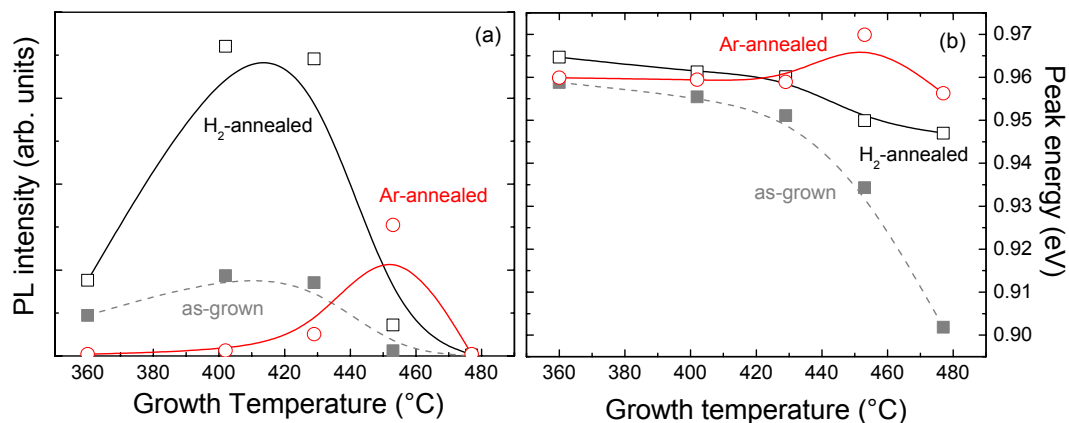
Figure 3.12.: (a) PL peak intensity and (b) PL peak position of an $In_{0.37}Ga_{0.63}As_{0.983}N_{0.017}$ SQW sample after H_2-annealing (open squares) and Ar-annealing (open spheres). For comparison, the results for the as-grown samples are shown with dashed lines.

Figure 3.13 (a-b-c) compares the PL peak energy variation with temperature for the samples annealed in different atmospheres. As for the as-grown case, the Ar-annealed S-curves show an increase of the degree of localization with increasing growth temperature. Moreover, while for the samples grown at Tg = 400 °C and 430 °C the blue shift induced by the Ar-annealing is similar to that induced by the H_2-annealing, for the samples grown at Tg = 450 °C it is clearly stronger. With the

exception of this different blue shift however, the S-curves of the annealed samples behave basically in the same way. For each Tg, in fact, the localization degree after annealing does not depend on the annealing atmosphere, suggesting a similar morphological structure of the QW.
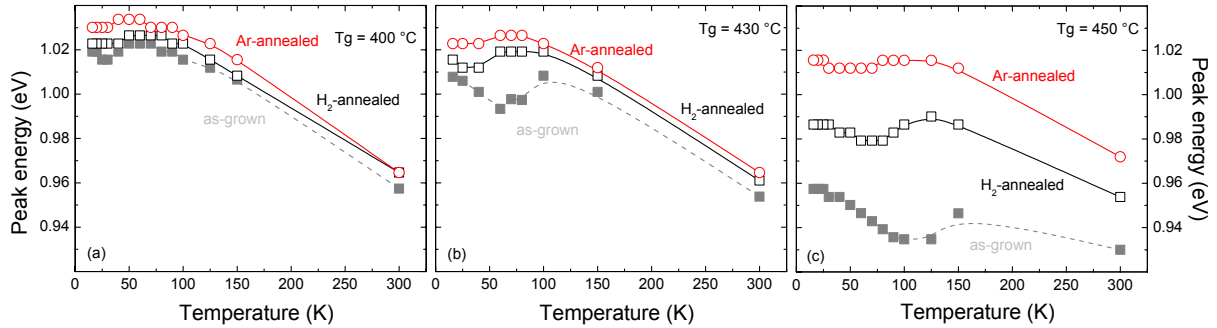
Figure 3.13.: Variation with temperature of the PL peak emission for H_2-annealed (open squares) and Ar-annealed (open spheres) $In_{0.37}Ga_{0.63}As_{0.983}N_{0.017}$ SQW samples grown at 400 °C, 430 °C and 450 °C. For comparison, the results for the as-grown samples are shown with dashed lines.

In order to confirm this conclusion, (002)- and (004)-dark field TEM images were acquired for these samples. In figure 3.14 the TEM micrographs of the H_2- and Ar-annealed samples for Tg = 400 °C and Tg = 450 °C are compared. From the TEM images it is possible to see that the samples annealed in two different atmospheres show the same morphological structure of the QW: smooth interfaces for Tg = 400 °C and strong fluctuations for Tg = 450 °C.
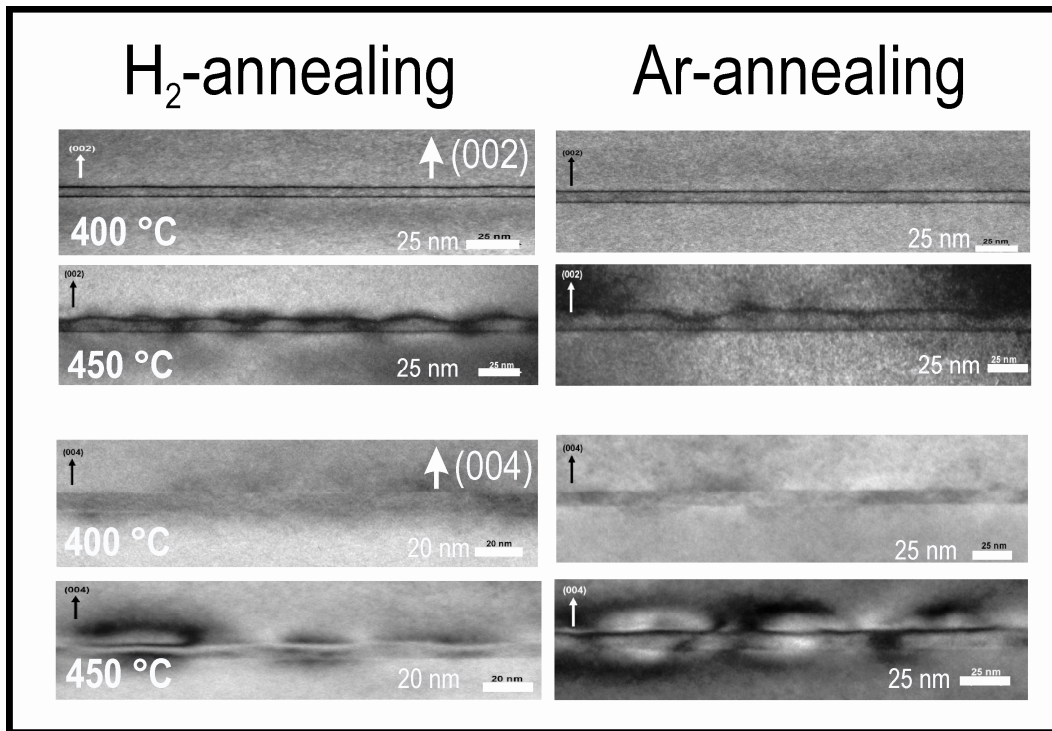
Figure 3.14.: (002)- and (004)-darkfield TEM images of $In_{0.37}Ga_{0.63}As_{0.983}N_{0.017}$ SQW H_2- and Ar-annealed samples. Comparison between the samples grown at 400 °C and 450 °C.

Although the PL efficiency of the samples annealed in argon atmosphere varies with Tg in a different way if compared to that of the samples annealed in hydrogen atmosphere, the morphological variations with Tg of the QW samples do not depend on the annealing environment. This means that the optical properties are not directly connected to the morphology of the system. This result is very interesting and opens new questions regarding the employment of annealing for the optimization of the PL intensity of the QWs. In particular, the annealing environment is found to be a key-factor. Compared to the as-grown case, the correlation between the morphology and the PL intensity of the Ar-annealed samples is completely modified. While for the as-grown samples, an increase of the homogeneity corresponds to an increase of the PL intensity (§ 3.1 and § 3.2), for the Ar-annealed case the homogeneity of samples corresponds to a very low PL intensity.

In the following, an attempt to find possible correlations between optical and morphological properties will be presented.

3.3.4 Correlation between optical and morphological properties of dilute nitrides

In the following, different approaches will be illustrated in order to describe the role played by defect passivation and structural modifications on the PL intensity variation of a QW after a thermal treatment. Moreover, an attempt to find out which type of defects is present in InGaAsN QW structures will be presented.

3.3.4.1 Time resolved PL measurements

In order to investigate in more detail the influence of annealing on the optical recombination processes, time resolved photoluminescence (TRPL) measurements have been performed on the same series of samples, as-grown and after the two different annealing procedures. The measurements have been carried out on samples grown at different temperatures with varying the measuring temperature from 4 K to 300 K.

In general, the PL decay time at a given temperature T can be expressed by the following expression

$$\frac{1}{\tau_{PL}(T)} = \frac{1}{\tau_{rad}(T)} + \frac{1}{\tau_{nonrad}(T)},$$ (3.1)

where τ_{rad} and τ_{nonrad} describe the lifetimes of radiative and non-radiative processes, respectively.

In addition, the PL efficiency is defined by

$$\eta_{PL}(T) = \frac{\tau_{nonrad}(T)}{\tau_{nonrad}(T) + \tau_{rad}(T)}.$$ (3.2)

Therefore, it is possible to estimate the temperature dependence of radiative and non-radiative lifetimes, by monitoring both $\tau_{PL}(T)$ and $\eta_{PL}(T)$. However, it is generally difficult to measure the value of the PL efficiency directly by experiment. As an approximation, the value of $\eta_{PL}(T)$ is assumed as the

integrated photoluminescence at a specific temperature normalised to the value of the integrated PL taken at the lowest temperature. The results are shown in figure 3.15.
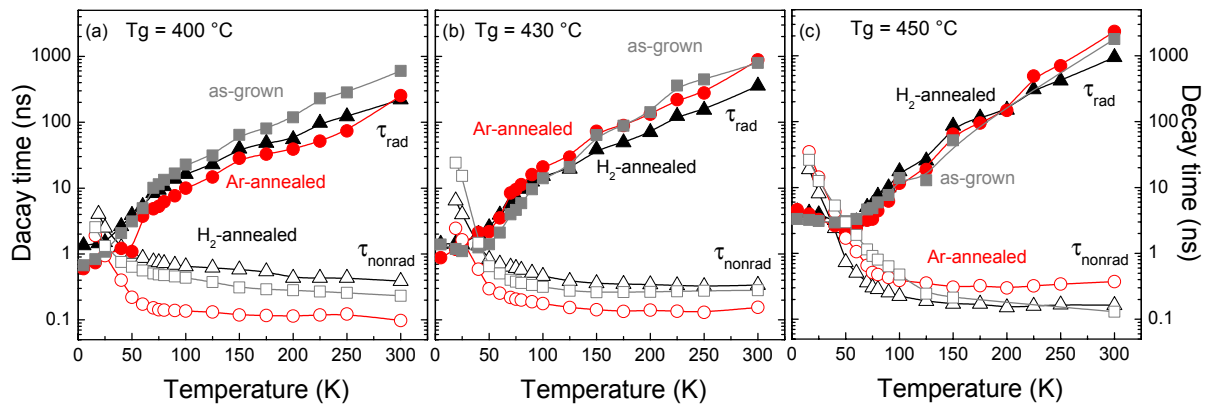
Figure 3.15.: Radiative (closed symbols) and non-radiative (open symbols) decay times with varying the measured temperature for $In_{0.37}Ga_{0.63}As_{0.983}N_{0.017}$ SQW samples as-grown (squares), H_2-annealed (triangles), and Ar-annealed (spheres). Comparison of samples grown at Tg = 400 °C (plot a), Tg = 430 °C (plot b), and Tg = 450 °C (plot c).

As expected, with increasing measurement temperature, the radiative decay time increases while the non-radiative decay time decreases. In particular, τ_{rad} increases by three orders of magnitude passing from 4 K to 300 K for all the samples, while τ_{nonrad} decreases by two orders of magnitude for the samples grown at Tg = 430 °C and 450 °C and by only one order of magnitude for the samples grown at Tg = 400 °C. Moreover, comparing the H_2- and Ar-annealed samples for each growth temperature, it is possible to notice that the radiative decay times assume almost the same values while the non-radiative decay times are in some cases very different. For the samples grown at Tg = 400 °C, for example, the values of τ_{nonrad} of the Ar-annealed sample are about one order of magnitude smaller than those of the H_2-annealed sample. This suggests that the non-radiative centres play an important role in order to understand the different optical properties between the samples annealed in hydrogen and argon atmosphere. In order to corroborate this thesis, a comparison between the behaviour of the life times and the PL intensity with varying growth temperature is presented.

In figure 3.16 the values of τ_{rad} (plot a) and τ_{nonrad} (plot b) obtained from TRPL measurements taken at 300 K for as-grown (open squares), H_2-annealed (open triangles), and Ar-annealed (open spheres) samples are plotted as a function of growth temperature.
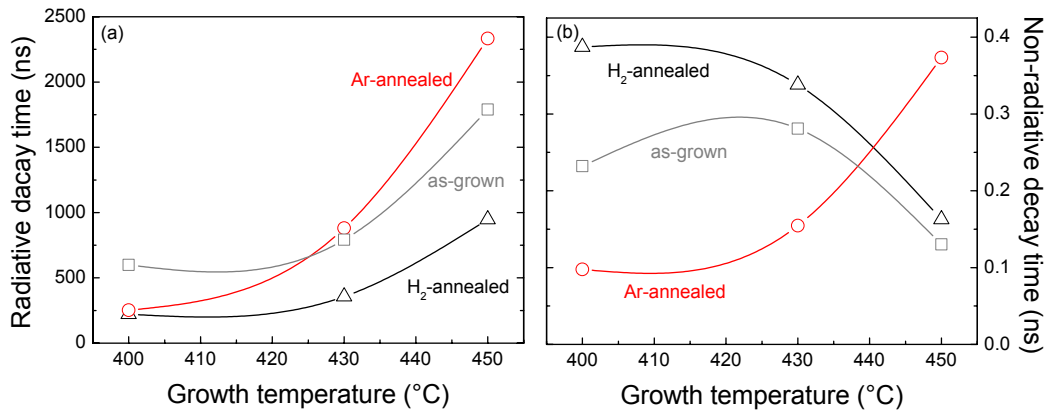
Figure 3.16.: (a) Radiative decay times extracted for 300 K as a function of growth temperature of $In_{0.37}Ga_{0.63}As_{0.983}N_{0.017}$ SQW samples as-grown (squares), H_2-annealed (triangles), and Ar-annealed (spheres). (b) Non-radiative decay times extracted for 300 K as a function of growth temperature of $In_{0.37}Ga_{0.63}As_{0.983}N_{0.017}$ SQW samples as-grown (squares), H_2-annealed (triangles), and Ar-annealed (spheres).

For all conditions, τ_{rad} rises with increasing Tg. The different behaviour of the PL intensity between H_2- and Ar-annealed samples (figure 3.12 (a)) cannot be explained on the basis of τ_{rad}. The dependence of τ_{nonrad} on Tg is more complex and changes with annealing conditions. Most importantly, for all three cases the behaviours of non-radiative decay time (figure 3.16(b)) and the room temperature PL intensity (figure 3.12 (a)) as a function of Tg are qualitatively the same. Moreover, for each growth temperature the evolution of τ_{nonrad} with annealing is very similar to the one of the room temperature PL intensity. Therefore, the improvement of the PL efficiency is directly correlated to the decrease of the density of non-radiative recombination centres.

3.3.4.2 Modification of the carrier localization degree after annealing

In § 3.3.3, it has been shown that annealing changes the PL efficiency of a QW. However, it has been also concluded that variations of PL efficiency are not directly correlated to modifications of the morphology of the structure. For this reason, it is interesting to understand how strong is the influence of the morphology modification of the QW and of the change of the number of defects / impurities in the system on the PL efficiency after annealing.

In order to make this point clear, the variation of the PL intensity and PL energy with annealing of an $In_{0.37}Ga_{0.63}As_{0.983}N_{0.017}$ SQW sample have been investigated employing photoluminescence measurements in two different ranges: the *localized temperature range* that means the range of temperatures in which the carriers are trapped in localized states and the *delocalized temperature range* representing the region of temperatures in which the carriers are completely delocalized. In figure 3.17 these ranges are marked with arrows on the S-curves of the analysed samples.
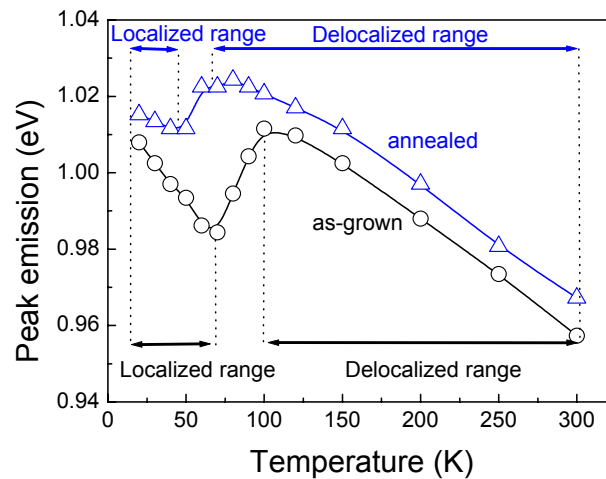
Figure 3.17.: Energy peak emission with varying temperature for an $In_{0.37}Ga_{0.63}As_{0.983}N_{0.017}$ SQW sample as-grown (open spheres) and H_2-annealed (open triangles) grown at 430 °C. Localized and delocalized ranges are marked with double-arrows. The power density is about 100 W/cm².

Figure 3.18 shows the comparison of the PL spectra of the as-grown and annealed samples taken at 20 K (i.e. in the localization temperature range of both samples) and at 300 K (i.e. in the delocalization temperature range of both samples). In both cases, annealing induces a blue shift and an increase of the PL intensity. As is well known, annealing can passivate defects created during the growth of the structure and improve the radiative efficiency of the QW.[101,102,103] However, while the PL intensity at 300 K is strongly increased after annealing (by almost one order of magnitude), at 20 K the improvement is very small, almost negligible. This result is plausible if one thinks that non-radiative processes play a more important role at higher measurement temperatures.

81
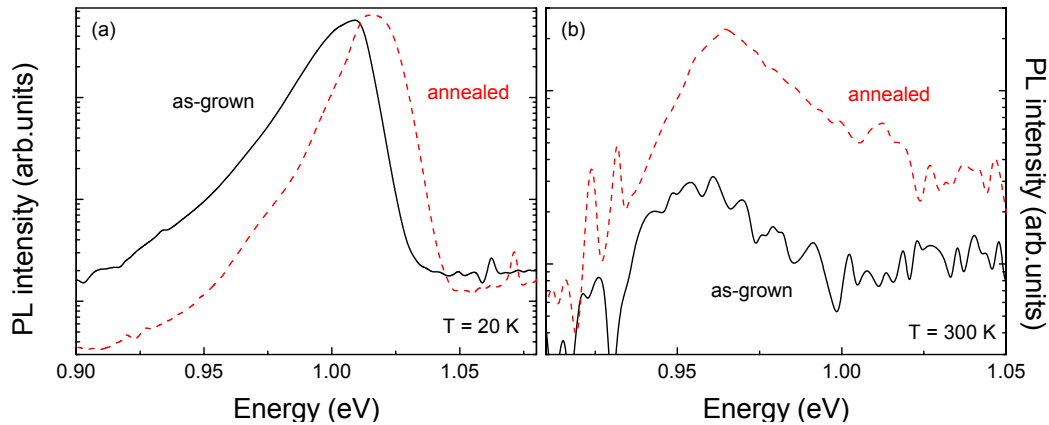
Figure 3.18.: PL intensity spectra for an $In_{0.37}Ga_{0.63}As_{0.983}N_{0.017}$ SQW sample as-grown (solid line) and annealed (dashed line) taken at 20 K (a) and at 300 K (b). The power density is about 100 W/cm^2.

Considering the localized temperature range, the main effect of annealing is the reduction of the red-blue-red shift characteristic of the S-curve (see figure 3.17). It has been shown that the carrier localization is directly correlated with the morphology of the QW (§ 3.1) and that a variation of the carrier localization degree changes the typical S-shape of the temperature dependence of the PL peak energy. Annealing modifies the morphology of the QW (§ 1.2.1) and, consequently, the degree of localization. On the other hand, it has been shown that the S-curve can also be modified without changing the morphology of the system (§ 1.3.3). By increasing the excitation power density, the PL peak emission in the localized temperature range blue shifts, resulting in a fictitious reduction of the localization degree.

Assuming that annealing passivates defects, compared to the as-grown case the number of carriers trapped by defects should be reduced. As a consequence, more carriers are able to occupy the higher lying energetic states of the QW. In this way, the system would behave as if more carriers were generated in the QW. As a result, the lower energy localized states would be filled by the "carriers in excess" compared to the as-grown sample and the radiative recombination would take place at higher energy values. This would mean that the reduction of the S-shape after annealing could not only be due to structural modifications but also to an increased number of carriers due resulting from defect passivation.

In order to investigate this problem, power dependent PL measurements were performed on the same samples as shown in figure 3.17. The power of the laser was varied from a density of about 1 W / cm^2 to 5 KW / cm^2 and the measurements were performed at 70 K. At that temperature, while the carriers of the as-grown sample are strongly localized, the carriers of the annealed sample are already in the delocalized range (figure 3.17). The peak energy variation with varying excitation power density for the two samples is shown in figure 3.19 (a). The correspondent PL spectra are shown in figures 3.19 (b) and (c).
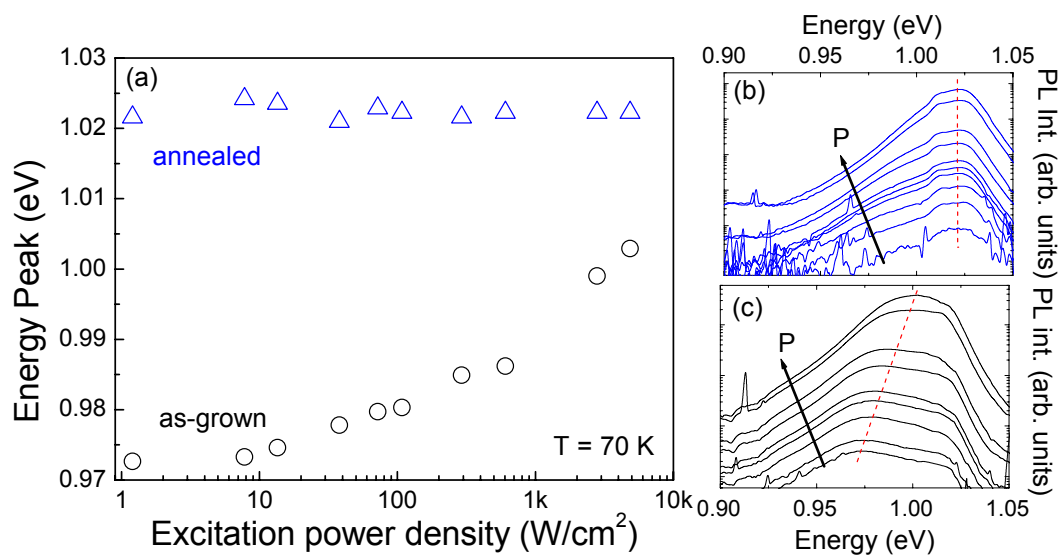
Figure 3.19.: (a) Peak emission energy variation with excitation power taken at 70 K for an In$_{0.37}$Ga$_{0.63}$As$_{0.983}$N$_{0.017}$ SQW sample as-grown (open spheres) and annealed (open triangles). (b)-(c) PL spectra of the annealed and as-grown sample, respectively.

The results show that while the PL peak position of the as-grown sample strongly decreases with decreasing excitation power (open spheres, from about 1.00 eV to about 0.97eV), the energy peak of the annealed sample remains constant (open triangles, about 1.02 eV) although the excitation power density is reduced by more than three orders of magnitude. The red shift of the peak energy of the as-grown sample with decreasing excitation power shows the presence of localized states. For power densities lower than 10 W / cm^2 the peak emission energy does not change any more. This means that the carriers recombine from the lowest possible localized states. These results exclude any improvement of the number of carriers due to defect passivation after annealing, because in that case the energy peak of the annealed sample should have shown a decrease in its value, at least for the very

low excitation power density. Therefore the reduction of degree of localization after thermal treatment can be ascribed only to a structural modification of the quantum well.

The above presented approach is a simple method to establish that a measurement of the variation of the carrier degree of localization after annealing gives information on the modification of the morphology of the system. On the other hand, this is a qualitative method and cannot give information regarding the origin of the variation of the potential fluctuations after annealing from a quantitative point of view.

Recently, a theoretical model has shown interesting results if applied to describe the properties of InGaAsN structures in the localization region.[104,105] This model, based on a kinetic Monte-Carlo simulation of the hopping energy relaxation of excitons, establishes proportionality factors between the disorder energy scale and the characteristics of the PL spectra. On the basis of a direct comparison between experimental data and theoretical calculations, this method gives quantitative information about the energy scale of the potential fluctuations in InGaAsN QWs. In the model, the three dimensionless parameters $\nu_0\tau_0$, $N_0\alpha^2$, and $k_B T / E_0$ have been employed in the calculations, where k_B is the Boltzmann constant, T is the lattice temperature, N_0 is the density of localized states, α is the decay length of the localized exciton centre-of-mass wave function, ν_0 is the attempt-to-escape frequency, τ_0 is the exciton radiative recombination rate and E_0 is the characteristic energy scale representing the disorder parameter. Simulating the variation of the energy peak emission and of the FWHM with temperature, the model is able to give quantitative information about the parameter E_0, that means the disorder energy scale in the QW. A comprehensive description of the method can be found elsewhere.[106]

In the following, the application of this method to an InGaAsN SQW sample before and after annealing is presented.
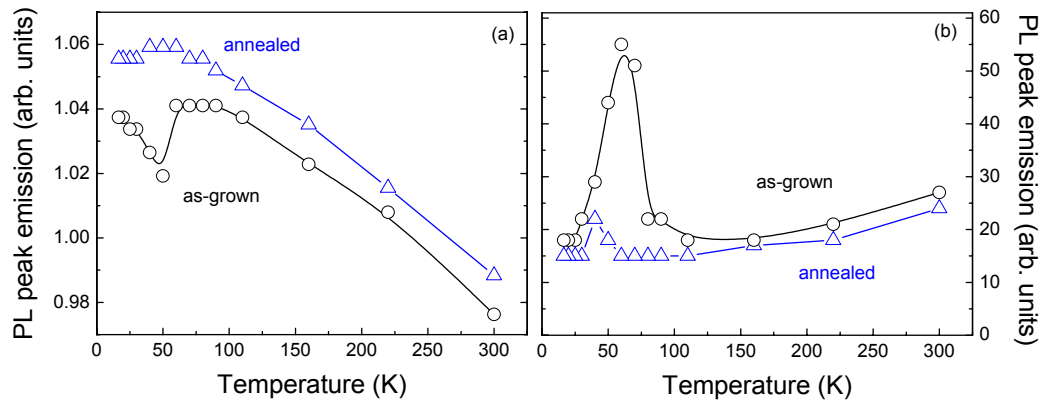
Figure 3.20.: Variation with temperature of the peak emission energy (a) and of the FWHM (b) for an $In_{0.30}Ga_{0.70}As_{0.984}N_{0.016}$ SQW sample as-grown (open spheres) and annealed (open triangles).

In figure 3.20 (a) the photoluminescence peak emission of an $In_{0.30}Ga_{0.70}As_{0.984}N_{0.016}$ SQW sample as-grown (open spheres) and annealed (open triangles) with varying temperature is shown. After annealing, the degree of localization is clearly reduced. In the annealed sample in fact, the peak emission energy describes almost a monotonous decrease with increasing temperature as in the case of fully delocalized carriers. This is also well described by the behaviour of the PL linewidth (plot b). The maximum energy value of the FWHM decreases in the low temperature region almost by a factor of 3.

The application of the above discussed theoretical model to these samples provides a decrease of the value of the characteristic energy E_0 by approximately 20% after annealing. In particular, by estimating E_0 from the temperature of the maximum linewidth (T_2), the following values have been found: E_0 = 4-5 meV (T_2 = 60K) for the as-grown sample, and E_0 = 3 meV (T_2 = 40K) for the annealed sample. As said before, this reduction is attributed to the modification of the morphology of the annealed samples (smoothing of the interfaces, homogenisation of compositional fluctuations, changes in the local environment, dissolution of nitrogen complexes). Moreover, combining the experimental data of the FWHM with the extracted values of E_0, a value for the coupling parameter $N_0\alpha^2 \approx 1$ was found for the as-grown sample and $N_0\alpha^2 \leq 0.25$ was found for the annealed sample. This means that either the concentration of localized states decreases by a factor of 4 or the localization length decreases by a factor of 2 due to the effect of the annealing. Also simultaneous changes in N_0 and α are not excluded.[104]

This method has several potentialities but its application to dilute nitrides has been very limited. So far, it has been employed only to describe the properties of InGaAsN / GaAs QWs in terms of carrier localization. It would be interesting to use this method with a dedicated series of samples. Combined with a micro-structural analysis, it would be possible, for example, to investigate in more detail the effects of annealing on the QW structures from a quantitative point of view.

3.3.4.2 Defects in dilute nitrides

It has been shown that the improvement (or the worsening) of the PL efficiency of the InGaAsN QW does not depend on the morphology of the quantum well but rather on the decrease (or increase) of the density of non-radiative recombination centres. The non-radiative recombination processes are caused by the presence of defects which play an important role within the delocalization temperature range.

Annealing can modify these defects however the resulting PL efficiency can be different on the basis of the annealing environment. This means that annealing conditions are determining factors for the modification of the density of defects and / or that different type of defects are present in the system.

The purpose of the analysis of the following series of samples is to elucidate the role of indium and nitrogen in the changes induced by annealing in different environments. By comparing the results for the two ternary compounds (GaAsN and InGaAs) with those for the quaternary compound (InGaAsN) it is possible to understand if the peculiar behaviour described above and shown in figure 3.12 and 3.13 depends on the presence of only either indium or nitrogen separately or on a combination of both.

Figure 3.21 shows the photoluminescence peak intensity and the peak energy position with varying growth temperature (from about 360 °C to about 480 °C) for three series of samples: (a) and (d) $GaAs_{0.983}N_{0.017}$/GaAs SQWs, (b) and (e) $In_{0.37}Ga_{0.63}As$/GaAs SQWs, (c) and (f) $In_{0.37}Ga_{0.63}As_{0.983}N_{0.017}$/GaAs SQWs. The results are compared for the as-grown (open squares), H_2-annealed (open triangles) and Ar-annealed (open spheres) case.
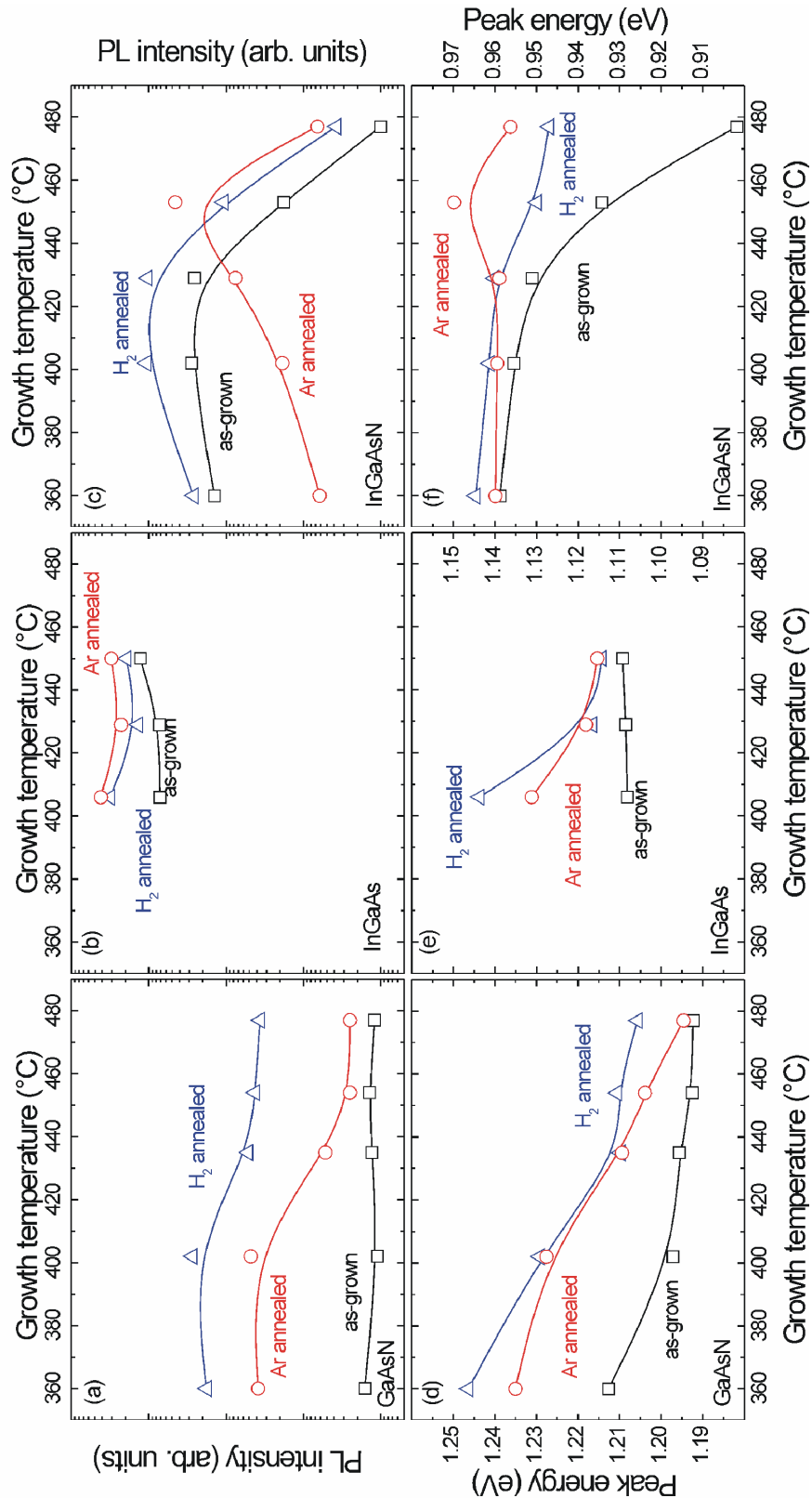
Figure 3.21.: (a, d) PL peak intensity and peak energy position taken at 300 K with varying growth temperature for GaAs$_{0.983}$N$_{0.017}$ SQW samples as-grown (open squares), H$_2$-annealed (open triangles), and Ar- annealed (open spheres). (b, e) PL peak intensity and peak energy position taken at 300 K with varying growth temperature for In$_{0.37}$Ga$_{0.63}$As SQW samples as-grown (open squares), H$_2$-annealed (open triangles), and Ar- annealed (open spheres). (c, f) PL peak intensity and peak energy position taken at 300 K with varying growth temperature for In$_{0.37}$Ga$_{0.63}$As$_{0.983}$N$_{0.017}$ SQW samples as-grown (open squares), H$_2$-annealed (open triangles), and Ar- annealed (open spheres).

Comparing plots (a), (b), and (c) in figure 3.21, it is clear that the N-free samples show the highest PL efficiency. The as-grown PL intensity of the InGaAs samples is three orders of magnitude greater than that of the GaAsN samples. This suggests that nitrogen causes the presence of non-radiative centres which strongly deteriorate the PL efficiency of the QW. On the other hand, it should be mentioned that the low PL intensity of GaAsN/GaAs QWs can also be attributed to the almost absent confinement of the holes. Annealing has a beneficial effect on these defects, however, only the intensities of the H_2-annealed InGaAsN samples reach almost the same order of magnitude compared to that of the InGaAs samples. The best intensity obtained for the GaAsN samples (H_2-annealed) is one order of magnitude lower than the N-free case. This means that the negative effects of nitrogen on the optical efficiency of the system are somehow reduced if indium is also present in the structure. Also in this case, carrier confinement can play an important role to the final PL efficiency of the QW. In fact, by inserting indium into GaAsN, the holes become more confined.

Considering the GaAsN and InGaAs samples, it is possible to notice that in both cases the PL intensity is always improved after the thermal treatments and that the best improvement is obtained for the samples grown at low temperature. The PL intensity of samples annealed in Ar- and H_2 shows the same Tg-dependence. However, while in the GaAsN case the H_2-annealed samples show the highest PL intensity values, in the InGaAs case the Ar-annealed samples show the strongest increase in PL intensity. In the InGaAsN case, as shown in § 3.3.3, the different behaviour between hydrogen and argon-annealed samples depends on the growth temperature. Whilst the H_2-annealed samples show the best PL intensity improvement in the case of low Tg (that is also the behaviour of the as-grown samples), the Ar-annealed samples show the strongest PL intensity increase at high Tg. In addition, for low growth temperatures, annealing in argon atmosphere reduces the radiative efficiency of the as-grown samples. The worsening of the PL intensity can be explained with the appearance, after Ar-annealing, of non-radiative recombination centres. This is shown in figure 3.22 where TEM plan-view images of the InGaAsN sample grown at 400 °C as-grown and Ar-annealed are presented.
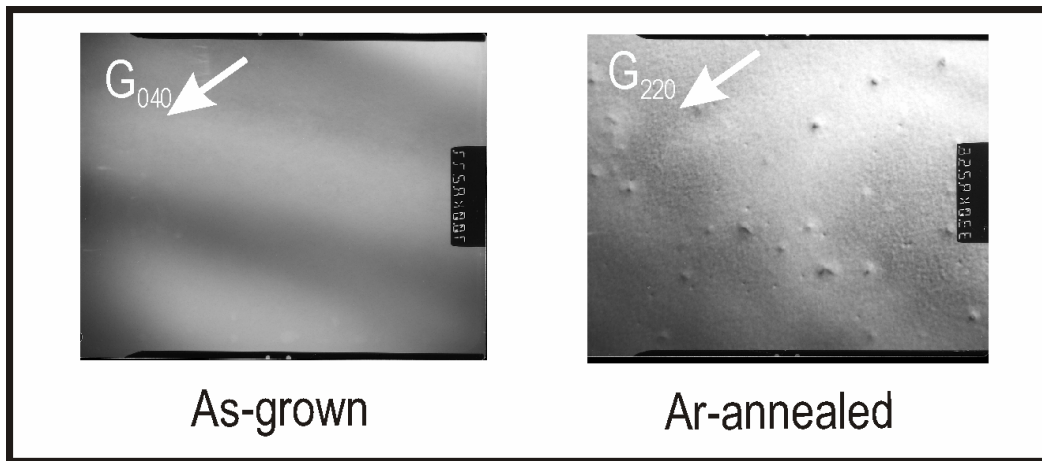
Figure 3 22.: TEM Plan view images of an $In_{0.37}Ga_{0.63}As_{0.983}N_{0.017}$ SQW sample as-grown and Ar-annealed grown at 400 °C.

The TEM images give a "top-view" of the samples. The different bright contrast shows that both the samples have similar structural fluctuations. However, while in the as-grown case the surface of the sample is generally homogeneous, in the Ar-annealed case "point-structures" are present. A more detailed analysis has shown that annealing InGaAsN samples in argon atmosphere leads to the formation of point defect agglomeration and to the possible creation of dislocations.[107] The presence of these non-radiative recombination centres explains therefore the degradation of the PL intensity after Ar-annealing.

Concerning the peak emission energy, it decreases with increasing growth temperature for all the samples. The only exception is constituted by the peak energy value of the as-grown InGaAs and Ar-annealed InGaAsN samples which do not show a clear dependence on Tg. An interesting aspect is that while for the GaAsN and InGaAs materials the blue shift due to annealing (H_2 or Ar) increases with decreasing Tg, for the InGaAsN samples it increases with increasing growth temperature. The behaviour of the peak emission energy with Tg has been explained in § 3.1 for InGaAsN considering the self annealing phenomenon. In Ref. 92 the Tg dependence of the peak position is ascribed to the formation of In-N bonds induced by a point-defect-assisted phenomenon.

In figure 3.21 some interesting results can be found concerning the different effects of H_2 and Ar annealing. Annealing in hydrogen atmosphere induces the strongest beneficial effects on the PL

intensity only for the N-containing samples. This suggests that optical defects related to the presence of nitrogen can be passivated by hydrogen. Moreover, concerning the PL intensity of samples annealed in different environments, InGaAsN QWs behave in a different way compared to the GaAsN and InGaAs QW cases. Particularly, while for GaAsN and InGaAs samples the PL intensity shows the same T_g-dependence after Ar- and H_2-annealing, for InGaAsN samples the two annealing environments lead to a completely different T_g-dependence of the PL intensity. This means that another defect related to the simultaneous presence of In and N should be taken into account and that annealing acts on it differently if performed in H_2 or Ar environment.

In order to describe the peculiar behaviour of the PL efficiency with varying T_g for samples annealed in H_2 and Ar atmosphere, a qualitative model is introduced. This model takes into account the presence of defects in InGaAsN systems. Due to the different nature of these defects, their density varies on the basis of the annealing environment.

Considering the conclusions of the results presented in figure 3.21, one can imagine that during the growth of InGaAsN structures at least two different types of optical defects are formed: Defects $A_{(N)}$, related to the presence of nitrogen, and defects $B_{(In-N)}$ related to the simultaneous presence of In and N.

It is important to emphasize that annealing has two different effects: thermal and chemical. While during annealing in Ar atmosphere, which is an inert gas, only the thermal component is present, during H_2-annealing both the thermal and chemical components must be considered.

The density of defects $A_{(N)}$ increases with increasing T_g. They do not react with the annealing environment and are reduced by thermal treatment. The density of defects $B_{(In-N)}$ decreases with increasing T_g. They react with the H_2-annealing atmosphere and agglomerate during thermal treatment (see figure 3.22).

Defects $B_{(In-N)}$ are passivated by annealing in H_2 atmosphere. This means that in the H_2-annealed samples only defects $A_{(N)}$ are active. Since the number of these defects increase with the growth temperature, before and after H_2-annealing the samples grown at low T_g show the best PL efficiency.

This is consistent with the PL intensity behaviour of the GaAsN and InGaAsN samples annealed in hydrogen.

Defects $B_{(In-N)}$ are present basically only in samples grown at low temperatures. Since they agglomerate after a thermal process, samples grown at low T (Tg < 430 °C) worsen the PL intensity after annealing. This happens only during annealing in inert gas atmosphere such as Ar or As_4. For higher growth temperatures (Tg > 430 °C), the number of these defects is very low and the PL intensity behaves similar to the H_2-annealing case. The presence of defects $B_{(In-N)}$ explains the behaviour of the PL efficiency of the Ar-annealed InGaAsN samples with varying growth temperature.

The above proposed defect-model is a speculative microscopic model that is consistent with the observations made in this chapter. In reality, further experiments, employing different techniques, would be required in order to have a detailed understanding of which type of defects are present in InGaAsN quantum wells and what their role is during annealing. Due to the lack of adequate investigation methods to unambiguously identify these defects, this has been not performed in this thesis work.

3.4 Conclusions of the third chapter

Dilute nitride semiconductors have attracted an increasing amount of attention due to their potential for applications in various electronic and optoelectronic devices and in particular in efficient light emitting quantum well (QW) devices operating within the infrared region. For this reason, in the last years much work has been dedicated to optimise the photoluminescence (PL) intensity and the peak emission energy of (In)GaAsN/GaAs QWs. It has been shown that dilute nitrides are very sensitive to the growth conditions and that the latter strongly affect the morphology of the material.

In this chapter it has been shown the influence of growth conditions, such as the growth temperature and QW composition (indium content) on the morphological and optical properties of InGaAsN / GaAs SQW samples. In particular, annealing effects have been investigated finding out a correlation between the structural and optical modifications in terms of peak energy and PL intensity.

Combining photoluminescence measurements and transmission electron microscopy (TEM) analysis, a correlation between the degree of localization and the homogeneity of the QW has been determined. In particular, it has been found that strongly inhomogeneous structures show a stronger localization effects. On the basis of this result, it has been found that with increasing QW growth temperature and with increasing QW indium content the inhomogeneity of the sample increases.

Concerning the optical properties, both the PL intensity and the peak emission energy vary with the growth temperature although the QW composition remains the same. In particular, the PL intensity decreases with increasing Tg and the emission energy increases with decreasing Tg. This latter blue shift has been explicitly explained by the self-annealing process. On the other hand, varying the indium concentration does not remarkably influence the PL intensity of the QW, especially after annealing. The only exception is for the samples having high indium content ([In] > 34%). In this case, the PL intensity is very low due to the presence of In-rich cluster and / or dislocations due to the high strain induced by the high indium concentration.

From the morphological point of view, annealing has been found to cause a general homogenisation of the QW layer. After annealing in fact, there is a reduction of the localization degree for all the investigated samples.

Most interestingly, the blue shift induced by annealing is dependent on the growth temperature. In addition, after the thermal treatment the emission energy differences among samples grown at different temperatures are strongly reduced. This has been explained considering the modification with annealing of the nitrogen nearest-neighbours configuration. The configuration varies on the basis of the growth temperature. After annealing this difference is eliminated or strongly reduced because the samples reach a similar, common, more stable configuration, that is the In-rich one.

Comparing the optical properties of the QW samples studied in this thesis work with the performance of final devices (lasers), it has been shown that the annealing environment is a very important factor one needs to consider in order to optimise the optical properties of InGaAsN structures. In particular, if the samples are annealed *ex-situ* in an inert gas like argon, the growth conditions to

obtain the best optical properties of the QW coincide with those to obtain the best performance of the lasers, that means high PL intensity and low threshold current at the same growth temperature (Tg $\approx$ 450 °C). On the other hand, if the samples are annealed *ex-situ* in hydrogen, the behaviour is the opposite: the highest PL intensity is reached at growth conditions at which the laser performances are the worst (Tg $\approx$ 400 °C). Most notably, annealing does not always improve the PL intensity of the as-grown samples. The Ar-annealed samples grown at low temperatures (Tg < 430 °C), in fact, worsen their PL intensity considerably compared to that of the as-grown case.

Most remarkably, although on the one hand the annealing environment strongly influences the optical properties of the samples, on the other hand the morphology is not affected by different annealing atmospheres. PL measurements and TEM images have shown that the degree of localization and the homogeneity of the QW is changed in the same way if the samples are annealed in Ar or H_2 atmosphere. As main conclusions it has been found that the PL efficiency is not necessarily correlated to the morphology of the system and, by employing time resolved photoluminescence measurements, that the increase (decrease) of the PL efficiency strongly depends on the decrease (increase) of the density of non-radiative centres.

In the range of temperatures where the carriers are localized, performing a PL analysis with varying excitation power density, it has been verified that the variation of the localization degree after annealing is only due to morphology modifications and not also to defect passivation. These modifications have been quantified in terms of the variation of the density of localized states and localization lengths by using a theoretical model.

Finally, a simple microscopic model has been presented in order to describe which types of defects are created during the growth of InGaAsN QWs and the main effects of annealing. By comparing the evolution with Tg of the PL efficiency and PL energy peak of InGaAsN, GaAsN, and InGaAs SQW samples as-grown and annealed in hydrogen and argon environment, two possible types of optical defects have been proposed. Defects $A_{(N)}$ are related to the presence of nitrogen and do not react with the annealing environment. Their density increases with increasing the growth temperature and is

reduced by thermal treatment. Defects $B_{(In-N)}$ are related to the simultaneous presence of nitrogen and indium and their number decreases with increasing the growth temperature. They react with the annealing atmosphere and are passivated by hydrogen environment. Moreover, they agglomerate by Ar-annealing.

Chapter 4

Band Offsets Analysis in Dilute Nitrides

In semiconductor heterojunctions, the edges of the valence and conduction bands produce band discontinuities across the heterojunction interface. These discontinuities are called valence and conduction band offsets. The band offsets are important parameters in device design and in understanding the physical properties of heterojunction structures. They influence the carrier transport properties both along and across the heterojunctions. The experimental determination of the band offsets in quantum well structures is still a controversial subject. A few methods, including photoemission spectroscopy,[46] capacitance-voltage techniques,[47] optical transition measurements,[48] and charge-transfer techniques [108] are used. Concerning the dilute nitride structures, very few experimental studies were dedicated to analyse the band alignment of (In)GaAsN /GaAs QW structures, and most of them were focussed on the controversial question of identifying the band configuration of GaAsN/GaAs QWs.[49,50,51] Up to now, the study of the band offsets in dilute nitrides has been limited to investigate the influence of nitrogen on the conduction band states of specific sample structures. However, a systematic and quantitative description of the influence of QW parameters such as QW width or QW composition on the band offsets is still missing. Moreover, a study about the influence of the above parameters distinguishing the behaviour of the conduction band offset from that of the valence band offsets is completely absent.

In this chapter, a method based on surface photovoltage measurements will be presented to determine the value of the conduction and valence band offsets in $In_xGa_{1-x}As_{1-y}N_y$/GaAs SQW samples. This method was recently conceived and developed at Infineon Technologies. [87,88,89] At first, the

understanding of this method will be deepened and refined in section 4.1. In section 4.2 and 4.3, this method will be applied to study the influence of various QW parameters on the band offsets of $In_xGa_{1-x}As_{1-y}N_y$/GaAs SQW samples.

4.1 Application of surface photovoltage spectroscopy to determine the band offsets of quantum well structures

Surface photovoltage spectroscopy (SPS) has been employed to study the surface and interface properties of a wide variety of materials and structures, including bulk materials, thin films, nano and quantum structures and (opto) electronic devices.[109] The good sensitivity of SPS to analyse buried interfaces has allowed this technique to obtain successful results for the characterization of multilayer structures. In particular, the possibility has been demonstrated to resolve, at room temperature, all the "symmetric allowed" electron-hole transitions in multi quantum well (MQW) structures.[110] Moreover, a successful application has been found in the field of process monitoring and quality control of multilayer quantum devices due to the possibility to perform a contactless and non-destructive electro-optical characterization.[109]

Only recently, a method based on SPV measurements has been developed to determine the band offsets of a hetero quantum structure.[87,88,89] With this method, the band offsets can be extracted directly from the SPV spectra without the need for additional simulations or the knowledge of other parameters. In the report describing this technique for the first time,[88] however, only a simple case was used to prove its validity and no deep analysis was performed in order to unambiguously identify the different features present in the SPV spectra. In this section, an extended study is presented that gives a more general understanding of the SPV technique applied to type I QW structures. In particular, more features have been found in the spectra for different samples and the transitions they are attributed to have been unambiguously clarified.

For this purpose, two series of samples have been investigated: A series of $In_{0.3}Ga_{0.7}As$/GaAs SQW samples with different well width to study the carrier confinement related to the heavy-hole states, and a series of $In_{0.15}Ga_{0.85}As$ / $Al_xGa_{1-x}As$ SQW samples with different aluminum content in the barrier to investigate the energy level involving the light-hole states. The results obtained from the SPV measurements have been compared with results taken on the same samples employing other optical techniques (like photoluminescence and contactless electroreflectance). Moreover, theoretical calculations and simulations of spectra have been performed to determine the quantized energy levels of the structures investigated.

4.1.1 Optical transitions detected by surface photovoltage measurements

As described in § 2.3.2, this method measures variations in the photovoltage created near the surface by the collection of photo-generated carriers. As the energy of the incident light is varied, the SPV signal can vary whenever photo-generated carriers of different origin are produced, resulting in steps in the spectra. The SPV spectrum of an $In_{0.30}Ga_{0.7}As$/GaAs single quantum well sample is presented in figure 4.1. The SPV signal increases with increasing energy of the incident light in four pronounced steps. The spectrum in figure 4.1 (a) is qualitatively typical for many samples, but it will be later shown that the number of steps may differ depending on the QW parameters. For a low injection of excess carriers, the SPV spectrum can be considered as an absorption spectrum.[109] Thus, the steps therein indicate the onset of different absorption processes occurring in the sample. Figure 4.1 (b) depicts the optical transitions that were discussed in Ref. 88 as the origin of the different steps. Transition 1 is the optical transition with the lowest possible energy, which is the transition between the bound ground states in the valence band and the conduction band of the QW (e_1-hh_1). Transition 2 is the transition from the extended state in the valence band to the bound state of the conduction band (e_1-ch). In Ref. 88, no distinction could be made between two possible origins of transition 3. As indicated in figure 4.1 (b) with dashed lines, transition 3 may originate from the transition between the bound state of

the valence band and the extended state of the conduction band (ce-hh$_1$). However, it may also be due to the transition between the first excited QW states (e$_2$-hh$_2$), i.e. between two bound states. Finally, transition 4 is the excitation of electrons from the extended states of the valence band to the extended states of the conduction band (ce-ch), i.e. it is due to the absorption in the GaAs barrier.[*]
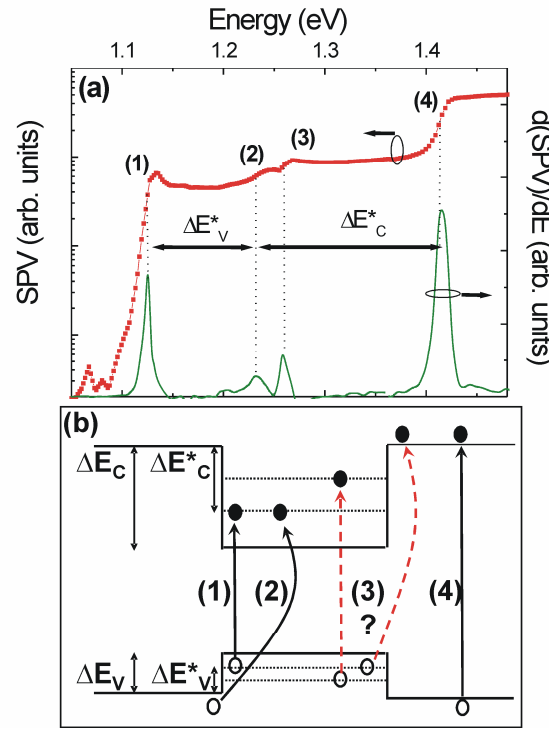
Figure 4 1.: (a) SPV and d(SPV)/dE spectra for a 9 nm-thick In$_{0.3}$Ga$_{0.7}$As SQW acquired at 300 K (line with data points and solid line, respectively). (b) The possible optical transitions as discussed in Ref. : (1) e$_1$-hh$_1$ (ground state), (2) e$_1$-ch, (3) ce-hh$_1$ / e$_2$-hh$_2$, and (4) ce-ch (continuum).

By determining simply the differences between the energies corresponding to these optical transitions, as indicated by the double arrows in figure 4.1 (a), one is able to extract the quantities ΔE^*_C and ΔE^*_V which are related to the band offsets by the expressions

$$\Delta E_C = \Delta E^*_C + e_1$$

$$\Delta E_V = \Delta E^*_V + h_1, \qquad\qquad (4.1)$$

---

[*] It should be mentioned that in Ref. 88, transition 3 was assumed to originate from a bound-to-extended state transition. It will be shown in the following that the assumption is generally incorrect, which means that transition 3 cannot be used for the determination of the band offsets. The values obtained in Ref. 88 are correct because coincidentally the energies of two possible transitions are identical.

where e_1 and h_1 are the first quantized state of electrons and holes, respectively. The energy quantities ΔE^*_C and ΔE^*_V will be called hereafter "practical band offsets" (PBOs). In fact, for the operation of a real device, only ΔE^*_C and ΔE^*_V are of practical interest because they express the real carrier confinement in the QW.

In the SPV spectrum (figure 4.1 (a)), the onset of the optical transitions is indicated by steps in intensity. For the precise determination of the transition energies the derivative of the SPV spectrum as a function of the detected energy has been numerically computed (also shown in figure 4.1 (a)). The maxima of the peaks of the derivative indicate the energy at which the steps appear, i.e. the optical transitions in the structure. All the error bars of the experimental results shown in this thesis are the full widths at half maximum (FWHM) of the peaks in the derivative spectrum. Typically, the resulting precision of these measurements is about 10%.

In the following, a complete identification of the features present in the SPV spectra will be presented.

4.1.1.1 The first and the last step in the spectra

In figure 4.2 the temperature dependence of the ground state and of the barrier of an $In_{0.3}Ga_{0.7}As_{0.984}N_{0.016}$/GaAs SQW are compared as determined by different techniques. The data points with error bars are extracted from SPV spectra using the values of the maxima in the derivative spectra which correspond to the steps 1 and 4. The crosses show the photoluminescence (PL) peak positions of the same sample, and the dashed line the theoretical behaviour of the GaAs band gap as a function of temperature (Varshni equation).[78,111] The good agreement between the SPV data and the PL results for step 1 and the theoretical prediction for step 4 confirms the interpretation of the step 1 and 4 as described in figure 4.1 (b).
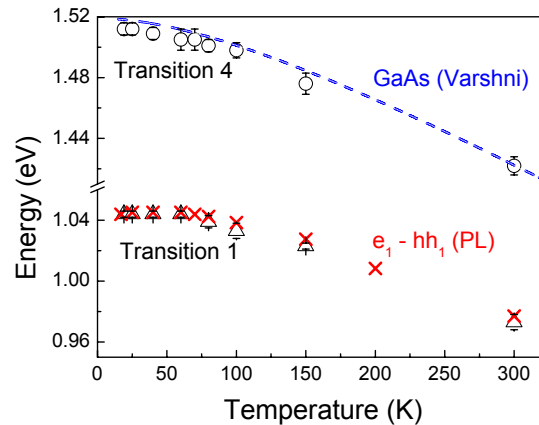
Figure 4.2.: Temperature dependence of the ground state (transition 1) and of the barrier (transition 4) of a 6.5 nm-thick $In_{0.3}Ga_{0.7}As_{0.984}N_{0.016}$ SQW as determined from SPV spectra (data points with error bars). Comparison of the same quantities measured with different techniques: PL for the ground state (crosses) and theoretical Varshni curve for the GaAs barrier (dashed line).

4.1.1.2 The third step in the spectra

As already said above, in the paper describing the method to determine the band offsets employing SPV measurements for the first time,[88] the interpretation of step 3 was not unambiguous. The clear distinction between e_2-hh_2 and ce-hh_1 as the origin of step 3 was prevented by the very small energy difference between these two transitions for that sample (less than 10 meV). In the following, with the help of dedicated samples it will be clarified whether step 3 comes from a bound-to-free (ce-hh_1) or from a bound-to-bound transition (e_2-hh_2).

In order to elucidate the origin of step 3, a series of InGaAs samples with different QW widths has been analysed. As all the other structural parameters remained the same, the only difference between the samples of this series is the quantization energy of the electron and hole states in the QW. While this influences all states, the effect is greater on states of higher order. Moreover, for the thinner QWs only the ground states are bound. Correspondingly, step 3 should vanish for these samples, if it is due to e_2-hh_2.

The SPV spectra for this series are shown in figure 4.3 (a). As expected, the transitions related to the GaAs barrier (step 4) have always the same energy. The experimental value of (1.42 ± 0.01) eV is

in good agreement with the value of the band gap of GaAs at 300 K (1.425 eV). This is well illustrated in

4.3 (b) where the derivative of the surface photovoltage spectra is shown. The ground state (transition 1)

moves towards higher energy values for decreasing well width, since the quantization energy increases.

The position of step 3 depends also on the well width. Passing from a width of 9 nm to 7 nm, it moves

towards higher energies and completely disappears for the samples with a QW width of 5 nm and 3 nm.

This implies that the occurrence and the energy position of step 3 depend on the confinement of the

carriers in the QW.
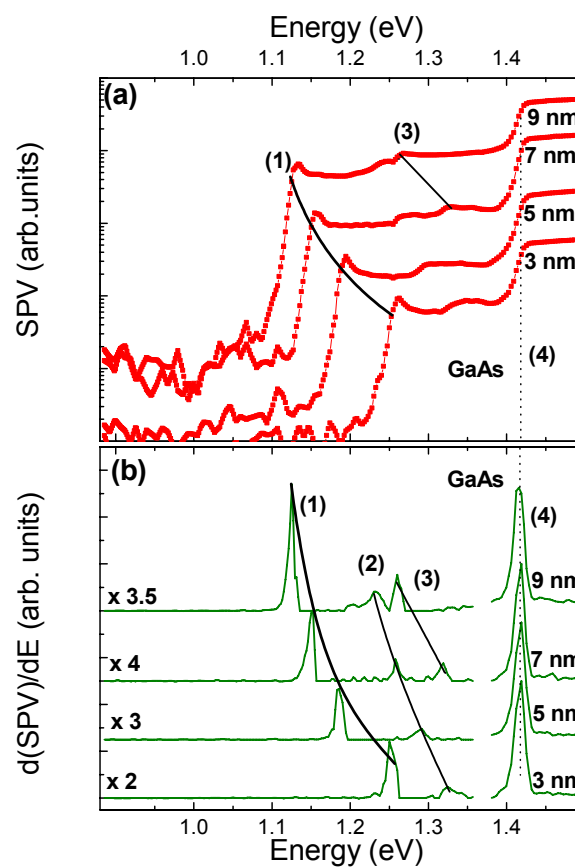
Figure 4.3.: (a) SPV spectra for $In_{0.3}Ga_{0.7}As$ SQWs with different well widths acquired at 300K. The change of the position of transition 1 for different well widths is indicated by a solid line. The band gap of GaAs at 300 K is indicated by a dotted vertical line. The position of step 3 is also indicated. (b) Derivatives of the SPV spectra as a function of the detected energy. The peaks correspond to the steps in intensity of the SPV spectra. The first part of each spectrum (up to 1.38 eV) has been magnified for clarity; on the left-hand side of the curves the multiplication factors are shown.

InGaAs/GaAs quantum wells have been studied for many years, and all the necessary material

parameters are well known.[111, 112] This allows to simulate the energy levels of the measured

$In_{0.3}Ga_{0.7}As$/GaAs QWs with high accuracy. The calculations were performed taking into consideration

both the hydrostatic and the uniaxial strain including the relevant deformation potentials. To determine the quantized states, the analytical solution of the Schrödinger equation for a square well potential has been used. The excitonic binding energy was taken equal to 8 meV.[113]

The simulated energies of the transitions e_1-hh_1 and e_2-hh_2 at 300 K are presented in figure 4.4 (solid and dashed lines, respectively). The calculated position of the transition ce-hh_1 is also shown (dotted line). The positions of the steps 1 and 3 were extracted from the spectra in figure 4.3 (b) and were also included in figure 4.4 (open squares and open spheres, respectively). In order to obtain a good agreement between the simulated and the experimental data for the ground state emission energy of the QW (e_1-hh_1), the conduction band offset ratio $Q_C = \Delta E_C/(\Delta E_C + \Delta E_V)$ was varied in the range of $0.6 \div 0.7$, as suggested by other groups.[112,114] The best fit was obtained for $Q_C = 0.65$. Also, simulations were carried out assuming slightly different indium contents [In]. The best agreement was found for [In] = 32.5%[*]. As one can see in figure 4.4, the resulting simulation of the transition e_2-hh_2 matches the experimental points corresponding to the transition 3. While for the 7 nm-QW the experimental value could also be explained by the transition ce-hh_1, this is clearly not the case for the 9 nm-QW. Also, if the transition ce-hh_1 caused a feature in the spectrum, this should occur for the QW widths 3 nm and 5 nm as well, which is not observed. All of this suggests that step 3 is due to the transition between the first excited electron and heavy-hole states.

---

[*] The deviation from the nominal value is explained by the fact that the ion gauge monitoring the beam flux was not operational at the time these samples were grown.
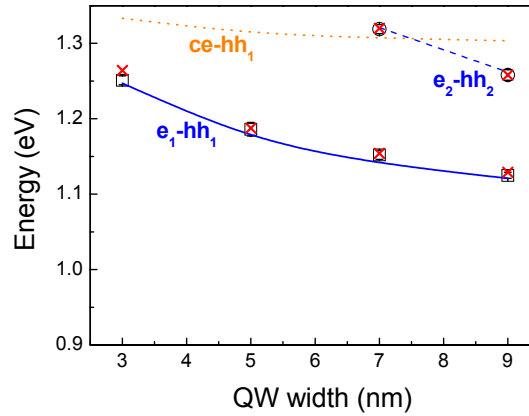
Figure 4.4.: Energy values of transition 1 (squares) and step 3 (spheres) in dependence of the well width. The solid and the dashed lines are the calculated values of e_1-hh_1 and e_2-hh_2, respectively. The dotted line is the calculated value of the transition ce-hh_1. The small crosses are the results from the electroreflectance measurements.

In order to further validate this interpretation, another optical technique able to identify the different energy levels in the QW was employed. Thus, contactless electroreflectance (ER) measurements were performed on the same series of samples. In figure 4.5 the experimental data (open circles) of the samples with the well widths of 7 nm (a) and 9 nm (b) are shown. The good agreement with the simulations, shown as solid lines in the figure, allows to accurately determine the energetic positions of the different optical transitions in the SQWs (marked by arrows). For the analysis of the contactless ER measurements, multi-oscillator fits assuming a Gaussian broadening have been employed in order to extract the energetic positions of the different transitions (oscillators) from the spectra. For the quantum well transitions, the first derivative functional form (FDFF) has been applied, which is the suitable lineshape for excitons in such structures. For bulk material (GaAs), the common third derivative functional form (TDFF) has been used. Also in this case, in order to have a good simulation, the nominal sample parameters had to be slightly modified. The indium content was assumed to be 32% and the value of the QW widths was assumed to be about 3% larger than the nominal one. In figure 4.4 the transitions corresponding to the ground (e_1-hh_1) and to the excited states (e_2-hh_2) extracted from the ER spectra are shown (small crosses). The excellent agreement gives further evidence that step 3 in the SPV spectra corresponds to the transition e_2-hh_2.

Figure 4.5 shows that ER measurements allow the determination also of optical transitions between subbands of different quantum number, i.e. e_1-hh_2, e_2-hh_1, e_2-hh_3... Since the built-in electric field generated in the SPV measurements is at least five times smaller than the typical electric field employed for ER measurements, SPV spectra show only bound-to-bound transitions between subbands of the same quantum number. This will be discussed in § 4.1.4.
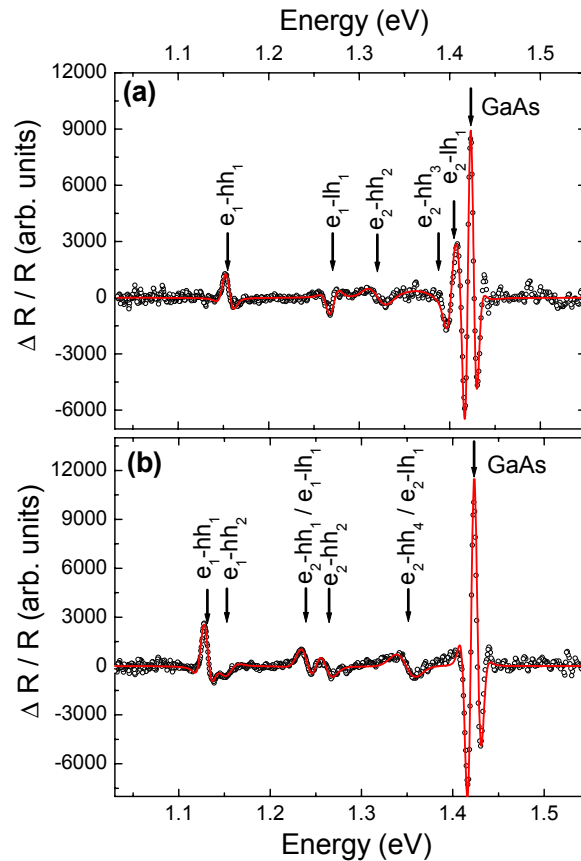
Figure 4.5.: Contactless electroreflectance measurements (open circles) at 300 K of a 7 nm-thick $In_{0.30}Ga_{0.70}As$ (a) and a 9 nm-thick $In_{0.30}Ga_{0.70}As$ SQW (b). The solid lines are the multi-oscillator fits which were used to determine the energetic positions of the different transitions in the QWs (indicated by arrows in the figure).

In order to elucidate if the transition ce-hh_1 could give rise to a step in such SPV-spectra, an absorption spectrum corresponding to the SPV-spectrum shown in figure 4.1 (a) has been simulated. For this purpose the multiband 8 x 8 **k · p** method was employed. The electron and hole levels and their wave functions have been calculated by using the nano device simulation tool nextnano³ taking into account strain, deformation potentials and the coupling between the conduction and valence bands.[115] For simplicity, the exciton correction for the energy levels was neglected. From these levels, the optical

absorption spectra have been calculated considering the non-parabolic $\mathbf{k} \cdot \mathbf{p}$ dispersion, i.e. also the energies and wave functions for $\mathbf{k}_{\parallel} \neq 0$.

The 9 nm-thick InGaAs SQW has been considered because in this case the transitions e_2-hh_2 and ce-hh_1 differ from each other by about 40 meV, as can be seen in figure 4.4. This offers the possibility of a clear distinction between these two transitions. In figure 4.6 the experimental SPV spectrum is shown along with the simulated absorption spectra for light propagation perpendicular to the QW along the z-direction (solid line) and in the QW-plane with perpendicular electric field polarization (dashed line). The calculated spectrum (x-polarized) fits the experimental data quite well, which confirms the validity of the method and the conclusions regarding the nature of step 3. In both the experimental and simulated spectra the transition from the bound state of the valence band to the extended state of the conduction band is absent. In the region of the spectrum where the transition ce-hh_1 would be expected (about 1.30 eV, see figure 4.4) there is no variation in intensity.

In conclusion of this section, step 3 in the SPV spectra is caused by the bound-to-bound transition e_2-hh_2, and the bound-to-free transition ce-hh_1 does not induce any step.
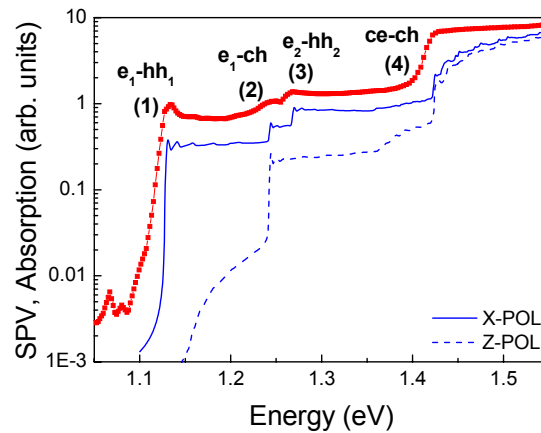
Figure 4.6.: SPV spectrum for a 9 nm-thick $In_{0.3}Ga_{0.7}As$ SQW acquired at 300 K (line with data points) compared with calculated (using k·p method) InGaAs absorption spectra for light propagation perpendicular to (solid line) and in the QW plane with perpendicular E-field polarization (dashed line).

4.1.1.3 The second step in the spectra

In Ref. 88, the nature of step 2 was analyzed partly with the help of a QW transmission spectrum for in-plane light propagation and perpendicular electric field polarization. For this geometry, only optical transitions involving light holes are allowed. Since the transmission decreased at the position of step 2 and since light holes were not confined in the respective QW, step 2 was associated with the transition e_1-ch. An analogous behaviour can be seen in figure 4.6. The z-polarized curve corresponds to the absorption in transverse magnetic mode (TM) for which only transitions involving light hole can contribute. In the structures here analysed the energy level of the light holes lies within a few meV to the valence band energy. For this reason, the onset of the absorption in the z-polarized mode must occur in the immediate proximity of the step attributed to e_1-ch, as it is indeed the case in figure 4.6.

All the samples investigated until now have the peculiarity that the light-hole energy level is located very close to the valence band edge of the QW barrier. Hence, step 2 in the SPV spectra could possibly have been caused by a transition between e_1 and the lightly bound level lh_1. This could possibly mean that bound-to-free transitions might not be observable at all. In order to clarify this uncertainty, a series of samples for which the light-hole level changes from free to bound has been studied.

The SPV spectra of $In_{0.15}Ga_{0.85}As/Al_xGa_{1-x}As$ SQW samples with $0 < x < 0.3$ are shown in figure 4.7 (a). The derivatives of the spectra are shown in figure 4.7 (b). As expected, the position of the step on the right-hand side of the spectrum, which is attributed to the transition in the barrier (ce-ch), moves to higher energies as the aluminum content in the barrier is increased from 0% to 7.5%. For higher aluminum contents, this step is located beyond the range of energies accessible to the experimental set-up employed for these measurements. Most notably, the presence of aluminum in the barrier gives rise to an additional step (indicated by a dotted-dashed line in the figure) close to the one related to the transition e_1-hh_1 (solid line). Thus, there are altogether five steps in the spectrum. It is known that light holes are not confined for an $In_{0.15}Ga_{0.85}As/GaAs$ structure.[114] Adding more and more Al to the barrier,

the carrier confinement increases and the light holes become bound. This suggests that the additional step is related to bound light holes, with the transition e_1-lh_1 being the most likely candidate.
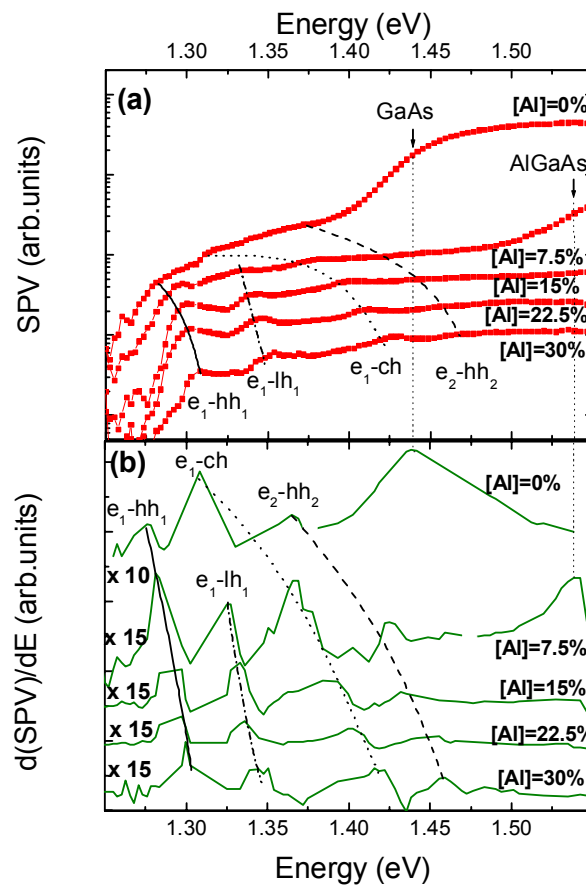
Figure 4.7.: (a) SPV spectra for 9nm-thick $In_{0.15}Ga_{0.85}As/Al_xGa_{1-x}As$ SQWs with different aluminum content in the barrier (0 < x < 0.3) acquired at 275 K. The optical transitions visible in the spectra are indicated with different lines as guides for the eye: solid line (e_1-hh_1), dotted-dashed line (e_1-lh_1), dotted line (e_1-ch), and dashed line (e_2-hh_2). The band gap of the barrier GaAs and of the barrier $Al_{0.075}Ga_{0.925}As$ at 275 K are indicated by a dotted vertical line. (b) Derivatives of the SPV spectra as a function of the detected energy. The peaks correspond to the steps in intensity of the SPV spectra. The first part of each spectrum has been magnified for clarity; on the left-hand side of the curves the multiplication factors are shown.

Employing the same method used for the series of InGaAs SQW samples, the relevant QW states were simulated in order to verify the nature of the different steps. The results of these simulations are displayed in figure 4.8 along with the experimental values for the first four steps in the spectra. The good agreement confirms that the additional step is caused by the transition e_1-lh_1.

It is important to stress here that independently of the presence of the other steps, the transition e_1-ch induces a step in the spectrum in any case. This is a fundamental feature for this method on the basis of which one is always able to determine the band offsets of the structure, provided that the

bound-to-free transition e_1-ch can be identified with one of the steps in the spectrum. This will be discussed in more detail in section 4.1.3.
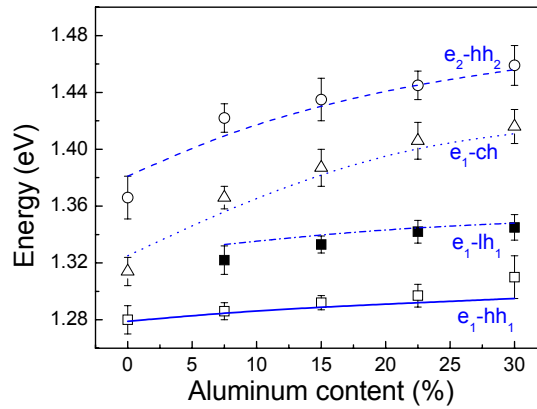
Figure 4.8.: Experimental points of the energy transitions extracted by the SPV spectra in function of the aluminum content. The solid, the dotted-dashed, the dotted, and the dashed lines are the calculated values of the transitions e_1-hh_1, e_1-lh_1, e_1-ch, and e_2-hh_2, respectively.

4.1.2 Refined interpretation of the surface photovoltage spectra

Combining the results obtained in the previous section, it is possible to give a complete interpretation of the surface photovoltage spectra. SPV spectra are characterized by different steps which correspond to different optical transitions in the QW. These transitions have been recognized as bound-to-bound (e_1-hh_1, e_1-lh_1, e_2-hh_2), bound-to-free (e_1-ch), and free-to-free transitions (ce-ch). This is well described by the spectrum of the sample with [Al] = 7.5% in the barrier which contains all the transitions mentioned above (see figure 4.9 (a)). These optical transitions are indicated in figure 4.9 (b). Passing from low to higher energies, the first step (1) is clearly associated to the absorption of the ground state (e1-hh1). The last one (5) is, without doubt, related to the absorption in the barrier. It has been demonstrated that between these two steps the transition from the extended state of the valence band to the bound state in the conduction band (e_1-ch) (3) can always be detected. The observation of this bound-to-free transition distinguishes this SPV method from many other techniques like PL or photoreflectance (PR) and enables the easy determination of band offsets, as will be discussed in more detail later. Depending on the QW parameters, the bound-to-bound transitions e_1-lh_1 (2) and e_2-hh_2 (4)

generate steps in the SPV spectrum. Further bound-to-bound transitions could also generate steps if the QW contains more bound states.
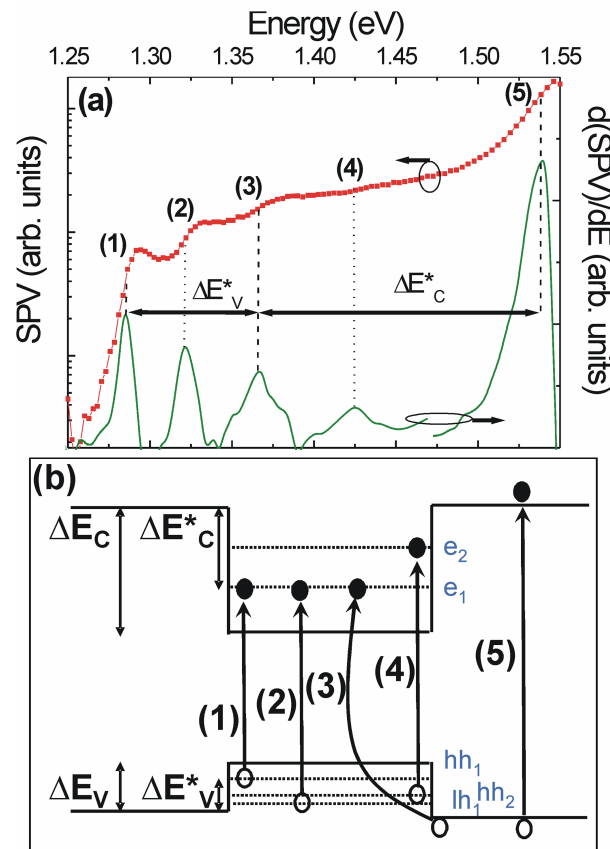
Figure 4.9.: (a) SPV and d(SPV)/dE spectra for a 9nm-thick $In_{0.15}Ga_{0.85}As/Al_{0.075}Ga_{0.925}As$ SQW acquired at 275 K. (b) Schematic drawing of the optical transitions visible in the spectrum: (1) e_1-hh_1, (2) e_1-lh_1, (3) e_1-ch, (4) e_2-hh_2, and (5) ce-ch (continuum).

In the spectra no bound-to-free transitions other than e_1-ch have been seen. Transitions involving the conduction extended states and valence confined states (e.g. ce-hh_1, ce-lh_1, ce-hh_2) do not seem to generate any step in the SPV spectra, at least with the sensitivity and resolution of these measurements. This suggests that these transitions are very weak. The above finding is in accordance with a previous report. Ksendzov et al., [116] employing polarization-modulated absorption measurements for an $In_{0.25}Ga_{0.75}As/GaAs$ SQW structure, have shown a strong difference in intensity between the bound-to-free transitions involving the confined electrons or the confined holes states. In particular, in their absorption spectra only the e_1-ch transition generates a clear step in intensity. Although they do not give any explanation for that, they found that the geometry of the structures can influence the step intensity.

In a calculation, they demonstrated that increasing the number of the wells in the sample one is able to improve the step-like feature in an absorption spectrum derived from a bound-to-free transition and, in this way, improve the intensity of the weakest transitions. Further investigations are necessary in order to verify this point.

4.1.3 Determination of the band offsets

Band offsets of a QW structure are not simple to measure. The majorities of the electronic and optical methods are indirect and, in order to give reasonable results, need the support of simulations.[117] For such simulations it is necessary to know accurately the parameters of the structures. This is not always possible, especially for some particular materials like the dilute nitrides for which many fundamental parameters still remain unknown.

The main advantage of the presented method here is the possibility to determine the value of the band offsets (in first approximation considering the practical band offsets) of a QW structure simply by analysing a SPV spectrum. The basis of this possibility is the fact that, in contrast to most other techniques like PL, excitation photoluminescence (PLE) and PR, a bound-to-free transition induces a clear feature in the SPV spectra. The only difficulty consists in the exact identification of the steps in the spectrum without employing any type of simulation or calculation to determine the energy states of the structure. In particular, the identification of the transitions related to the ground state and to the barrier as well as of the bound-to-free transition e_1-ch is fundamental for the determination of the band offsets. The former two transitions are easily found as the first and the last step in the spectrum. Thus, the crucial point is to identify the transition from the electron bound state to the extended valence state (e_1-ch).

It has been seen that for QW structures with $\Delta E_C > \Delta E_V$, with a well width less than 10 nm and with a type I band configuration, e_1-ch is the first step at energies above the step corresponding to the transition e_1-hh_1 (figure 4.3). However, if the light hole levels are bound in the QW, this rule does not

apply any more because in this situation a step corresponding to the transition e_1-lh_1 appears between the steps related to the transitions e_1-hh_1 and e_1-ch, respectively (figure 4.10). In this case, however, the excitonic enhancement characteristic for the two ground states can be used as the discerning element. An example is shown in figure 4.10 in which the SPV spectra of an $In_{0.3}Ga_{0.7}As/GaAs$ SQW and of an $In_{0.15}Ga_{0.85}As/Al_{0.15}Ga_{0.85}As$ SQW are compared. The excitonic features of the ground states e_1-hh_1 and e_1-lh_1 are clearly visible in the spectra. Therefore a guiding rule could be that e_1-ch is associated with the first step at energies above the ground state without excitonic enhancement.
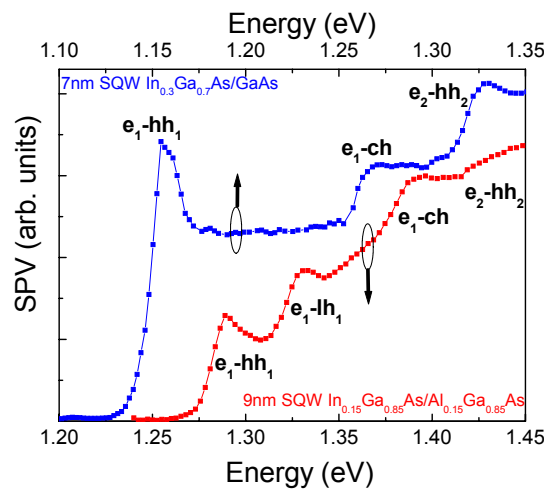
Figure 4.10.: SPV spectra of a 7 nm-thick $In_{0.3}Ga_{0.7}As/GaAs$ SQW sample and a 9 nm-thick $In_{0.15}Ga_{0.85}As/Al_{0.15}Ga_{0.85}As$ SQW sample taken at 300K. The transitions e_1-hh_1 and e_1-lh_1 show excitonic features. This helps to identify the position of the step e_1-ch. Note that the two spectra refer to two different energy scales.

In an unknown sample with arbitrary type I band offsets and unknown well width, SPV measurements alone cannot be used unambiguously to identify the nature of all the steps present in the spectra. In this case, additional optical investigations (e.g. PLE or ER) are necessary in order to identify the bound-to-bound transitions characteristic for that structure and to recognize in the SPV spectrum the transition e_1-ch required to calculate the practical band offsets.

Once the bound-to-free transition e_1-ch is identified, the practical band offsets ΔE^*_V and ΔE^*_C can easily be extracted from the SPV spectra simply by determining the differences between the energetic positions of the steps related to the transitions e_1-hh_1 and e_1-ch, and e_1-ch and ce-ch, respectively (see

_____

figure 4.1 (a)). In the InGaAs/GaAs SQW thickness series (figure 4.3) for example, these transitions correspond to the steps 1, 2, and 4. This is not the case for the InGaAs/AlGaAs [Al] series (figure 4.7), for which the detection of the transition ce-ch was in most cases prevented by the limitations of the experimental set-up employed: only signals up to 1.55 eV could be detected.

From the derivatives of the SPV spectra in figure 4.3 (b), the practical band offsets of the InGaAs/GaAs series have been extracted and plotted, as a function of the well width, in figure 4.11. The experimental data points show an increase of both ΔE^*_C and ΔE^*_V with increasing well width. Since the band offsets remain unchanged, this increase is due only to the decrease in energy of the values of the first quantized state for electrons and holes. Using again the value of $Q_C = 0.65$ and the other structural parameters described in 4.1.1.2, the PBOs were simulated (dashed lines in figure 4.11). The very good agreement between the experimental data and the simulations confirms that what one can extract from the surface photovoltage spectra is exactly the energy difference between the conduction (valence) band offset and the first quantized energy state of electrons (holes).
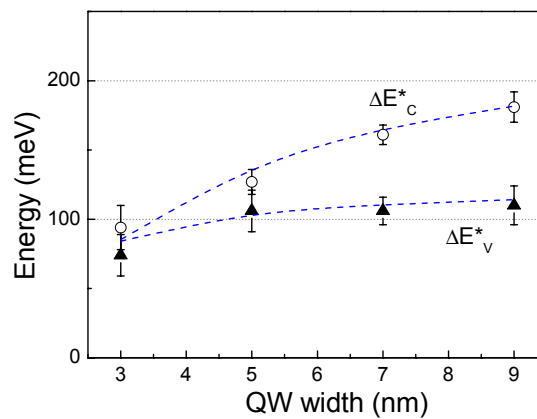
Figure 4.11: Experimental values of the practical band offsets ΔE^*_C and ΔE^*_V extracted from the SPV spectra of $In_{0.3}Ga_{0.7}As$ SQWs as a function of the well width. The dashed lines are the theoretical simulations of the same quantities.

4.1.4 Advantages of the method: comparison with other techniques

It is well known that the energy dependence of the density of states of a QW leads to a staircase-like absorption spectrum for the transitions between confined states.[118] However, little attention has

been paid to the effects of transitions between confined and extended states on the absorption spectra. Different groups,[116, 119] employing different experimental techniques (PLE, PR), have shown the possibility to detect bound-to-free transitions. The majority of the experiments were performed on multi quantum well structures and it was shown that the contribution of these transitions was small compared to the contribution of the transitions between confined states. It should be noted here that the use of multi QW samples is not always possible due to strain considerations. In one case for a SQW sample,[116] however, employing polarization-modulated absorption measurements, it was shown that bound-to-free transitions have the same strength and produce the same step-like absorption features as bound-to-bound transitions, at least for the transition e_1-ch. Nevertheless in this reference, the data in the spectra were reliable only up to the energy position of the first excited state. At that point, in fact, the strong absorption in the substrate prevented the possibility to detect other transitions inside the SQW.

In contrast to this, SPV has the advantage to allow the detection of all bound-to-bound transitions and also of bound-electron-to-free hole-transitions, with high sensitivity even in single quantum well samples. Bound-to-bound transitions must be intended here between subbands of the same quantum number (e.g. e_1-hh_1, e_1-lh_1, e_2-hh_2,…). Transitions between subbands of different quantum number (e.g. e_1-hh_2, e_2-hh_3,…) do not generate any step in our SPV spectra.

Compared to photoluminescence spectroscopy that gives clear information only about the first quantum transition (the excited states can be detected only with a large excitation power density), SPV spectra easily resolve transitions between excited states in the QW. Further advantages of this measurement technique are the simple experimental set-up compared to other optical measurement techniques like PLE and the fact that the samples must not be subject to special treatments (e.g. thinning process for some cases in transmission spectroscopy). Moreover, the simple structure of the samples employed in the measurements allows the simulation of the energy levels in the QW with high accuracy.

The presented results here show that simply by employing SPV it is possible to obtain comprehensive information about SQWs which otherwise could be achieved only by combining different optical techniques and theoretical calculations.

4.2 Application of the method to InGaAsN / GaAs structures

The results presented in section 4.1 have shown that from the SPV spectrum, the transitions between the ground and the excited states in the QW and the practical band offsets can be extracted at the same time. Thus, by measuring the SPV spectra of a small series of samples the influence of different QW parameters on both the conduction and valence band states can be studied.[120] This is a very interesting aspect in order to improve the knowledge about the band offsets of dilute nitrides. In fact, a systematic analysis of the influence of QW parameters on the conduction and valence band offsets separately is a novelty in the literature of III-N-V compounds. In this section, the results of two series of $In_xGa_{1-x}As_{1-y}N_y$/GaAs SQW samples with varying nitrogen and indium content are presented. The evolution of the practical conduction and valence band offsets was found in dependence of both nitrogen and indium concentration. In addition, employing the band anti-crossing model, the variation of the conduction band offset ratio with N and In content was obtained for the same series of samples.

4.2.1 Influence of the nitrogen content on the energetic states and band offsets of InGaAsN quantum wells

In order to understand the influence of nitrogen on the band states of dilute nitride quantum structures, a series of several $In_{0.34}Ga_{0.66}As_{1-y}N_y$ SQWs samples with varying nitrogen concentration has been investigated. In figure 4.12 the SPV spectra taken at 300 K and the corresponding derivatives of four samples of the N-series with a nitrogen content of 0%, 0.3%, 1.25%, and 2.4% are shown. As expected, the transition related to the ground state in the QW (e_1-hh_1) shifts toward lower energy values

with increasing nitrogen content, while the transition corresponding to the GaAs barrier is fixed in energy. With increasing nitrogen content, the derivative spectra become noisier. This is attributed to a degradation of the crystal quality with increasing nitrogen concentration.
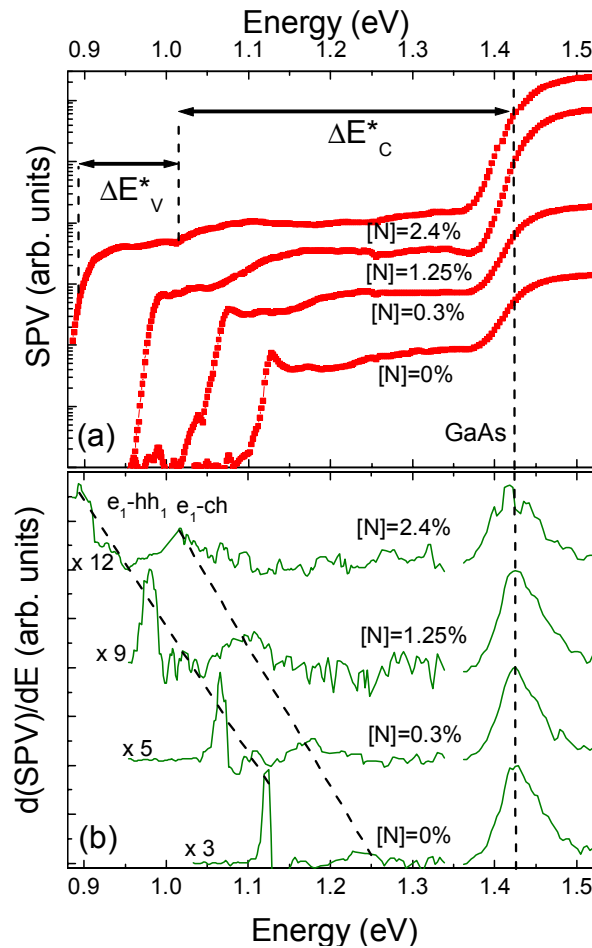
Figure 4.12.: (a) SPV spectra acquired at 300 K for $In_{0.34}Ga_{0.66}As_{1-y}N_y$/GaAs SQWs with varying nitrogen content. (b) Derivatives of the SPV spectra as a function of the detected energy. The parts below 1.35 eV have been magnified by a factor that is indicated on the left-hand side of the spectra.

Looking at the spectra in figure 4.12, it is possible to notice the strong red shift of the step related to the ground state with adding a small amount of nitrogen. Moreover, a different behaviour of ΔE^*_C with varying [N] is notable compared to ΔE^*_V. The three dashed lines in figure 4.12 (b) denote the transitions e_1-hh_1, e_1-ch, and ce-ch, respectively (§ 4.1.3). While the relative distance of the first two lines (ΔE^*_V) remains almost constant with varying nitrogen content, the relative distance of the last two (ΔE^*_C) is strongly modified by varying the N concentration. However, for a deeper and more complete description

of the evolution of the energy states in dilute nitrides with nitrogen content, theoretical support is desirable. This will be discussed in the following subsection.

4.2.1.1. Application of the band anti-crossing model to simulate the energy levels in dilute nitrides

Due to the highly localized nature of the perturbation introduced by the N atoms, it is not possible to use the same theoretical methods as described for the N-free structures in 4.1.1.2 in order to simulate the energy levels of dilute nitride SQWs. For this reason the band anti-crossing model (BAC) was employed for the calculations.[19,32] As described in § 1.1.2.1, this model consists of two interacting energy levels, one at the energy E_M associated with the extended conduction band edge states of the (In)GaAs matrix, and the other one at energy E_N associated with the localized N impurity states. The interaction between these two levels is described by a matrix element $V_{NM} = C_{NM}\sqrt{y}$, where C_{NM} is the band interaction parameter and y is the nitrogen concentration. This interaction leads to a characteristic splitting of the conduction band into two non-parabolic sub-bands. For k = 0, the energies of the sub-bands for InGaAsN QW structures can be expressed as

$$E_{\pm}(\mathrm{In}_x\mathrm{Ga}_{1-x}\mathrm{As}_{1-y}\mathrm{N}_y) = \frac{E_M(x) + E_N \pm \sqrt{[E_M(x) - E_N]^2 + 4V^2{}_{NM}(x,y)}}{2}. \qquad (4.2)$$

In addition, the electron effective mass can be approximated as[45]

$$\frac{1}{m^*{}_e} = \frac{1}{2m_M}\left[1 - \frac{E_M - E_N}{\sqrt{(E_M - E_N)^2 + 4V^2{}_{NM}}}\right], \qquad (4.3)$$

where m_M is the effective mass of the InGaAs ternary compound (E_M band near k = 0). Taking into account the indium dependence of the nitrogen impurity level, the following expression has been employed to calculate E_N:[121]

$$E_N(x) = 1.65(1-x) + 1.44x - 0.38x(1-x).$$

(4.4)

In addition, by means of tight-binding calculations it has been found that

$$E_M = E_{(In)GaAs} - [N]\alpha,$$

(4.5)

where α = 1.55 eV.[32]

In this way it is possible to calculate the band gap of the quaternary material and then, by solving the Schrödinger equation for a square well potential, the quantized states in the QW. In the simulation, the strain effects are calculated considering the hydrostatic (δE_H) and uniaxial (δE_S) deformation potentials of the N-free semiconductor matrix (InGaAs, in this case). The presence of nitrogen is taken into consideration in the strain element $\varepsilon = (a_s - a_w)/a_w$, where a_s and a_w are the lattice constant of the substrate (GaAs) and well (InGaAsN), respectively.

This approach, that is only an approximation, is able to reproduce the experimental data in a satisfactory way. In figure 4.13, the ground states of a series of $In_{0.34}Ga_{0.66}As_{1-y}N_y$ SQW samples with varying nitrogen content are measured with SPV spectroscopy and are presented along with the calculated values of the same quantities. The simulation was performed taking C_{NM} and the conduction band offset ratio $Q_C = \Delta E_C / (\Delta E_C + \Delta E_V)$ as fitting parameters.
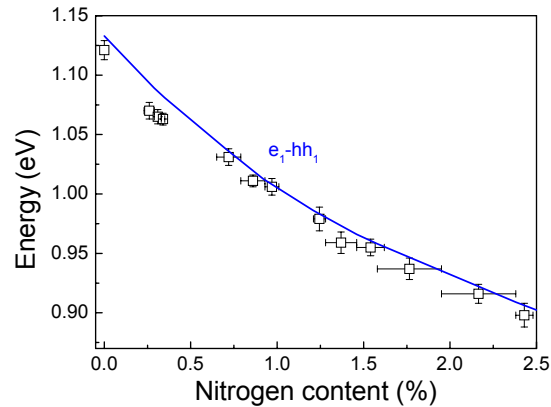
Figure 4.13.: Experimental values of the ground states of $In_{0.34}Ga_{0.66}As_{1-y}N_y$ SQW samples extracted from SPV spectra (open squares) and simulation of the same quantities employing the BAC (solid line).

The data are in agreement with the theoretical calculations within the experimental error bars. The difference between the experimental data and the simulation in the region of very low nitrogen content is explained considering the presence of different N-cluster states for [N] < 0.3%.[122] The results show that with varying the nitrogen content from 0% to 2.4% the ground state emission energy changes from a value of 1.121 eV to a value of 0.898 eV yielding a red shift of about 225 meV. This is consistent with the findings of other groups who report a reduction rate of the dilute nitride band gap of about 100 meV per 1% of nitrogen.[19,52]

4.2.1.2. Evolution of the conduction and valence practical band offsets with varying nitrogen content

The energy values of the practical conduction and valence band offsets were extracted from the SPV spectra as explained in figure 4.12 (a). The PBO values of the complete N-series are shown in figure 4.14 (a). While the energy value of ΔE^*_C (spheres in the figure) strongly increases with increasing nitrogen content (from about 170 meV for 0% of nitrogen to about 400 meV for 2.4% of nitrogen), the value of ΔE^*_V (triangles in the figure) is basically unaltered by the incorporation of nitrogen (about 100 meV).
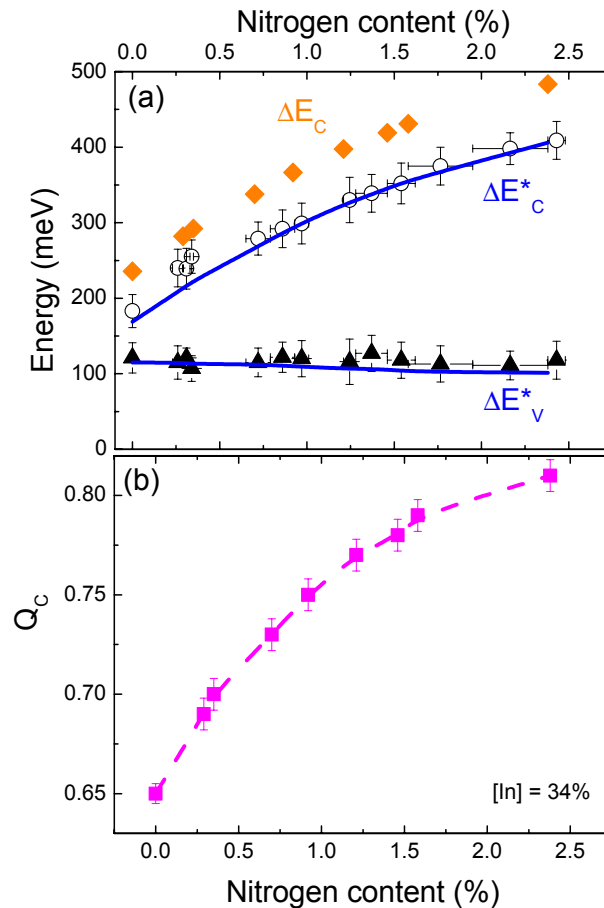
Figure 4.14.: (a) Experimental values of the conduction (spheres) and valence (triangles) practical band offsets and theoretical simulations of the same quantities (solid lines) and of the conduction band offset (diamonds) of $In_{0.34}Ga_{0.66}As_{1-y}N_y$ SQWs samples. (b) Fitting parameter values of the conduction band offset ratio for varying nitrogen concentration.

Many theoretical papers predict that the incorporation of N into (In)GaAs affects mostly the conduction band and has a negligible effect on the electronic structure of the valence band.[19,20] The only experimental studies that investigated this phenomenon employed photoreflectance measurements.[37,123] On the basis of the unchanged value of the spin-orbit splitting energy Δ_0 for different nitrogen contents, the negligible effect of N on the electronic structure of the valence band was demonstrated. In the study presented here the different influence of N on the valence and the conduction band is visible directly in the experimental data.

The simulations of the data, employing the BAC, are shown in figure 4.14 (a) (solid lines); setting the interaction parameter C_{NM} = 2.55 eV, the theoretical curves fit the experimental data very well. The calculations confirm that the main contribution to the reduction of the band gap with increasing nitrogen

content is due to the conduction band and that ΔE^*_V is almost unaltered. In addition, the values of the conduction band offset ΔE_C resulting from the simulations are given in 4.14 (a) (full diamonds). The corresponding values of ΔE_V are only about 12 meV larger than the experimental values of ΔE^*_V and are not shown for reason of clarity. In general the band offsets vary with the nitrogen content like the PBOs.

The conduction band offsets in similar series of samples have been determined by other groups as well. Choulis et al.[124] showed the N-dependence of ΔE_C by simulating the energy states of InGaAsN QW samples obtained by photo reflectance measurements. Their data points up to about 0.5% N content are similar to our results. However, at about 2.5% of N they obtained a much lower value for ΔE_C [≈ 0.32 eV compared to ≈ 0.5 eV in Fig. 3 (a)]. Consequently, their simulated curve for ΔE_C increases slower with nitrogen content than our fit. By fitting the ground state energy levels from photoluminescence measurements, also Xin et al.[52] determined the values of the conduction band offset as a function of the nitrogen content. In this case, there is a good quantitative agreement with our results for the entire range of investigated nitrogen concentrations (0% - 2.5%). Neither report contains quantitative information on the valence band offset.

In figure 4.14 (b), the fitting parameter values of Q_C are plotted as a function of the nitrogen content. The value of Q_C rises monotonously with rising nitrogen content in the QW. Since the valence band states are basically unchanged by the incorporation of N, the behaviour of Q_C essentially reflects the modification of the conduction band offset with varying nitrogen content.

SPV measurements have been also performed on an analogous series of $In_{0.31}Ga_{0.69}As_{1-y}N_y$ SQW samples, i.e. the indium content in the SQWs of this series is lower.[120] The data, shown in figure 4.15, have been simulated following the same approach described in § 4.2.1.1.
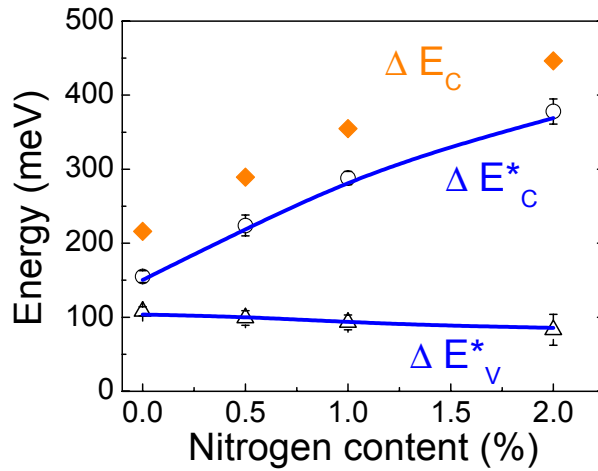
Figure 4.15.: Experimental values of the conduction (spheres) and valence (triangles) practical band offsets and theoretical simulations of the same quantities (solid lines) and of the conduction band offset (diamonds) of $In_{0.31}Ga_{0.69}As_{1-y}N_y$ SQWs samples.

The behaviour of the band offsets with varying N content is the same for the two series of samples. However, a slight difference is present in the value of the conduction band offset. Due to the fact that the indium content in the samples shown in figure 4.14 is higher than that of the samples in figure 4.15, for this latter series of samples ΔE_C is slightly smaller.

The experimental values of ΔE^*_V in figure 4.15 show a small downward shift with increasing nitrogen content. This behaviour is difficult to recognise in figure 4.14 due to the big error bars of the experimental data. This shift is consistent with the findings of Héroux et al..[125] They have shown a regular decrease of the hh-lh splitting as the nitrogen fraction increases. They explain this reduction by a decrease of the compressive strain in high indium content (> 10%) InGaAsN QWs due to nitrogen incorporation.

4.2.2 Influence of the indium content on the energetic states and band offsets of InGaAsN quantum wells

A series of $In_xGa_{1-x}As_{0.984}N_{0.016}$/GaAs SQW samples with different indium content has been analysed to investigate the influence of indium on the band structure of dilute nitrides. The SPV spectra and the corresponding derivatives are shown in figure 4.16. As in the nitrogen series, the transition

corresponding to the GaAs region is fixed in position (vertical dotted line) and the ground state shifts towards smaller energy values with increasing indium content. Compared to the case of figure 4.12, the region between the transitions e_1-ch and the ch-ce shows additional features. The reason for this is most likely the GaAsN barrier layers present in these particular samples. This feature, however, does not affect the results in a significant way.
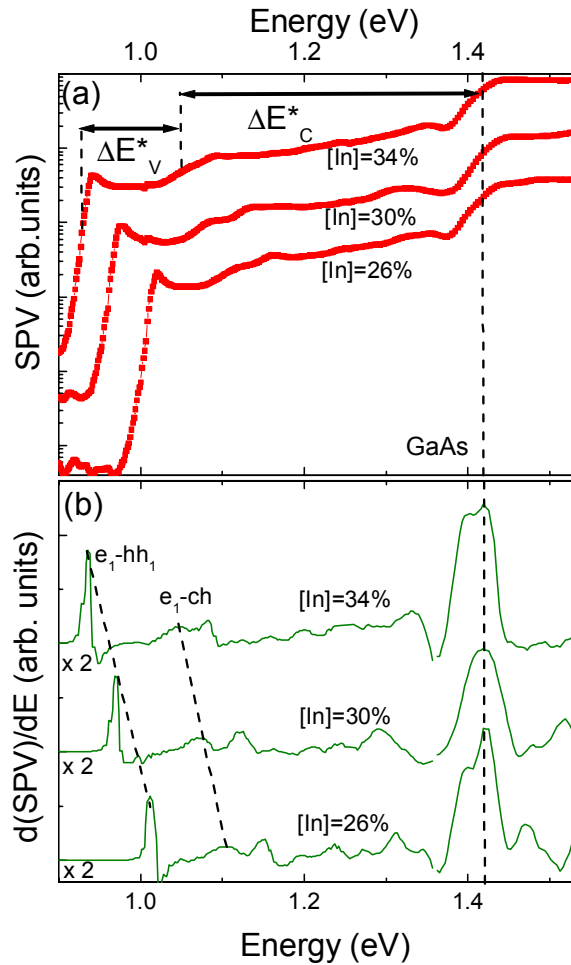
Figure 4.16.: (a) SPV spectra acquired at 300 K for $In_xGa_{1-x}As_{0.984}N_{0.016}$/GaAs SQWs with varying indium content. (b) Derivatives of the SPV spectra as a function of the detected energy. The parts below 1.36 eV have been magnified by a factor that is indicated on the left-hand side of the spectra.

The experimental values of the ground states are obtained considering the position of the lowest peak in energy in the derivative spectra in figure 4.16 (b) and are shown in figure 4.17. Employing the BAC with C_{NM}=2.55 eV the calculated values fit the experimental data very well.
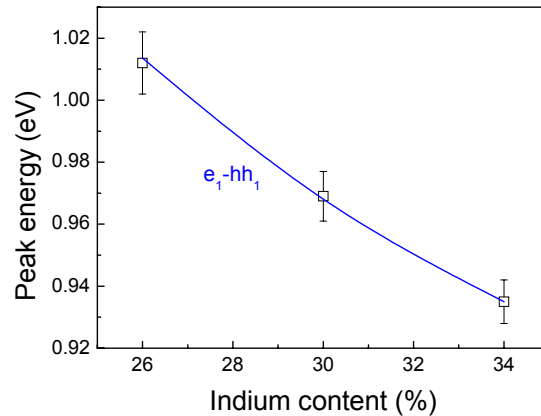
Figure 4.17.: Experimental values of the ground states of $In_xGa_{1-x}As_{0.984}N_{0.016}$ SQWs samples (open squares) and simulation of the same quantities employing the BAC (solid line).

The values of the practical band offsets have been extracted from figure 4.16 (a) and are shown in Fig. 4.18 (a). Both the conduction and the valence PBOs increase with increasing In concentration in the quantum well. In particular, passing from an indium content of 26% to 34%, the practical conduction band offset increases from a value of about 330 meV to a value of about 380 meV and the practical valence band offset from a value of about 90 meV to a value of about 120 meV. This behaviour is expected, since both electrons and holes are affected by changing the indium content in the QW. The theoretical calculations (solid lines in figure 4.18 (a)) agree very well with the tendency shown by the experimental data.

In the upper part of figure 4.18 (a), the energy values of ΔE_C (full diamonds) are shown along with a theoretical expression [126] (dashed line) describing the variation of the conduction band offset with increasing In content in N-free InGaAs QWs. The theoretical description fits our results very well if it is shifted in energy by about 195 meV. This shift is reasonable if one takes into account the variation of the energy gap and of Q_C due to nitrogen incorporation ([N] = 1.6%). The result shows that in dilute nitrides ΔE_C varies with In content like the conduction band offset in N-free QWs. The corresponding values of ΔE_V are only about 12.5 meV higher than the ones of ΔE^*_V and are not shown. So far, no other work in the literature has shown the indium dependence of the band offset in dilute nitrides.

The values of the fitting parameter Q_C employed in the calculations for this series of samples are shown in figure 4.18 (b). In contrast to the N-series, the value of Q_C decreases with increasing indium content. This tendency is consistent with the fact that in the limiting case of GaAsN / GaAs structures Q_C is close to one due to the change of bandgap being almost entirely in the conduction band offset.[50,51]
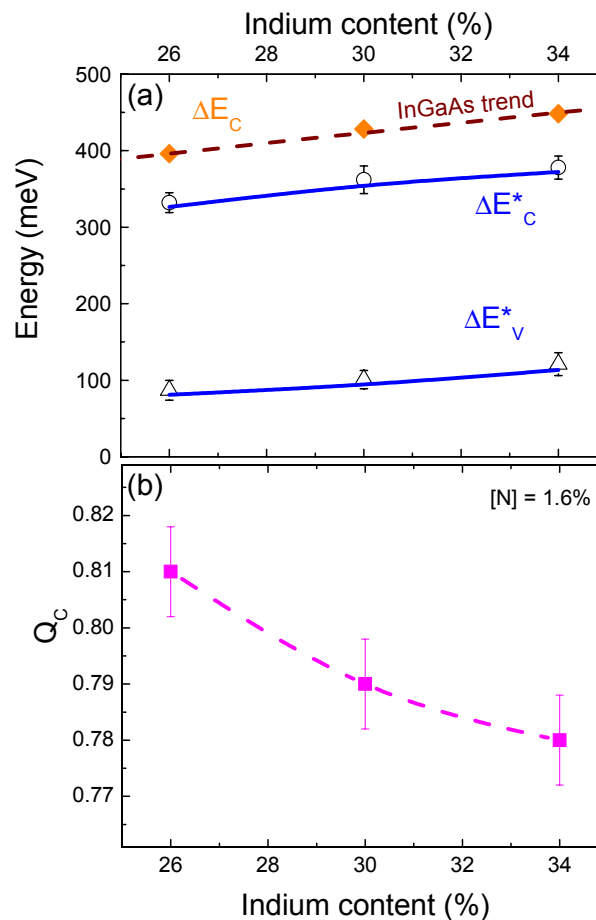
Figure 4.18.: (a) Experimental values of the conduction (open spheres) and valence (open triangles) practical band offsets and theoretical simulations of the same quantities (solid lines). The dependence of the conduction band offset on indium content (full diamonds) is compared with the theoretical description for N-free InGaAs QWs (dashed line). The dashed line is derived from the dependence of the conduction band offsets for InGaAs given in Ref. and was shifted by 195 meV to higher energies in order to fit our data for InGaAsN. (b) Fitting parameter values of the conduction band offset ratio for varying indium concentration.

4.2.3 Combined indium and nitrogen influence on the conduction band offset ratio

In figure 4.19 the evolution of the conduction band offset ratio with nitrogen content is shown for two N-series. The two series of samples are $In_{0.34}Ga_{0.66}As_{1-y}N_y$ SQWs with a N-content varying between 0% and 2.4% (squares) and $In_{0.31}Ga_{0.69}As_{1-y}N_y$ SQWs with 0% < N < 2% (triangles). In the figure, the

influence of both indium and nitrogen content on the band offset of dilute nitride structures is described.

In the case of the N-free samples, the conduction band offset ratio assumes the same value (Q_C = 65%) even though the indium content in the well is different. Despite the reduction in the band gap with increasing indium content, the band offset ratio does not change, at least in this range of indium variation. In contrast, for the case in which nitrogen is present, Q_C assumes different values for different indium contents. This difference in Q_C between the two series increases with increasing nitrogen concentration; suggesting that the more nitrogen is present in the quantum well, the greater is the difference between the variation rate of the valence and the conduction band offsets with varying indium content. Thus, by appropriately changing both nitrogen and indium concentrations, electron and hole confinement can be modified in a different way while the band gap remains constant. In figure 4.19, a dashed line shows the region where the emission wavelength of the QW corresponds to 1.3 µm. For this emission wavelength, the variation of the indium content from 34% to 31% induces an increase of the value of Q_C from 79% to 82%.
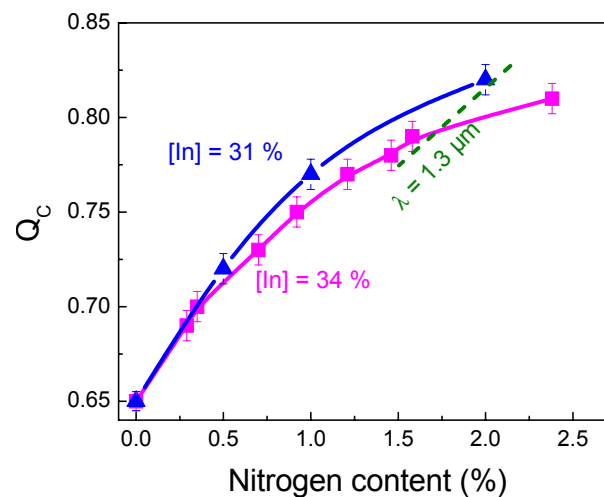
Figure 4.19.: Evolution of the conduction band offset ratio with nitrogen content for two series of samples having two different indium concentrations: 31% (triangles) and 34% (squares).With a dashed line the 1.3 µm emission wavelength region is shown.

4.3 Further investigation of the band offsets of dilute nitrides

As explained in the previous sections, the application of SPV measurements in order to study the band offsets of dilute nitrides offers the possibility to understand fundamental physical properties of these types of quantum structures. In the following, two examples will be presented in which this method is applied to find out practical properties useful, for example, for the design of QW devices.

4.3.1 Quantum well width analysis

In order to study how the practical band offsets change with varying QW width in dilute nitrides, a series of $In_{0.30}Ga_{0.70}As_{0.98}N_{0.02}$/GaAs SQW samples with different well width has been analysed. To investigate the effect of the nitrogen content, the results were compared with those from an analogous series of samples without nitrogen inside ($In_{0.30}Ga_{0.70}As$/GaAs SQW samples presented in 4.1.3).

The SPV spectra are shown in figure 4.20 (a) along with the corresponding derivatives in figure 4.20 (b). In the GaAs absorption region above 1.38 eV the 7 nm-thick and the 9 nm-thick samples show an unusual behaviour. At the moment, there is not a clear explanation for this phenomenon but similar spectra have been reported before.[127] The ground state energy value increases with decreasing well width and the transition corresponding to the barrier has the same value for all the samples. The energy position of the step related to the transition e_2-hh_2, varies with the well width here as well. However, differently from the case of the InGaAs series (4.1.1.2), it is possible to detect this transition also for the sample having a well width of 5 nm. Since the presence of nitrogen reduces the band gap energy of the QW and increase the carrier effective mass compared to InGaAs, thus increasing the carrier confinement, it is reasonable that bound excited states occur for smaller well widths.
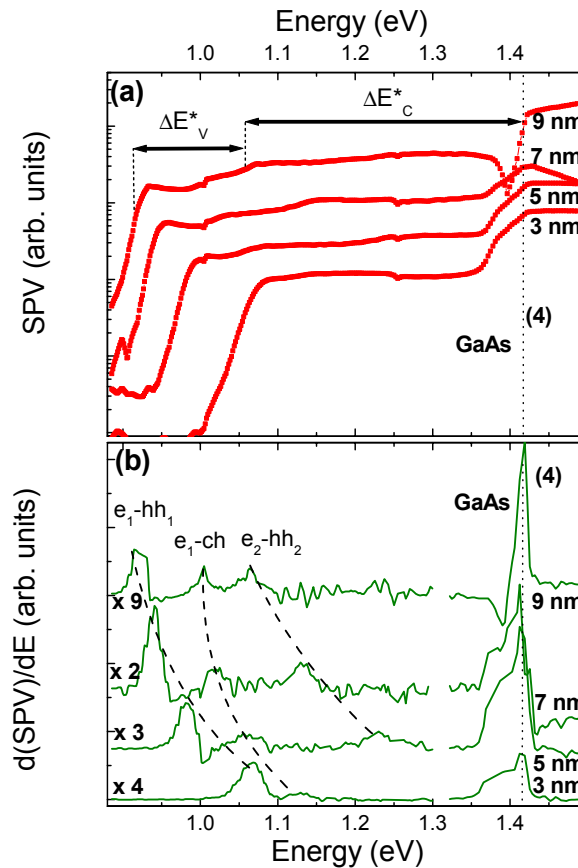
Figure 4.20.: (a) SPV spectra for $In_{0.3}Ga_{0.7}As_{0.098}N_{0.02}$ SQWs with different well widths acquired at 300 K. The different positions of transition 1 for different well widths are indicated by a solid line. The fixed position of the barrier (GaAs) is indicated with a dotted vertical line. The presence of step 3 is also indicated. (b) Derivatives of the SPV spectra as a function of the detected energy. The peaks correspond to the steps in intensity of the SPV spectra. The first part of each spectrum (up to 1.30 eV) has been magnified for clarity; on the left-hand side of the curves the multiplication factors are shown.

The energetic positions of the steps related to the ground and to the first excited state are depicted in figure 4.21 (a) versus the QW width and are marked with open squares and open spheres, respectively. The comparison of figure 4.4 and figure 4.21 (a) reveals the influence of nitrogen on the energetic states in the QW. The incorporation of 2% of nitrogen into InGaAs generates a redshift of the transition of the confined QW states e_1-hh_1 of about 200 meV. In particular, passing from the 3 nm-thick to the 9 nm-thick samples, the redshift increases from 185 meV to about 215 meV, showing thus a dependence on the QW width (figure 4.21 (b)). The excited states, corresponding to the transition e_2-hh_2, show the same trend. The influence of the well width will be explained below. The average redshift of

roughly 200 meV is in line with other studies that state an energy gap reduction rate of about 100 meV per percent of nitrogen.
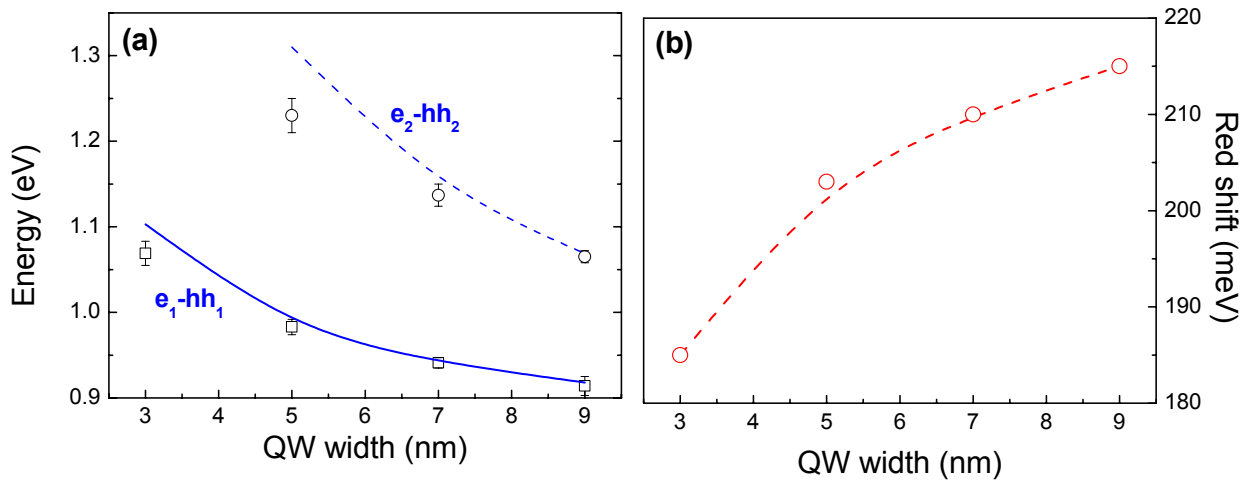
Figure 4.21.: (a) Energy values of transitions 1 (squares) and 3 (spheres) in dependence of the well width. The solid and the dashed lines are the calculated values of e_1-hh_1 and e_2-hh_2, respectively. (b) Redshift of the QW ground state transition e_1-hh_1 induced by the incorporation of 2% of nitrogen into $In_{0.30}Ga_{0.70}As$ QWs.

In figure 4.20 (a) the simulations of e_1-hh_1 and e_2-hh_2 (solid and dashed lines, respectively) performed employing the BAC are shown. For these calculations, the conduction band offset ratio has been slightly varied around the value of 80% which is the value that several groups[42,43] reported for InGaAsN SQWs with an indium content of about 30% and a low nitrogen concentration (< 2%). Good results were obtained taking $Q_C = 0.82$ and $C_{NM} = 2.36$ eV. For the ground states, experimental data and simulation are in agreement. However, for the transition e_2-hh_2 the agreement is not as good, in particular at the smallest well width of 5 nm. This effect can be explained by the strongly non-parabolic dispersion of the InGaAsN conduction band, which was not considered in these calculations of the confined states. This non-parabolicity affects mostly the quantization energies for the conduction band states with high values of the wave vector k (e.g. excited conduction band states).

The values of the practical conduction and valence band offsets were extracted from the SPV spectra depicted in figure 4.20 (a) and (b) and are shown in detail in figure 4.22 (a). In order to make the comparison with the N-free samples easier, figure 4.22 (b) reproduces the results already shown in figure 4.11 but in a different energy scale. This comparison gives the additional possibility to distinguish

between the effect of nitrogen on the conduction and on the valence band. While the practical valence band offsets assume almost the same values in both series of samples (between 75 meV and 110 meV for well widths between 3 nm and 9 nm), the values of ΔE^*_C for the InGaAsN samples are remarkably greater than the ΔE^*_C values for the N-free samples. A close inspection of figure 4.22 (a) and (b) reveals for InGaAsN a slight decrease in the values of the valence practical band offset for the same well width. This phenomenon has already been discussed in section 4.2.1.2 and is attributed to the reduction in strain by the incorporation of nitrogen.
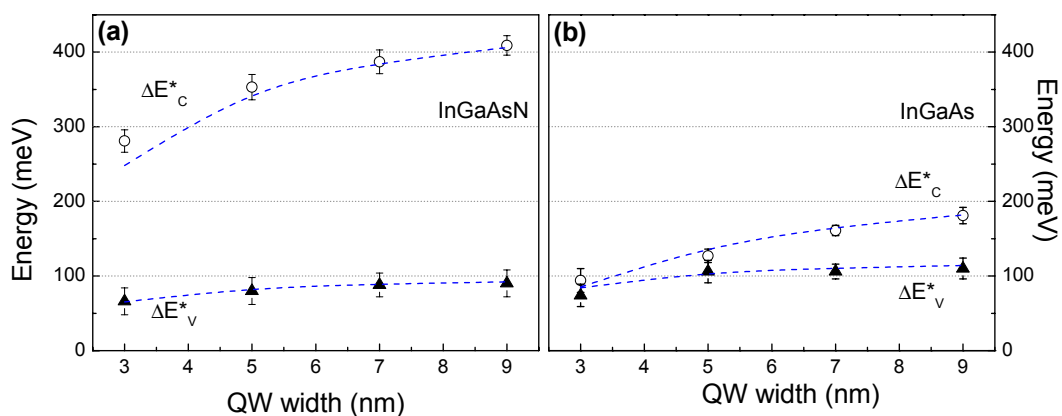
Figure 4.22.: (a) Experimental values of the practical band offsets ΔE^*_C and ΔE^*_V extracted from the SPV spectra of $In_{0.3}Ga_{0.7}As_{0.98}N_{0.02}$ SQWs as a function of the well width. The dashed lines are the theoretical simulations of the same quantities. (b) Experimental values of the practical band offsets ΔE^*_C and ΔE^*_V extracted from the SPV spectra of $In_{0.3}Ga_{0.7}As$ SQWs as a function of the well width. The dashed lines are the theoretical simulations of the same quantities (figure 4.14).

In figure 4.22 (a) the theoretical simulations of the practical band offsets for the InGaAsN samples are shown as well (dashed lines). Also in this case, there is a good agreement between the simulations and the experimental data. For these series of samples the values of $\Delta E_C = 454$ meV and $\Delta E_V = 100$ meV were found for the conduction and valence band offsets, respectively (independently of the QW width). For the N-free samples the conduction band offset was found to be $\Delta E_C = 226$ meV and the valence band offset $\Delta E_V = 122$ meV.

The comparison of the two QW width series yields another interesting result that has been mentioned already above. Apparently, the variation of e_1-hh_1 with the well width is significantly stronger for the nitrogen-containing samples. Passing from 3 nm to 9 nm-thick QWs, the change of e_1-hh_1 is

about 125 meV in the case of InGaAs but about 155 meV for InGaAsN, as can be seen from the comparison of the experimental data in figure 4.4 and figure 4.21 (a). In other words, the redshift induced by the incorporation of N depends on the well width [figure 4.21 (b)]. The comparison of the two graphs in figure 4.22 shows that the origin of this phenomenon must be related to the conduction band states. The presence of nitrogen in the InGaAsN samples increases the conduction band offset remarkably. This leads to an enhancement of the quantum well confining potential, whose influence on the confined states depends on the width of the QW. The evolution of the electron quantized states for the two extreme well widths is illustrated in figure 4.23 for both InGaAs and InGaAsN. Since it has been shown that nitrogen influences mostly the conduction band, only the case of the electron states will be discussed here. While for the 3 nm-thick QW the incorporation of 2% of nitrogen produces an increase of the energy value of the quantized state e_1 by about 40% (from about 141 meV to about 205 meV), for the 9 nm-thick QW e_1 remains almost unchanged (around 45 meV). This means that, although the change in the conduction band offset is the same, the increase of the practical band offset is stronger for the samples with a wider QW. For the 3 nm-thick QW sample the value of ΔE^*_C increases by about 175 meV, while for the 9 nm-thick QW sample the same quantity increases by about 230 meV.
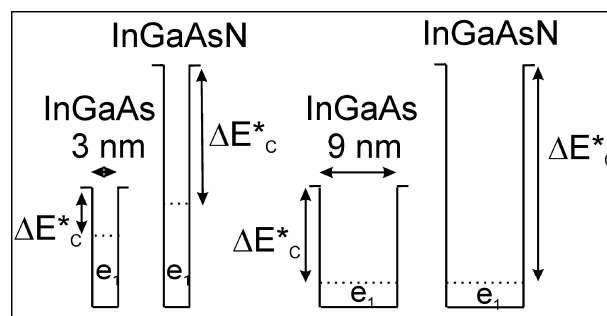
Figure 4.23.: Influence of the well width on the structure of the electron states of $In_{0.3}Ga_{0.7}As$ and $In_{0.3}Ga_{0.7}As_{0.098}N_{0.02}$ SQWs is shown. For illustrative purposes, the bottoms of the QWs are aligned. In reality, the energetic level of the GaAs-barrier is the same for all the QWs.

Properties like that are of great interest for the design of quantum well devices. For the high-temperature performance of a quantum well laser, for example, a large practical band offset is desirable. At the same time, the degradation of InGaAsN with increasing nitrogen content suggests that as long wavelengths as possible should be reached with as little nitrogen as possible. Both findings imply the

use of thick QWs. However, these results need to be balanced with strain considerations and the dependence of gain on the QW width.

4.3.2 Laser structure characterization

As mentioned previously in this chapter, the determination of band offsets employing conventional methods requires the exact knowledge of particular parameters, which for dilute nitrides are not always unambiguously known. Furthermore, the simulation of the structure of the system is necessary in order to calculate the energy states of the samples. The latter requirement is a further difficulty if one intends to analyse the band offsets of a real device whose structure is more complicated to simulate as compared to that of a test structure.

One of the most interesting properties of the method presented here is the possibility to obtain direct information about the structures investigated in a very simple and fast way, even if these structures are real devices. In figure 4.24 the SPV spectra of two InGaAsN samples having a laser structure and emission wavelengths of about 1.3 μm and 1.5 μm are shown. These wavelengths are very important for applications in the telecommunication field.
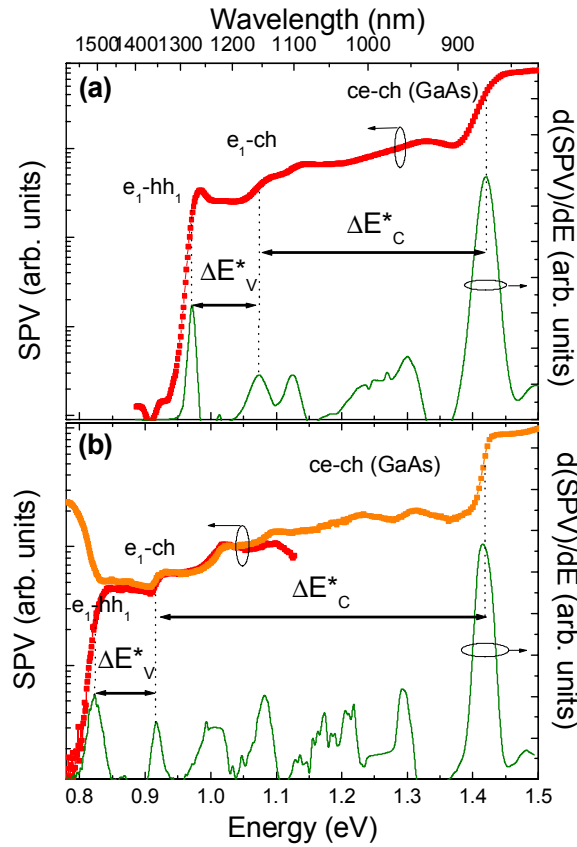
Figure 4.24.: (a) SPV spectrum and corresponding derivative spectrum of a $In_{0.30}Ga_{0.70}As_{0.984}N_{0.016}$/GaAs SQW sample emitting at 1.3 μm. (b) SPV spectrum and corresponding derivative spectrum of a $In_{0.40}Ga_{0.60}As_{0.961}N_{0.039}$/GaAs SQW sample emitting at 1.5 μm. The spectra are taken at 300 K.

As explained in § 4.1 the practical band offsets can be extracted directly from the spectra (double arrows in the figure). For the laser emitting at 1.3 μm [(figure 4.24 (a)], it has been found that the practical conduction band offset is ΔE^*_C = (360±15) meV and the practical valence band offset is ΔE^*_V = (101±12) meV. Looking at figure 4.24, it can be noticed that, in order to reach an emission wavelength of 1.5 μm, the conduction band states are the most affected. The spectrum of the laser shown in figure 4.24 (b) shows in fact a value of ΔE^*_C = (500±14) meV and a value of ΔE^*_V = (94±13) meV.

The spectrum in figure 4.24 (b) is a composition of two different spectra. The first one covers the entire range of energies from 0.8 eV to 1.5 eV. The SPV intensity decreases monotonously till the energy value of 0.83 eV, and after that it increases. The increase of the SPV intensity for low energy values is explained by the grating replicas characteristics of the light source employed in the experiment.

In order to cut off these replicas, an optical filter was employed. In this way, a second spectrum was acquired describing the SPV intensity cleaned by the effects of the replicas but only in the range of wavelengths which are allowed to pass through the filter (λ > 1100 nm), that means for energies below the value of about 1.1 eV.

With this example it has been shown that, employing a non-destructive method, it is possible to obtain information regarding the energy levels and the carrier confinement of samples having the structure of a laser.

4.4 Conclusions of the fourth chapter

In this chapter a new electro-optical technique has been presented. With this technique, more detailed understanding about the lacking knowledge of the band offsets in dilute nitrides has been obtained. This contactless technique, based on surface photovoltage measurements, can be applied to a large variety of semiconductor heterostructures.

Firstly, the understanding of the number and the kind of optical transitions that can be detected by surface photovoltage measurements in type I quantum well (QW) structures has been generalized. Most importantly, with this method it is possible to detect in addition to the bound-to-bound transitions (ground and excited states involving both the heavy and light holes), also one bound-to-free transition. This allows the direct determination of band offsets energies, which are one of the main parameters to characterize heterostructures. This speciality, together with the simple experimental set-up, gives this method several advantages compared to other techniques. Simply by employing surface photovoltage spectroscopy, it is possible to obtain comprehensive information about SQWs which otherwise could be achieved only by combining different optical techniques and theoretical calculations.

The method was applied to investigate the evolution of the band offsets of InGaAsN / GaAs SQWs varying different quantum well parameters. In particular, the behaviour of the conduction and valence band offsets was separately analysed as a function of nitrogen and indium content. Confirming

theoretical predictions, it was found that with varying nitrogen concentration only the conduction band states are affected while the valence band states remain almost unaltered. For changing indium content, it has been shown that both the conduction and the valence band states are modified and, in particular, that the conduction band offset ΔE_C varies with indium content like that in nitrogen-free quantum wells. Furthermore, it has been found that the value of the conduction band offset ratio increases with increasing nitrogen content and decreases with increasing indium concentration. This effect shows the possibility to design structures with a fixed band gap but varied confinement of electrons and holes by changing the In / N ratio.

Finally, the possibility to apply the method to obtain information about important parameters for the design of devices has been shown. Comparing two series of QW samples having different well width, it has been found that thicker QWs produce a larger red shift for the incorporation of the same quantity of nitrogen. In addition, the method has been employed to determine the band offsets of real devices. The practical band offsets for two laser structures emitting at the telecommunication wavelengths 1.3 µm and 1.5 µm have been determined.

General Conclusions

In the last decade great attention has been given to the characteristics of dilute nitrides. Both their peculiar physical properties and their wide range of possible applications have attracted the interest of many experimental and theoretical groups. In this thesis work some open questions about the fundamental properties of dilute nitrides have been answered. Two important topics have been investigated: the correlation between the optical and morphological properties of InGaAsN / GaAs single quantum well samples (SQWs) and a quantitative, model-independent determination of the band offsets for the same types of structures.

In chapter 3, a combined study of photoluminescence (PL) measurements and transmission electron microscopy (TEM) analysis has allowed to find a direct correlation between the degree of carrier localization in the sample and the homogeneity of the material. In particular, the degree of localization increases with increasing the inhomogeneity of the QW layer. On the basis of that, it has been found that the growth temperature (Tg) and the indium content strongly influence the morphology of the InGaAsN QW samples. With increasing Tg or with increasing [In], the inhomogeneity of the sample increases.

The growth temperature affects also the optical properties of InGaAsN SQWs. By raising Tg, the PL intensity degrades and the peak emission energy red shifts. On the other hand, the indium content does not remarkably influence the PL efficiency of the QW. The only exception is for very high indium contents ([In] > 34%). In this case, dislocations due to strain relaxation and / or other types of non-radiative recombination centres are created causing a drastic decrease of the PL intensity.

General conclusions

After annealing both the morphological and the optical properties are modified. Most notably, by employing samples grown in the range of temperatures between 360 °C and 480 °C annealed in different environments, two important conclusions have been found. First of all, *morphology and PL efficiency are not always correlated* and secondly, *the PL efficiency of a QW directly depends on the density of non-radiative centres.* Annealing samples in different atmospheres is a novelty in the literature and it has been the key-point to reach these findings.

The first conclusion has been obtained by performing photoluminescence measurements on samples annealed in hydrogen and argon environment, and comparing the results with those of as-grown samples. It has been shown that while the PL intensity of H_2-annealed samples is maximum for low values of Tg ($\approx$ 400 °C) and minimum for high Tg ($\approx$ 450 °C), the PL intensity of the Ar-annealed samples is maximum for high values of Tg ($\approx$ 450 °C) and minimum for low Tg ($\approx$ 400 °C). In contrast, the degree of localization and the TEM images have shown the same Tg-behaviour, independently of the annealing environment.

The second conclusion has been reached by performing time resolved photoluminescence measurements on the same series of samples. It has been shown that whilst the radiative decay time varies with Tg in the same manner for the two annealing atmospheres, i.e. it increases with increasing Tg, the non-radiative decay time varies with the growth temperature in a different way for different annealing environments. In particular, the non-radiative decay time decreases with increasing Tg for H_2-annealed samples and increases with increasing Tg for Ar-annealed samples. This behaviour correlates in both cases with the dependence of the PL intensity on the growth temperature.

In addition to that, by performing power dependent PL measurements, it has been verified that changes of degree of localization after annealing are only due to morphological modification of the sample.

By comparing the results obtained performing PL measurements on GaAsN / GaAs, InGaAs / GaAs, and InGaAsN / GaAs SQW samples, it has been shown that at least two different type of defects are created during the growth of InGaAsN SQWs. One type of defect is related to the presence of nitrogen.

The density of these defects increases with Tg and decreases by annealing. Defects of another type are related to the simultaneous presence of indium and nitrogen. They are created at low Tg and tend to agglomerate under annealing. These two types of defects have been employed in a simple model in order to justify the main results obtained in this chapter.

In chapter 4, a much debated topic has been analysed: the evolution of the band offsets of InGaAsN / GaAs structures with varying QW parameters. The chapter has been initially focussed on the refinement of the information which can be obtained employing an experimental method developed at Infineon Technologies based on surface photovoltage (SPV) measurements. With this method it is possible to identify optical transitions involving bound states and extended states in a QW sample. In particular, in addition to the bound-to-bound transitions, also the indirect transition from the extended state of the valence band to the first confined state of the conduction band can be identified. This allows the easy determination of the practical band offsets of the QW. These quantities represent the energy values of the conduction (valence) band offset of the heterostructures without the value of the first quantized state of the electrons (holes). For the design of a device, the practical band offsets are fundamental quantities because they quantify the real confinement of the carriers in the well.

SPV measurements have been performed on several dedicated series of samples. The results have been compared with those obtained employing other optical techniques and performing theoretical simulations. It has been shown that by using this method, it is possible to gather comprehensive information about a single quantum well which otherwise could be obtained only by combining different experimental techniques and theoretical calculations. With this method transitions related to the ground states of the QW involving both the heavy and light holes states can be detected. Also, the excited states can be identified. As a main condition, it has been shown that only bound-to-bound transitions having the same parity can generate a step in the spectra.

This method has been employed to investigate the band states of dilute nitrides SQWs. In particular, the effect of varying nitrogen and indium content on the practical band offsets of $In_xGa_{1-x}As_{1-y}N_y$ /GaAs SQW samples has been analysed. As a main result, it has been found that *with increasing nitrogen*

content, the conduction band offset strongly increases (with a rate of about 100 meV / [N]), while the valence band offset is almost unchanged. Moreover, with increasing indium concentration both the conduction and the valence band offsets are modified. In particular, _the conduction band offset varies with indium content as in the case of N-free samples._ These results represent the first quantitative analysis which directly, i.e. independently of any model, determines the band offsets in dilute nitrides quantum wells. More importantly, it allows to analyse the effect of nitrogen and indium on the conduction and valence band states separately.

The practical band offsets are highly important parameters in the design of many devices. Therefore, in the end of this thesis, it has been shown that the SPV method can be employed to determine the practical band offsets of real device structures. In particular, the practical conduction and valence band offsets of lasers emitting at 1.3 µm and 1.5 µm have been determined from the SPV spectra.

Optische Charakterisierung von InGaAsN/GaAs Quantentöpfen: Tempereffekte und Bestimmung von Band-Offests (Doktorabeitzusammenfassung)

In den letzten Jahrzehnten wurden „Dilute Nitrides" wegen ihrer besonderen physikalischen Eigenschaften und ihres großen Anwendungsbereiches von vielen experimentellen und theoretischen Gruppen untersucht. In dieser Doktorarbeit werden einige offene Fragen zu den fundamentalen Eigenschaften dieser Materialien beantwortet. Zwei wichtige Themen werden behandelt: Zum einen die Korrelation zwischen den optischen und morphologischen Eigenschaften von InGaAsN/GaAs Einzelquantentopfproben und zum anderen eine quantitative, modell-unabhängige Bestimmung der Band-Offsets für die gleichen Strukturen.

Photolumineszenzmessungen (PL) und Transmissionselektronenmikroskopieanalyse (TEM) zeigen in Kapitel 3, dass es eine direkte Korrelation zwischen der Lokalisierung von Ladungsträgern und struktureller Inhomogenität des Quantentopfes gibt.. Der Lokalisierungsgrad steigt dabei mit zunehmender struktureller Inhomogenität der Quantentopfschicht. Es wurden InGaAsN/GaAs Quantentöpfe untersucht, die bei verschiedenen Temperaturen T_W gewachsen wurden und/oder sich im Indiumgehalt [In] unterscheiden. Beide Parameter beeinflussen stark die Morphologie des Quantentopfes. Wenn T_W oder [In] steigen, nimmt die Inhomogenität des Quantentopfes zu. Die Wachstumstemperatur beeinflußt auch die optischen Eigenschaften von InGaAsN Quantentöpfen. Mit zunehmender T_W verschlechtert sich die PL Intensität, und es kommt zu einer Rotverschiebung der Emissionsenergie. Von der In-Konzentration hängt die PL Intensität dagegen kaum ab. Nur die Proben mit hohem Indiumgehalt ([In] > 34%) bilden eine Ausnahme. Aufgrund von Versetzungen und / oder anderen nichtstrahlenden Rekombinationszentren nimmt die PL Intensität drastisch ab.

Tempern modifiziert sowohl die morphologischen als auch die optischen Eigenschaften der Quantentöpfe. Hierzu wurden bei der Untersuchung von Proben, die bei Temperaturen zwischen

360 °C und 480 °C gewachsen und in verschiedenen Atmosphären getempert wurden, zwei wichtige Ergebnisse erzielt. Zum einen wurde festegestellt, dass die Morphologie und die PL Effizienz nicht direkt zusammenhängen, und zum anderen, dass die PL Effizienz des Quantentopfes von der Dichte nichtstrahlender Zentren abhängt. Hierbei spielt die Atmosphäre, in der das Tempern durchgeführt wird, eine zentrale Rolle. Diese Untersuchung des Einflusses der Temperatmosphäre ist eine Neuheit in der Literatur.

Das erste Ergebnis wurde durch den Vergleich von PL Messungen an Proben erreicht, die entweder in Wasserstoff, in Argon oder gar nicht getempert worden waren. Hierbei zeigte sich, dass die PL Intensität der H_2 – getemperten Proben für tiefe Wachstumstemperaturen ($\approx$ 400 °C) am höchsten und für hohe Wachstumstemperaturen ($\approx$ 450 °C) am niedrigsten ist, während die PL Intensität der Ar – getemperten Proben für hohe T_W ($\approx$ 450 °C) am höchsten und für tiefe T_W ($\approx$ 400 °C) am niedrigsten ist. Der Lokalisierungsgrad und die TEM-Bilder sind jedoch für gleiche T_W gleich und damit unabhängig von der Temperatmosphäre.

Das zweite Ergebnis wurde durch zeitaufgelöste Photolumineszenzmessungen an derselben Probenserie erzielt. Es zeigte sich hierbei, dass die strahlende Zerfallzeit für beide Temperatmosphären mit der Wachstumstemperatur zunimmt, also auf die gleiche Art und Weise variiert. Die nichtstrahlende Zerfallzeit dagegen ändert sich mit der Wachstumstemperatur für die beiden Temperatmosphären auf unterschiedliche Art und Weise. Für die H_2 - getemperten Proben nimmt die nichtstrahlende Zerfallzeit mit zunehmender Wachstumstemperatur ab, während sie für die Ar – getemperten Proben steigt. Dieses Verhalten ist in beiden Fällen analog zu der Wachstumstemperaturabhängigkeit der PL Intensität.

Ferner zeigten leistungsabhängige PL Messungen, dass Änderungen in der Lokalisierung, die nach dem Tempern beobachtet werden, nur durch morphologische Modifizierungen verursacht werden und nicht durch eine Abnahme in der Dichte nichtstrahlender Rekombinationszentren.

Der Vergleich von PL Messungen an GaAsN/GaAs, InGaAs/GaAs und InGaAsN/GaAs Einzelquantentopf-Proben ergab, dass mindestens zwei verschiedene Defekte während des

Wachstums der InGaAsN/GaAs Einzelquantentöpfe auftreten. Der eine Defekt wird durch den Einbau von Stickstoff verursacht. Die Anzahldichte dieses Defektes nimmt mit steigender Wachstumstemperatur zu und wird durch Tempern reduziert. Die Defekte der anderen Art entstehen, wenn sowohl Indium als auch Stickstoff vorhanden sind. Diese Defekte bilden sich vor allem bei tiefer Wachstumstemperatur aus und neigen beim Tempern zu Agglomeration. Das Verhalten beider Defekte wird in einem spekulativen Modell zusammengefaßt, mit dem die Ergebnisse dieses Kapitel erklärt werden können.

In Kapitel 4 wird ein wichtiges und viel diskutiertes Thema behandelt: Die Veränderung der Band-Offsets von InGaAsN/ GaAs Heterostrukturen mit variierenden Quantentopf-Parametern. Zu Beginn dieses Kapitels wird das Verständnis einer experimentellen Methode verbessert und erweitert, die bei Infineon Technologies entwickelt wurde. Diese Methode basiert auf Messungen der Oberflächenfotospannung (surface photovoltage, SPV). Mit dieser Methode ist es möglich, optische Übergänge zwischen verschiedenen gebundenen und ungebundenen Zuständen in einer Quantentopfprobe zu beobachten. Eine Besonderheit ist dabei, dass zusätzlich zu den Übergängen zwischen gebundenen Zuständen des Quantentopfes der Übergang vom ungebundenen Zustand des Valenzbandes in den gebundenen Grundzustand des Leitungsbandes gemessen werden kann. Dies ermöglicht eine einfache Bestimmung der Praktischen Band-Offsets des Quantentopfes. Dieser in dieser Arbeit eingeführte Begriff repräsentiert die Band-Offsets des Leitungs- (Valenz-) bandes der Heterostrukturen abzüglich der Quantisierungsenergie des Grundzustandes für gebundene Elektronen (Löcher). Für die Entwicklung von Bauelementen sind die Praktischen Band-Offsets von fundamentaler Bedeutung, da sie den tatsächlichen elektronischen Einschluß der Ladungsträger im Quantentopf angeben.

SPV-Messungen wurden an mehreren speziell hierfür gewachsenen Probenserien durchgeführt. Diese Ergebnisse werden mit Resultaten verglichen, die mit konventionellen experimentellen optischen Methoden und theoretischen Simulationen erzielt wurden. Es wird gezeigt, dass mit einer einzelnen SPV-Messung umfangreiche Informationen über einen Einzelquantentopf gewonnen werden, die sonst

nur durch die Kombination mehrerer experimenteller Methoden und theoretischer Berechnungen erreicht werden könnten. Mit der SPV-Methode können Übergänge in die Grundzustände sowohl der schweren als auch der leichten Löcher des Quantentopfes beobachtet werden. Ferner können auch angeregte Zustände identifiziert werden. Als Bedingung wurde festgestellt, dass nur Übergänge zwischen gebundenen Zuständen gleicher Parität eine Stufe in den Spektren erzeugen können.

Diese Methode wurde eingesetzt, um die Bandzustände von Quantentöpfen aus „Dilute Nitrides" zu untersuchen. Insbesondere wurde analysiert, wie sich eine Änderung des Stickstoff- und des Indium-Gehaltes auf die Praktischen Band-Offsets von $In_xGa_{1-x}As_{1-y}N_y$ / GaAs Einzelquantentopfproben auswirkt. Als Hauptergebnis wird gezeigte, dass mit steigendem Stickstoffgehalt der Leitungsband-Offset stark zunimmt (mit einer Rate von ca. 100 meV/ 1% [N]), während der Valenzband-Offset unverändert bleibt. Ferner werden mit Zunahme des Indiumgehalts sowohl der Leitungsband-Offset als auch der Valenzband-Offset modifiziert. Insbesondere hängt der Leitungsband-Offset vom Indiumgehalt so ab, wie dies auch für analoge stickstofffreie Proben der Fall ist. Diese Ergebnisse sind die erste quantitative Analyse, welche direkt bzw. unabhängig von jeglichem Modell die Band-Offsets in „Dilute Nitrides" Quantentöpfen bestimmt. Dabei wurde auch der separate Einfluß von Stickstoff und Indium auf die Leitungsband- und Valenzband-Zustände untersucht.

Die Praktischen Band-Offsets sind sehr wichtige Parameter für die Entwicklung vieler Bauelemente. Dazu wird am Ende dieser Doktorarbeit gezeigt, wie die SPV - Methode angewendet wird, um die Praktischen Band-Offsets eines realen Bauelementes zu bestimmen. Insbesondere werden die Praktischen Leitungsband- und Valenzband-Offsets von Lasern bestimmt, die eine Emission von 1.3 µm bzw. 1.5 µm haben.

Acknowledgments

At this point, I would like to thank some persons which have been important for the conclusion of this PhD work.

Dr. habil. W. Stolz for his suggestions and interesting discussions.

Prof. S. Baranovski and Dr. habil. W. Stolz for the acceptance to evaluate this thesis work.

Henning Riechert for his extreme willingness and his helpful hints.

Lutz Geelhaar for his help to find interesting results and for the patience during the correction of this thesis.

Robert Averbeck for his kindness especially during my first weeks in Germany.

The rest of the *ex*-CPR-PH group at Infineon Technologies: Oliver, Gregor, Gert, Christian, Thomas, Harry, Bernhard, Brem, Martin ... Each of them contributed to a serene and pleasant working atmosphere.

The WZMW-group in Marburg (Bernadette, Thorsten, Kerstin, Oleg…) for their help and the interesting discussions.

Michael Hetterich and Andreas Grau for the helpful discussions and for the electroreflectance measurements.

Stefan Birner for the absorption simulations.

Matthias Dworzak and his colleagues at the Technical University of Berlin for the time-resolved measurements.

Martin Albrecht and his staff for the transmission electron microscopy analysis.

Oleg Rubel for the kinetic Monte Carlo simulations

My friends in Italy: Stefania, Francesco, Maddalena, Francesco M., Elena, Tullia, Cristian, Simona, Gianluca... *Always present!*

Giorgio. *Impredictable!*

My friends in Munich: Roberto, Sabrina, Elena, Miran, Jesús, Guillermo, Josè, Andrea, Dagmar, Isacco, Valerio, Pina, Tiziana…

Mosè. *There are no words to explain how much you are important for me!*

My family. Mamma, Papà, Simona, Luca, il piccolo Alessandro, gli Zii...*Grazie!*

Scientific Curriculum Vitae

29th March 1975   born in Rome (Italien)

1994   Maturità scientifica (Sientific Lyceum Diplom)

1994-1999   Student at the University of Rome "La Sapienza"

2000   Laurea in Physics at the University of Rome "La Sapienza". Thesis title:
"*Optical properties of Quantum Dots in In$_{0.5}$Ga$_{0.5}$As/GaAs heterostructures grown by MOCVD and their comparison with similar structures grown by MBE*"

2003-2005   PhD at the Philipps-University of Marburg in collaboration with Infineon Technologies in Munich, Thesis title:
"*Optical characterisation of InGaAsN/GaAs quantum wells: Effects of annealing and determination of band offsets*"

Wissenschaftlicher Lebenslauf

29 März 1975   geboren in Rom (Italien)

1994   Maturità scientifica (Abitur)

1994-1999   Studium der Physik an der La Sapienza-Universität in Rom

2000   Physik-Diplom an der La Sapienza-Universität in Rom, Titel der Arbeit:
„*Optical properties of Quantum Dots in In$_{0.5}$Ga$_{0.5}$As/GaAs heterostructures grown by MOCVD and their comparison with similar structures grown by MBE*"

2003-2005   Doktorarbeit an der Philipps-Universität in Marburg in Zusammenarbeit mit der Infineon Technologies AG in München, Titel der Arbeit:
„*Optical characterisation of InGaAsN/GaAs quantum wells: Effects of annealing and determination of band offsets*"

List of publications

1. <u>M. Galluppi</u>, L. Geelhaar, H. Riechert, M. Hetterich, A. Grau, S. Birner, and W. Stolz, Phys. Rev. B **72**, 155324 (2005) *"Bound-to-bound and bound-to-free transitions in surface photovoltage spectra: Determination of the band offsets for $In_xGa_{1-x}As_{1-y}N_y$ quantum wells"*

2. O. Rubel, <u>M. Galluppi</u>, S. D. Baranovski, K. Volz, L. Geelhaar, H. Riechert, P. Thomas, and W. Stolz, J. Appl. Phys. **98**, 063518 (2005) *"Quantitative description of disorder parameters in (GaIn)(NAs) quantum wells from the temperature-dependent photoluminescence spectroscopy"*

3. <u>M. Galluppi</u>, L. Geelhaar, and H. Riechert, Appl. Phys. Lett. **86**, 131925 (2005) *"Nitrogen and Indium dependence of the band offsets in InGaAsN quantum wells"*

4. <u>M. Galluppi</u>, L. Geelhaar, and H. Riechert, J. Electr. Materials **1568**, S40 (2006) *"Band offsets analysis of dilute nitride single quantum well structures employing surface photovoltage measurements"*

5. L. Geelhaar, <u>M. Galluppi</u>, G. Jaschke, R. Averbeck, H. Riechert, T. Rammele, M. Albrecht, M. Dworzak, R. Hildebrant, and A. Hoffmann, Appl. Phys. Lett. **88**, 011903 (2006) *"Influence of structural non-uniformity and non-radiative processes on the luminescence efficiency of InGaAsN quantum wells"*

Conferences and workshops participation

<u>22-24 Jun. 2005</u>   Electronic Material Conference, in Santa Barbara (USA). Oral presentation: *Band offset analysis of dilute nitride single quantum well structures employing surface photo voltage measurements*

24-28 May 2004   E-MRS 2004 Spring Meeting, in Strasbourg (France). Visual presentation: *Investigation on InGaAs(N) quantum well band offset properties employing surface photovoltage measurements*

31 Mar-2 Apr 2004 Workshop of the DFG Research Group on Metastable Compound semiconductors and Heterostructures, in Marburg (Germany). Visual presentation: *Surface photovoltage measurements employed to determine the conduction and the valence band offsets in InGaAs(N) quantum wells*

8-12 Mar 2004   Spring Meeting of the German Physical Society, in Regensburg (Germany). Oral presentation: *Band Offset determination in InGaAsN quantum well structures employing surface photovoltage*

15-20 Feb 2004   13th International Winterschool on New Developments in Solid State Physics, in Maunterdorf (Austria).Visual presentation: *Surface photo voltage measurements employed to determine the conduction and the valence band offset in InGaAs(N) quantum wells*

06 Oct 2003   Deutscher MBE Workshop, in Munich (Germany) Oral presentation: *Determination of band-offset in GaInNAs quantum wells using the surface photovoltage technique*

References

[1] S. Nakamura, Jpn. J. Appl. Phys. **30**, L1705 (1991)

[2] M. Weyers, M. Sato, and H. Ando, Jpn. J. Appl. Phys. **31**, L853 (1992)

[3] M. Kondow, K.Uomi, A. Niwa, T. Kitatani, S. Watahiki, and Y. Yazawa, Jpn. J. Appl. Phys. **35**, 1273 (1996); M. Kondow, T. Kitatani, S. Nakatsuka, M.C. Larson, K. Nakahara, Y. Yazawa, and M. Okai, IEEE J. Select Topics Quantum Electron. **3**, 719, (1997)

[4] N. Tansu, N. J. Kirsch, and L. J. Mawst, Appl. Phys. Lett. **81**, 2523 (2002)

[5] Y. Wei, S. Wang, X. Wang, P. Modh, Q. Gu, M. Sadeghi, and A. Larsson, Electr. Lett. **40**, 1338 (2004)

[6] G. Jaschke, R. Averbeck, L. Geelhaar, and H. Riechert, J. Cryst. Growth **278**, 224 (2005)

[7] H. Riechert, A. Ramakrishnan, and G. Steinle, Semicond. Sci. Technol. **17**, 892 (2002)

[8] S. Prakash, L. Chirovsky, R. Naone, D. Galt, D. Kisker, and A. Jackson, Proc. SPIE Int. Soc. Opt. Eng. **4994**, 44 (2003)

[9] M. A. Wistey, S.R. Bank, H. B. Yuan, L:L. Goddard, and J. S. Harris, Electron. Lett. **39**, 1822 (2003)

[10] A. Ramakrishnan, G. Steinle, D. Supper, W. Stolz, and G. Ebbinghaus, J. Cryst. Growth **248**, 457 (2003)

[11] S.R. Kurtz, A. A. Allerman, E. D. Jones, J. M. Gee, J. J. Banas, and B. E. Hammons, Appl. Phys. Lett. **74**, 729 (1999)

[12] J. B. Heroux, X. Yang, and W. I. Wang, Appl. Phys. Lett. **75**, 2716 (1999)

[13] Y. S. Jalili, P. N. Stavrinou, J. S. Roberts, and G. Parry, Electron. Lett. **38**, 343 (2002)

[14] H.P. Xin and C. W. Tu, Appl. Phys. Lett. **75**, 1416 (1999)

[15] W. G. Bi, and C. W. Tu, Appl. Phys. Lett. **70**, 1608 (1997)

[16] L. Bellaiche, S.-H. Wei, and A. Zunger, Phys Rev. B **54**, 17568 (1996)

[17] G. H. Wannier, Phys Rev. **52**, 191 (1937); J. C. Slater, Phys Rev. **76**, 1592 (1949); J. M. Luttinger and W. Kohn, Phys Rev. **97**, 869 (1955)

[18] M. Burt, J. Phys Condens. Matter **4**, 6651 (1992) ; *ibid.* **11**, R53 (1999)

[19] W. Shan, W. Walukiewicz, J. W. Ager III, E. E. Haller, J. F. Geisz, D. J. Friedman, J. M. Olson, and S. R. Kurtz, Phys Rev. Lett. **82**, 1221 (1999)

[20] P. R. C. Kent and A. Zunger, Phys Rev. Lett. **86**, 2613 (2001)

[21] S. Adachi, *GaAs and Related Materials* (World Scientific, Singapore, 1994)

[22] I.A. Buyanova, W. M. Chen, G. Ponzina, J. P. Bergman, B. Monemar, H. P. Xin, and C. W. Tu, Appl. Phys. Lett. **75**, 501 (1999)

[23] H. Grüning, L. Chen, Th. Hartmann, P. J. Klar, W. Heimbrodt, F. Höhnsdorf, J. Koch, and W. Stolz, Phys Stat. Sol. (b) **215**, 39 (1999)

[24] S. Sakai, Y. ueta, and Y. Terauchi, Jpn. J. Appl. Phys. **32**, 4413 (1993)

[25] J. Neugebauer and C. Van de Walle, Phys. Rev. B **51**, 10568 (1995)

[26] J. A. Van Vechten, Phys. Rev. **182**, 891 (1969)

References

[27] S.-H. Wei and A. Zunger, Phys Rev. Lett. **76**, 664 (1996)

[28] J. Toivonen, T. Hakkarainen, M. Sopanen, H. Lipsanen, J. Cryst. Growth **221**,456 (2000)

[29] K. Uesugi and I. Suemune, Jpn. J. Appl. Phys. **36**, L1572 (1997)

[30] J. Wu, W. Shan, W. Walukiewicz, K. M. Yu, J. W. Ager III, E. E. Haller, H. P. Xin, and C. W. Tu, Phys. Rev. B **64**, 085320 (2001)

[31] P. R. C. Kent and A. Zunger, Phys Rev B **64**, 115208 (2001)

[32] A. Lindsay and E. P. O`Reilly, Sol. State Comm. **112**, 443 (1999)

[33] C. Skierbiszewski, P. Perlin, P. Wisniewski, T. Suski, J. F. Geisz, K. Hingerl, W. Jantsch, D. E. Mars, and W. Walukiewicz, Phys Rev. B **65**, 035207 (2001)

[34] E. P. O`Reilly, A. Lindsay, S. Tomić, and M. Kamal-Saadi, Semicond. Sci. Technol. **17**, 870 (2002)

[35] J. Wu, W. Walukiewicz, and E. E. Haller, Phys Rev B **65**, 233210 (2002)

[36] N. Shtinkov, P. Desjardins, and R. A. Masut, Phys Rev B **67**, 081202(R) (2003)

[37] J. D. Perkins, A. Mascarenhas, Y. Zhang, J. F. Geisz, D. J. Friedman, J. M. Olson, and S. R. Kurtz, Phys Rev. Lett. **82**, 3312 (1999)

[38] W. Shan, W. Walukiewicz, K. M. Yu, J. W. Ager III, E. E. Haller J. F. Geisz, D. J. Friedman, J. M. Olson, S. R. Kurtz, H. P. Xin, and C. W. Tu, Phys. Stat. Sol. (b) **223**, 75 (2001)

[39] E. D. Jones, N. A. Modine, A. A. Allerman, S. R. Kurtz, A. F. Wright, S. T. Tozer, and X. Wei, Phys Rev. B **60**, 4430 (1999)

[40] T. Mattila, S.-H. Wei, and A. Zunger, Phys Rev B **60**, R11245 (1999)

[41] P. N. Hai, W. M. Chen, I. A. Buyanova, H. P. Xin, and C. W. Tu, Appl. Phys. Lett. **77**, 1843 (2000)

[42] Z. Pan, L. H. Li, Y. W. Lin, B. Q. Sun, D. S. Jiang, and W. K. Ge, Appl. Phys. Lett. **78** 2217 (2001)

[43] M. Hetterich, M. D. Dawson, A. Yu. Egorov, D. Bernklau, and H. Riechert, Appl. Phys. Lett. **76**, 1030 (2000)

[44] S. B. Zhang, A. Mascarenhas, H. P. Xin, and C. W. Tu, Phys. Rev. B **61**, 7479 (2000)

[45] C. Skierbiszewski, P. Perlin, P. Wisniewski, W. Knap, T. Suski, W. Walukiewicz, W. Shan, K. M. Yu, J. W. Ager, E. E. Haller, J. F. Geisz, and J. M. Olson, Appl. Phys. Lett. **76**, 2409 (2000)

[46] A. D. Katnani, and G. Margaritondo, Phys. Rev. B **28**, 1944 (1983)

[47] H. Kroemer, W.-Y. Chien, J. S. Harris, and D. D. Edwall, Appl. Phys. Lett. **36**, 295 (1980)

[48] R. Dingle, W. Wiegmann, and C. H. Henry, Phys Rev. Lett. **33**, 827 (1974)

[49] T. Kitatani, M. Kondow, T. Kikawa, Y. Yazawa, M. Okai, and K. Uomi, Jpn. J. Appl. Phys. **38**, 5003 (1999)

[50] P. Krispin, S. G. Spruytte, J. S. Harris, and K. H. Ploog, J. Appl. Phys. **88**, 4153 (2000)

[51] I. A. Buyanova, G. Ponzina, P. N. Hai, W. M. Chen, H. P. Xin, and C. W. Tu, Phys. Rev. B **63**, 033303 (2001)

[52] H. P. Xin, and C. W. Tu, Appl. Phys. Lett. **72**, 2442 (1998)

[53] T. Miyamoto, K. Takeuchi, T. Kageyama, F. Koyama, and K. Iga, J. Cryst. Growth **197**,67 (1999)

[54] V. Grillo, M. Albrecht , T. Remmele, H. P. Strunk, A. Yu. Egorov, and H. Riechert, J. Appl. Phys. **90**, 3792 (2001)

[55] L. Grenouillet, C. Bru-Chevallier, G. Guillot, P. Gilet, P. Duvaut, C. Vannuffel, A. Million, and A. Chenevas-Paule, Appl. Phys. Lett. **76**, 2241 (2000)

[56] H. P. Xin, K. L. Kavanagh, Z. Q. Zhu, and C. W. Tu, Appl. Phys. Lett. **74**, 2337 (1999)

[57] W. K. Loke, S. F. Yoon, T. K. Ng, S. Z. Wang, and W. J. Fan, J. Vac. Sci. Technol. B **20**, 2091 (2002)

[58] M.-A. Pinault and E. Tournié, Appl. Phys. Lett. **79**, 3404 (2001)

[59] K. Volz, A. Hasse, A.K. Schaper, T. E. Weirich, F. Höhnsdorf, J. Koch, and W. Stolz, Mat. Res. Soc. Symp. Proc **618**, 291 (2000)

References

[60] M.-A. Pinault and E. Tornié, Appl. Phys. Lett. **78**, 1562 (2001)

[61] A. Pomarico, M. Lomascolo, R. Cingolani, A. Yu. Egorov, and H. Riechert, Semicond. Sci. Technol. **17**, 145 (2002)

[62] S. B. Zhang and S.-H. Wei, Phys Rev. Lett. **86**, 1789 (2001)

[63] P. R. Berger, K. Chang, P. K. Bhattacharya, J. Singh, and K. K. Bajaj, Appl. Phys. Lett. **53**, 684 (1988)

[64] N. Grandjean and J. Massies, Semicond. Sci. Technol. **8**, 2031 (1993)

[65] D. Schlenker, T. Myamoto, Z. Chen, M. Kawaguchi, T. Kondo, E. Govardes, J. Gemmer, C. Gemmer, F. Koyama, and K. Iga, Jpn. J. Appl. Phys. **39**, 5751 (2000)

[66] R. Asomoza, V. A. Elyukhin, and R. Peña-Sierra, Appl. Phys. Lett. **81**, 1785 (2002)

[67] P. J. Klar, H. Grüning, J. Koch, S. Schäfer, K. Volz, W. Stolz, W. Heimbrodt, A. M. Kamal Saadi, A. Lindsay, and E. P. O`Reilly, Phys. Rev. B **64**, 121203 (R) (2001)

[68] M. Albrecht, V. Grillo, T. Remmele, H. P. Strunk, A. Yu. Egorov, Gh. Dumitras, H. Riechert, A. Kaschner, R. Heitz, and A. Hoffmann, Appl. Phys. Lett. **81**, 2719 (2002)

[69] L. Grenouillet, C. Bru-Chevallier, G. Guillot, P. Gilet, P. Ballet, P. Duvaut, G. Rolland, and A. Million, J. Appl. Phys. **91**, 5902 (2002)

[70] S.Kurtz, J. Webb, L. Gedvilas, D. Friedman, J. Geisz, J. Olson, R. King, D. Joslin, and N. Karam, Appl. Phys. Lett. **78**, 748 (2001)

[71] H. Ch. Alt, A. Yu. Egorov, H. Riechert, J. D. Meyer, and B. Wiedemann, Phisica B: Condensed Matter **308-310**,877 (2001)

[72] A. Moto, S. Tanaka, N. Ikoma, T. Tanabe, S. Tagagishi, M. Takahashi, and T. Katsuyama, Jpn. J. Appl. Phys. **38**, 1015 (1999)

[73] S.G. Spruytte, C. W. Coldren, J. S. Harris, W. Wampler, P. Kripsin, K. Ploog, and M. C. Larson, J. Appl. Phys. **89**, 4401 (2001)

[74] M. Oueslati, M. Zouaghi, M. E. Pistol, L. Samuelson, H. G. Grimmeiss, and A. Balkanski, Phys. Rev. B **32**, 8220 (1985)

[75] T Tiedje and A Rose, Solid State Commun. **37**, 49 (1980)

[76] K. L. Teo, J. S. Colton, P. Y. Yu, E. R. Weber, M. F. Li, W. Liu, K. Uchida, H. Tokunaga, N. Akutsu, and K. Matsumoto, Appl. Phys. Lett. **73**, 1697 (1998)

[77] A. Polimeni, M. Capizzi, M. Geddo, M. Fischer, M. Reinhardt, and A. Forchel, Appl. Phys. Lett. **77**, 2870 (2000)

[78] Y. P. Varshni, Physica (Utrecht) **34**, 149 (1967)

[79] P. Perlin, Ch. Kisielowski, V. Iota, B. A. Weinstein, L. Mattos, N. A. Shapiro, J. Kruger, E. R. Weber, and J. Yang, Appl. Phys. Lett. **73**, 2778 (1998)

[80] H. D. Sun, M. Hetterich, M. D. Dowson, A. Yu. Egorov, D. Bernklau, and H. Riechert, J. Appl. Phys. **92**, 1380 (2002)

[81] A. Kaschner, T. Lüttgert, H. Born, A. Hoffmann, A. Yu. Egorov, and H. Riechert, Appl. Phys. Lett. **78**, 1391 (2001)

[82] Y. Narukawa, Y. Kawakami, S. Fujita, S. Fujita, and S. Nakamura, Phys. Rev. B **55**, R1938 (1997)

[83] L. H. Li, Z. Pan, W. Zhang, Y. W. Lin, Z. Q. Zhou, and R. H. Wu, J. Appl. Phys. **87**, 245 (2000)

[84] P.J. Klar and K. Volz, J. Phys.: Cond. Mat. **16**,S3053 (2004)

[85] A review of the different growth techniques employed to grow dilute nitrides can be found in *Dilute Nitride Semiconductors* Ed. H. Henini Elsevier 2005

[86] A. Yu. Egorov, D. Bernklau, B. Borchert, S. Illek, D. Livshits, A. Rucki, M. Schuster, A. Kaschner, A. Hoffmann, Gh. Dumitras, M. C. Amann, and H. Riechert, J. Cryst. Growth **227-228**, 545 (2001)

[87] Gh. Dumitras, *Optical and electrical characterization of InGaAsN used for 1.3 μm lasers* PhD work (2003)

[88] Gh. Dumitras, H. Riechert, H. Porteanu, and F. Koch, Phys Rev B **66**, 205324 (2002)

References

[89] Gh. Dumitras and H. Riechert, J. Appl. Phys. **94**, 3955 (2003)

[90] E. Tournié, M.-A. Pinault, and A. Guzmán, Appl. Phys. Lett. **80**, 4148 (2002)

[91] J.-M. Chauveau, A. Trampert, K. H. Ploog, M.-A. Pinault, and E. Tournié, Appl. Phys. Lett. **82**, 3451 (2003)

[92] E.-M. Pavelescu, T. Jouhti, M. Dumitrescu, P. J. Klar, S. KAririnne, Y. Fedorenko, and M. Pessa, Appl. Phys. Lett. **83**, 1497 (2003)

[93] A. Hierro, J.-M. Ulloa, J.-M. Chauveau, A. Trampert, M.-A. Pinault, E. Tournié, A. Guzmán, J. L. Sánchez-Rojas, and E. Calleja, J. Appl. Phys. **94**, 2319 (2003)

[94] R. Kudrawiec, E.-M. Pavelescu, J. Andrzejewski, J. Misiewicz, A. Gheorghiu, T. Jouhti, and M. Pessa, J. Appl. Phys. **96**, 2909 (2004)

[95] S.-W. Feng, Y.-C. Cheng, Y.-Y. Chung, C.-C. Yang, Y.-S. Lin, C. Hsu, K.-J. Ma, and J.-I. Chyi, J. Appl. Phys. **92**, 4441 (2002)

[96] Y. Y. Chung, Y. S. Lin, S. W. Feng, Y. C. Cheng, E. C. Lin, C. C. Yang, K. J. Ma, C. Hsu, H. W. Chuang, c. T. Kuo, and J. S. Tsang, J. Appl. Phys. **93**, 9693 (2003)

[97] G. Mussler, L. Däweritz, K. Ploog, J. W. Tomm, and V. Talalaev, Appl. Phys. Lett. **83**, 1343 (2003)

[98] V.Lordi, V. Gambin, S. Friedrich, T. Funk, T. Takizawa, K. Uno, and J. S. Harris, Phys Rev Lett. **90**,145505 (2003)

[99] A. Polimeni, G. Baldassarri Höger von Högersthal, M. Bissiri, M. Capizzi, A. Frova, M. Fisher, M. Reinhardt, and A. Forchel, Semic. Sci. Technol. **17**, 797 (2002)

[100] I. A. Buyanova, M. Izadifard, W. M. Chen, A. Polimeri, M. Capizzi, H. P. Xin, and C. W. Tu, Appl. Phys. Lett. **82**, 3662 (2003)

[101] M. Ramsteiner, D. S. Jiang, J. S. Harris, and K.H. Ploog, Appl. Phys. Lett. **84**, 1859 (2004)

[102] P. Krispin, V. Gambin, J. S. Harris, and K. H. Ploog, J. Appl. Phys. **93**, 6095 (2003)

[103] J. Toivonen, T. Hakkarainen, M. Sopanen, H. Lipsanen, J. Oila, and K. Saarinen, Appl. Phys. Lett. **82**, 40 (2003)

[104] O. Rubel, M. Galluppi, S. D. Baranovskii, K. Volz, L. Geelhaar, H. Riechert, P. Thomas, and W. Stolz, J. Appl. Phys. **98**, 063518 (2005)

[105] H. Grüning, K. Kohary, S. D. Baranovskii, O. Rubel, P. J. Klar, A. Ramakrishnan, G. Ebbinghaus, P. Thomas, W. Heimbrodt, W. Stolz, and W. W. Rühle, Phys. Stat. Sol. (c) **1**, 109 (2004)

[106] S. D. Baranovski, R. Eichmann, and P. Thomas, Phys Rev B **58**, 13081 (1998)

[107] M. Albrecht, *private communication*

[108] W. I. Wang, T. S. Kuan, E. E. Mendez, and L. Esaki, Phys Rev B **31**, 6890 (1985)

[109] L. Kronik and Y. Shapira, *Surface Photovoltage Phenomena: Theory, Experiment, and Applications* (Elsevier, Amsterdam, 1999)

[110] N. Ashkenasy, M. Leibovitch, Y. Shapira, F. H. Pollak, G. T. Burnham, and X. Wang, J. Appl. Phys. **83**, 1146 (1998)

[111] I. Vurgaftman, J. R. Meyer, and L. R. Ram-Mohan, J. Appl. Phys. **89**, 5815 (2001)

[112] G. Ji, D. Huang, U.K. Reddy, T. S. Henderson, R. Houdré, and H. Morkoç, J. Appl. Phys. **62**, 3366 (1987); D. J. Arent, K. Deneffe, C. van Hoff, J. De Boeck, and G. Borghs, J. Appl. Phys. **66**, 1739 (1989); J. Micallef, E. H. Li, and B. L. Weiss, Superlattices and Microstructures **13**, 125 (1993)

[113] J.-P. Reithmaier, R. Höger, and H. Riechert, Phys Rev B **43**, 4933 (1991)

[114] J.-Y. Marzin, M. N. Charasse, and B. Sermage, Phys Rev B **31**, 8298 (1985)

[115] The nextnano³ software package can be downloaded from www.wsi.tum.de/nextnano3 and www.nextnano.de

[116] A. Ksendzov, W.T. Pike, and A. Larsson, Phys Rev B **47**, 2228 (1993)

References

[117] G. Ji, D. Huang, U. K. Reddy, H. Unlu, T. S. Henderson, and H. Morkoç, J. Vac. Sci. Technol. B **5**, 1346 (1987); J.-P. Reithmaier, R. Höger, H. Riechert, A. Haberle, G. Abstreiter, and G. Weimann, Appl. Phys. Lett. **56**, 536 (1990)

[118] G. Bastard, *Wave Mechanics Applied to Semiconductor Heterostructures* (Halsted, New York 1988)

[119] G. Bastard, U. O. Ziemelis, C. Delalande, M. Voos, A. C. Gossard, and W. Wiegmann, Solid State Comm. **49**, 671 (1984); G. Duggan, Proc. SPIE **1283**, 206 (1990)

[120] M. Galluppi, L. Geelhaar, and H. Riechert, Appl. Phys. Lett. **86** 131925 (2005)

[121] I. Vurgaftman and J. R. Meyer, J. Appl. Phys. **94**, 3675 (2003)

[122] P.J. Klar, Prog. Solid State Chem. **31**,301 (2003)

[123] W. Shan, W. Walukiewicz, J. W. Ager III, E. E. Haller J. F. Geisz, D. J. Friedman, J. M. Olson, S. R. Kurtz, J. Appl. Phys. **86**, 2349 (1999)

[124] S. A. Choulis, T.J.C. Hosea, S. Tomić, M. Kamal-Saadi, A.R. Adams, E.P. O´Reilly, B.A. Weinstein, P.J. Klar, Phys. Rev. B 66, 165321 (2002)

[125] J. B. Héroux, X. Yang, and W.I. Wang, J. Appl. Phys. **92**, 4361 (2002)

[126] V. I. Zubkov, M. A. Melnik, A. V. Solomonov, E. O. Tsvelev, F. Bugge, M. Weyers, and G. Tränkle, Phys Rev B **70**, 075312 (2004)

[127] S. Datta, B. M. Arora, and S. Kumar, Phys. Rev. B 62, 13604 (2000)